Dissertation zur Erlangung des Doktorgrades

der Fakultät für Chemie und Pharmazie

der Ludwig-Maximilians-Universität München

Structural Analysis of

No-go Decay and Ribosome Recycling in Archaea

Sibylle Franckenberg

aus

Bamberg

2012

Erklärung

Diese Dissertation wurde im Sinne von §13 Abs. 3 bzw. 4 der Promotionsordnung vom 29. Januar 1998 (in der Fassung der sechsten Änderungssatzung vom 16. August 2010) von Herrn Prof. Dr. Roland Beckmann betreut.

Ehrenwörtliche Versicherung

Diese Dissertation wurde selbständig, ohne unerlaubte Hilfe erarbeitet.

München,

Sibylle Franckenberg

Dissertation eingereicht am 09.01.2012

1. Gutachter   Prof. Dr. Roland Beckmann
2. Gutachter   Prof. Dr. Karl-Peter Hopfner

Mündliche Prüfung am 08.03.2012

Table of contents

Abbreviations

$A_{260/280}$	absorbance at a wavelength of 260 or 280 nm
aa-tRNA	aminoacyl tRNA
ABC	ATP binding cassette
ADPNP	5'-adenylyl-ß,γ -imidodiphosphate
A site	acceptor-site of the ribosome
ATP	adenosine triphosphate
bp	base pairs (kb kilo base pairs)
BSA	bovine serum albumin
CCD	charge coupled devise
CTD	carboxy-terminal domain
C-terminal	carboxy-terminal
CTF	contrast transfer function
CTP	cytosine triphosphate
Cryo-EM	cryo-electron microscopy
Da	Dalton (kDa = kilo Dalton, MDa = Mega Dalton)
DMSO	dimethyl sulfoxide
DNA	deoxyribonucleic acid
DTT	dithiotreitol
EF	elongation factor (a/eEF archaeal/eukaryotic elongation factor)
E site	exit-site of the ribosome
E. coli	*Escherichia coli*
EDTA	ethylenediaminetetraacetic acid

EF	elongation factor
FeS	$[4\text{Fe-4S}]^{2+}$
FSC	Fourier shell correlation
GDPNP	5'-guanylyl-ß,γ -imidodiphosphate
GTP	guanosine triphosphate
h	hour
HA	hemagglutinin
HLH	helix-loop-helix
HRP	horse reddish peroxidase
IF	initiation factor (eIF eukaryotic initiation factor)
IPTG	isopropyl-β-D-1-thiogalactopyranoside
min	minutes
mRNA	messenger ribonucleic acid
NBD	nucleotide binding domain
NGD	no-go decay
NMD	nonsense mediated decay
NMR	nuclear magnetic resonance
NSD	non-stop decay
NTD	N-terminal domain
N-terminal	amino-terminal
OD	optical density
P site	peptidyl-site of the ribosome
PAGE	polyacrylamide gel electrophoresis
PCR	polymerase chain reaction

P. furiosus	*Pyrococcus furiosus*
PMSF	phenylmethylsulfonyl fluoride
PTC	peptidyl transferase center
RBS	ribosomal binding site
RF	release factor (eRF eukaryotic release factor, aRF archaeal release factor)
RNA	ribonucleic acid
RNC	ribosome - nascent chain complex (SL-RNC stem loop ribosome-nascent chain-complex)
RRF	ribosome recycling factor
rRNA	ribosomal ribonucleic acid
RT	room temperature
sec	seconds
SDS	sodium dodecyl sulfate
SRL	sarcin-ricin-loop
TEM	transmission electron microscope
T. kodakarensis	*Thermococcus kodakarensis*
tmRNA	transfer-messenger ribonucleic acid
Tris	tris(hydroxymethyl)aminomethane
tRNA	transfer ribonucleic acid
UTP	uridine triphosphate

1. Introduction

1.1.   Archaea – the third domain of life

Since Woese's discovery in 1977, archaea are now generally accepted to be the third domain of life besides eukaryotes and bacteria (Woese and Fox, 1977; Woese et al., 1990). Initially, archaea were thought to occur only in extreme habitats regarding temperature, pH or salinity (Kates et al., 1993), but subsequent investigations have shown that species can be found also under moderate conditions and even associated with the human microbiome (DeLong, 1998; Dridi et al., 2011).

A large effort has been made to analyze the characteristics of the third domain of life. Archaea possess unique attributes that cannot be found in other domains: the membrane, for example, is made of ether linked lipids and sometimes even of tetra ether lipids that form a rigid monolayer which is nearly impermeable to ions (van de Vossenberg et al., 1998). However, often it is possible to draw parallels to bacteria and eukaryotes: like bacteria, archaea are prokaryotes that contain a simple cellular structure without organelles and sometimes similar metabolic pathways (Danson and Hough, 1992). Yet, in other aspects they resemble eukaryotes: several features of DNA replication, transcription and translation seem to be a simplified version of the more complex eukaryotic processes (Bell and Jackson, 1998). These observations are in concordance with the hypothesis of the origin of eukaryotes being the outcome of a fusion or endosymbiosis event between an archaeon and a bacterium (Poole and Penny, 2007). These characteristics make archaea interesting model organisms to analyse the evolution of contemporary metabolic processes.

1.1.1. Archaea as model organisms for structural analysis

Several metabolic processes in archaea – such as translation – are simplified models of processes known from eukaryotes. Often fewer factors are involved and the factors fulfil more functions than the eukaryotic counterparts (Bryant and Aves, 2011; Saito et al., 2010). The strong conservation of some proteins allows partial substitution of components in eukaryotes or bacteria with their archaeal counterpart. This has been shown for initiation factor a/eIF5B in a yeast knock-out strain and for a/eIF2 in a mammalian *in vitro* translation system (Allen and Frank, 2007; Dmitriev et al., 2011). In *Escherichia coli*, a temperature sensitive SecY mutant was complemented with archaeal SecY (Auer et al., 1991; Egea and Stroud, 2010). The functional homology is the prerequisite for archaea as model organisms to structurally analyze the principles of metabolic pathways that are conserved across domains. In addition, the occurrence of extremophile species provides an advantage for molecular analyses: The adaption of some archaeal species to extreme temperature or high osmotic pressure allowed the development of exceptionally robust proteins. These proteins are less prone to degradation and therefore ideal candidates for crystallisation. For example the halophilic family *Halobacteriaceae* and the hyperthermophilic *Methanococcacea* and *Thermococcacea* families have been proven useful for addressing multiple biochemical and structural questions associated with translation: The first ribosomal subunit to be crystallized at high resolution was the large subunit from the haloarchaeon *Haloarcula marismortui (Ban et al., 1999; Ban et al., 2000)*; the understanding of the signal recognition particle that mediates the interaction between protein translation and translocation machinery was greatly improved by numerous crystal structures obtained from archaeal homologues (Egea et al., 2008; Hainzl et al., 2011; Janda et al., 2010; Wild et al., 2010). Also structures of the archaeal protein conducting channel SecYEβ provided new insights into the general mechanism of protein insertion into or translocation across the membrane (Egea and Stroud, 2010; Van den Berg et al., 2004).

1.1.2. *In vitro* translation

Cell-free translation has been established in the early 1960s to investigate the principles of protein synthesis (Dvorak et al., 1967; Matthaei and Nirenberg, 1961). Since then *in vitro* translation has become an important tool for addressing diverse biochemical and mechanistic questions: It allows the expression of proteins that interfere with the viability of the host cell (Henrich et al., 1982) or the synthesis of proteins with unnatural amino acids (Noren et al., 1989). Besides these applications it also provides an environment for the analysis of specific aspects of protein synthesis that can be easily controlled and manipulated.

Since the 1960s reliable protocols have been established for bacterial (Liu et al., 2005) and eukaryotic (Endo and Sawasaki, 2004; Kozak, 1990) translation systems. More recently, protocols for *in vitro* translation of the hyperthermophilic archaea *Sulfolobus solfactarius* (Condo et al., 1999; Ruggero et al., 1993) and *Thermococcus kodakarensis* (Endoh et al., 2007; Endoh et al., 2006) have been published.

T. kodakarensis is an obligate anaerobic euryarcheote and was initially isolated from hydrothermal vents on Kodakara Island in Japan (Morikawa et al., 1994). The species grows at a temperature range from 60-100°C and thrives on sulphur reduction. The sequenced genome and the recently established *in vitro* translation system make this species an ideal candidate for structural studies on translation associated processes.

1.1.3. Programming ribosomes *in vitro*

The structural analysis of translation associated processes requires *in vitro* reconstitution of the respective factors with ribosomes that are caught in synchronized translation. This can be achieved by stalling the ribosomes at a defined moment during the translation process. This way, a population of homogeneous complexes of translating ribosomes with identical nascent chains can be obtained.

Several physiological and un-physiological mechanisms are known that interfere with translation: Some proteins are known that regulate their own translation rate by interactions of the nascent chain with the ribosomal exit tunnel. These mechanisms have been exploited successfully for ribosome-nascent chain-complex (RNC) generation in bacteria (Bhushan et al., 2011; Seidelt et al., 2009). Species independent generation of RNC is simply based on biochemical or sequence encoded properties of the mRNA: The usage of stable RNA stem-loop structures or truncated mRNA that lacks a stop codon at the 3'-end leads to ribosomal stalling and was successfully used for generating RNCs from eukaryotes (Becker et al., 2011; Halic et al., 2004) as well as bacteria (Frauenfeld et al., 2011).

So far, hardly anything is known about physiological stalling or pausing events during archaeal translation; therefore truncated mRNA is the most promising approach to start with. Truncated mRNA is independent of the coding sequence and the stalling mechanism is supposed to work universally. A ribosome stalled by truncated mRNA does not contain a codon in the A site, therefore translation as well as termination is impaired. The interesting question that remains is how efficient archaeal extracts can deal with the rescue of ribosomes stalled by truncated mRNA. These questions will have to be addressed experimentally.

1.2.   mRNA surveillance mechanisms

Several checkpoints ensure the correct interpretation of the genetic code from transcription to translation and proper folding of proteins: one aspect in this control scheme are the so called mRNA surveillance mechanisms. These mechanisms consist of several components that are

able to recognize and deal with different failures of mRNA translation and act directly on translating ribosomes. Translation of erroneous mRNA can lead to two major problems for the cell: Firstly, alterations in the open reading frame by mutations or inaccurate splicing generate premature stop codons. The resulting proteins are truncated and non-functional or even harmful for the cell metabolism (Hentze and Kulozik, 1999). Secondly, translation of mRNAs that lack stop codons or contain stable secondary structures like stem loops stall translating ribosomes (Isken and Maquat, 2007). If there is no way to release the ribosomes from these erroneous mRNAs the amount of functional ribosomes in the cell is reduced. This severely affects the rate of protein synthesis in the cell and thereby cell viability.

Since it is vital for all forms of life to overcome these problems, different mRNA surveillance mechanisms have evolved.

1.2.1. Nonstop decay in *Saccharomycetes* yeasts

mRNA lacking a stop codon leads to a translation arrest at the 3'-end of the mRNA and the ribosome remains bound to the mRNA. In yeast, a nonstop decay (NSD) surveillance mechanism has been identified that involves Ski7, a member of the EF-Tu family of translational GTPases (Fig. 1, A). This protein is restricted to *Saccharomycetes* yeasts and is most likely derived from duplication of the gene coding for Hbs1 (Atkinson et al., 2008; van Hoof, 2005). Ski7 is thought to recognize the empty A site of a stalled ribosome and to mimic the GTPase domain of eEF1α and eRF3 (van Hoof et al., 2002). The N-terminal domain of Ski7 recruits the exosome and the Ski-complex consisting of Ski2, Ski3 and Ski8. The exosome functions as 3'-5' RNase and degrades the defective mRNA after release of the ribosome (van Hoof et al., 2002).

So far, it is not known how the erroneous protein is targeted for degradation, but it was proposed that the translation of the poly(A)-tail provides a signal for subsequent proteolysis (Ito-Harashima et al., 2007). It is quite likely that more proteins are involved in this surveillance mechanism but the details of their interaction and their importance remain to be analysed

(Wilson et al., 2007). It was speculated that an unknown A-site factor like Pelota or RF1 is involved that senses the ribosomal stall at the end of the mRNA (Clement and Lykke-Andersen, 2006). It remains to be analyzed how non-stop mRNA is recognized and targeted in other eukaryotic species or even archaea since Ski7 is strictly restricted to *Saccharomycetes* yeast. Studies in yeast *ski2Δ* strains that are deficient of NSD have revealed that factors involved in no-go mRNA decay (see 1.2.4.) might also target ribosomes stalled on non-stop mRNA (Kobayashi et al., 2010).

1.2.2. tmRNA – nonstop decay in bacteria

A completely different mechanism addressing the problem of nonstop mRNA can be found in eubacteria. A ribonucleoprotein complex consisting of transfer-messenger RNA (tmRNA) and the protein SmpB recognises and releases stalled ribosomes: The chimeric tmRNA consists of two functional domains. The first domain mimics the tRNA acceptor branch and can be aminoacylated with alanine (Komine et al., 1994; Ushida et al., 1994). The second domain acts as translatable open reading frame that tags the emerging peptide with a C-terminal degradation signal (Gillet and Felden, 2001). So far no candidate genes for tmRNA could be identified in eukaryotes and archaea, which makes this system unique for eubacteria.

1.2.3. Nonsense mediated decay in eukaryotes

Nonsense mediated decay (NMD) is triggered when stop codons on the mRNA prematurely terminate translation. An mRNA with a premature stop-codon can be generated by incorrect splicing events in higher eukaryotes, frameshift mutations or transcription initiation upstream of the coding sequence. Even though translating ribosomes are not negatively affected by these mRNAs, the resulting truncated proteins might harbour a potential hazard for the cells (Pulak

and Anderson, 1993). Interestingly, NMD is also known to play a regulatory role in the expression level of some proteins like the polypyrimidine tract-binding protein (Wollerton et al., 2004).

The majority of potential NMD targets in mammals are characterised by the presence of the post-splicing exon junction complex 50-55nt downstream of a termination codon (Lykke-Andersen et al., 2000; Nagy and Maquat, 1998). In other eukaryotes where splicing is an exception, it is speculated in the "faux-UTR model" that the long distance between the premature termination codon and the poly(A)-tail interferes with normal termination and therefore activates NMD (Amrani et al., 2004). In the process of NMD the termination factors eRF1 and eRF3, members of the Upf family and Smg proteins are involved (Fig. 1, B). Even though the classical termination factors are involved, the process of aberrant termination differs from normal termination regarding initiation competence of the released ribosome (Amrani et al., 2004; Ghosh et al., 2010); So far, little is known about the biochemical difference between the aberrant and normal termination reaction. The Upf proteins (Upf1, Upf2 and Upf3) and the Smg proteins (Smg1, Smg5, Smg6, Smg7) are essential for the degradation of the mRNA, but the mechanism is not yet understood (Avery et al., 2011; Chamieh et al., 2008; Gatfield et al., 2003).

Until now, no homologues of the Upf and Smg protein family are known in archaea.
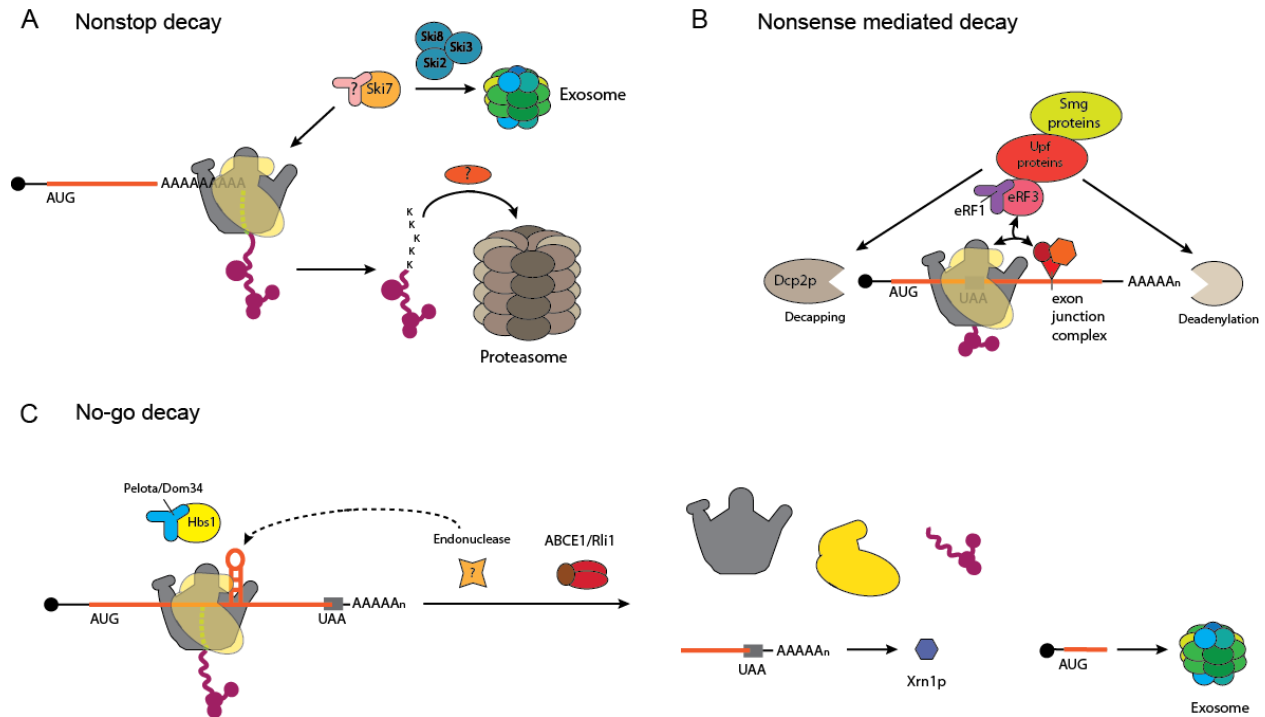
Figure 1: mRNA surveillance mechanisms in eukaryotes. (A) Nonstop decay in *S. cerevisiae*: The ribosome translates along the mRNA until the end of the Poly-(A) tail. Ski7 and eventually an unknown A-site factor bind to the ribosome and recruit the exosome and the Ski complex for degradation of the mRNA. The Poly-(K) stretch that is added to the nascent chain by translation of the Poly-(A) tail is thought to trigger rapid degradation of the protein by the proteasome. (**B**) Nonsense mediated decay: the presence of an exon-junction complex downstream of the stop-codon initiates NMD in higher eukaryotes. The mechanism involves release factors eRF1 and eRF3 and members of the Upf and Smg protein family. The later proteins initiate deadenylation and decapping of the mRNA. (**C**) No-go decay: The stalling of a ribosome during translation e.g. by secondary structures is recognized by Pelota/Dom34 and Hbs1. An endonuclease cleaves the mRNA near the stem loop structure and the mRNA fragments are further digested by Xrn1p and the exosome. Recycling of the ribosome involves the ATPase ABCE1/Rli1. Models adapted from (Clement and Lykke-Andersen, 2006).

1.2.4. No-go decay in eukaryotes

The no-go decay (NGD) pathway is initiated when translation is slowed down or even stopped by physical properties of the mRNA. Reasons for stalling can be pseudoknots, rare codons, RNA stem loop structures, truncated mRNA or depurination (Doma and Parker, 2006; Doma and Parker, 2007; Gandhi et al., 2008). All these structural alterations of the mRNA are assumed to

interfere with the correct codon-anticodon pairing and therefore inhibit translation elongation. In eukaryotes the stalled ribosome is recognised by two proteins, Pelota (Dom34 in yeast) and Hbs1 (Doma and Parker, 2006; Passos et al., 2009) (Fig. 1, C).

Pelota is related to eRF1, a termination factor that recognizes stop codons and catalyses release of peptidyl-tRNA in the termination reaction (Frolova et al., 1994) (Fig. 2). Pelota consists of three domains, an N-terminal domain (NTD) containing a RNA-binding motif and similar to eRF1 a central domain and a C-terminal domain (CTD) (Graille et al., 2008).
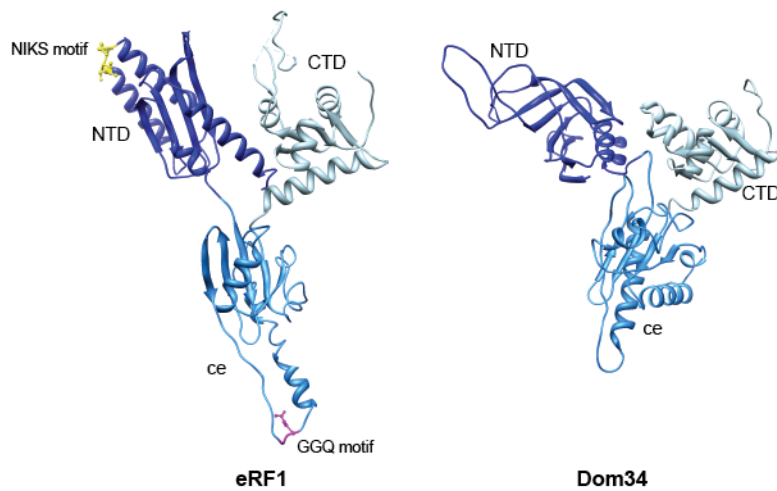
Figure 2: Comparison of the paralogs eRF1 and Dom34. Colors indicate domain architecture. Crystal structure of human eRF1 (Frolova et al., 2002) shown in comparison with the structure of yeast Dom34 (Chen et al., 2010; Lee et al., 2007). The domain architecture is essentially conserved, but the NIKS motif that recognizes stop codons (yellow) and the catalytically active GGQ motif (purple) are absent in Dom34.

Initially, the function of Pelota was assessed by mutation analysis in drosophila and yeast: In drosophila the phenotype of the deletion mutant is indicated by a failure in spermatogenesis and eye development (Eberhart and Wasserman, 1995) whereas in yeast, sporulation and pseudohyphal growth are affected (Davis and Engebrecht, 1998). It was soon postulated that Pelota mediates its effects via the translation machinery (Davis and Engebrecht, 1998).

As observed for its paralog eRF1, Pelota binds to the ribosomal A site by mimicking an aminoacyl-tRNA (aa-tRNA) (Becker et al., 2011; Kobayashi et al., 2010; Passos et al., 2009). In contrast to eRF1, Pelota neither contains the GGQ motif that is necessary to release the peptide from the P-site tRNA, nor the NIKS motif that recognizes stop codons (Fig. 2) (Frolova et al., 1999; Pisareva et al., 2011; Shoemaker et al., 2010).

In the process of NGD, the mRNA is cleaved near the stalling structure. The remaining mRNA fragments are targeted by the 5'→3' exonuclease Xrn1 and the exosome in concert with the Ski complex, a 3'→5' RNA degradation complex (Doma and Parker, 2006). Initially, it was proposed that Pelota functions as the initial endonuclease (Lee et al., 2007), but these results could not be confirmed (Becker et al., 2011; Passos et al., 2009; Shoemaker et al., 2010). So far the identity of the initial endonuclease is unknown.

Hbs1 belongs to the EF-Tu like family of translational GTPases. It consists of a conserved GTPase domain (domain I), domains II and III and a non-conserved N-terminal domain (NTD) which varies in length in different paralogs (Becker et al., 2011). Other members of this family are known to transport aa-tRNA (a/eEF1α, EF-Tu) or release factors (aEF1α, eRF3) to the ribosome. The function of these proteins is best described for tRNA delivery by EF1α; GTP-bound EF1α binds aa-tRNA and the complex binds to the ribosome. The correct codon-anticodon-pairing between the aa-tRNA and the mRNA leads to GTP hydrolysis in EF1α and induces a conformational change. Inactive EF1α-GDP then dissociates from the ribosome (Krab and Parmeggiani, 1998; Negrutskii and El'skaya, 1998). Presumably, the delivery mechanism is similar for all members of this family. Hbs1 in complex with Dom34 shows GTP hydrolysis only in the presence of both ribosomal subunits which is in concordance with the general delivery mechanism (Shoemaker et al., 2010). Also the cryo-EM structure of Dom34-Hbs1 bound to a stem-loop stalled ribosome (SL-RNC) resembles the crystal structure of a bacterial ribosome with bound EF-Tu and aa-tRNA (Becker et al., 2011; Schmeing et al., 2009).

A crystal structure of the Dom34-Hbs1 complex revealed that upon binding of Hbs1 the central domain of Dom34 is rotated by 142°C and interacts with domain II and III of Hbs1 compared to a crystal structure of Dom34 alone (Fig. 3, A) (Chen et al., 2010; Graille et al., 2008). Binding of Dom34 to Hbs1 increases the affinity of Hbs1 for GTP as was also observed for the interaction between eRF1 and eRF3 (Chen et al., 2010).
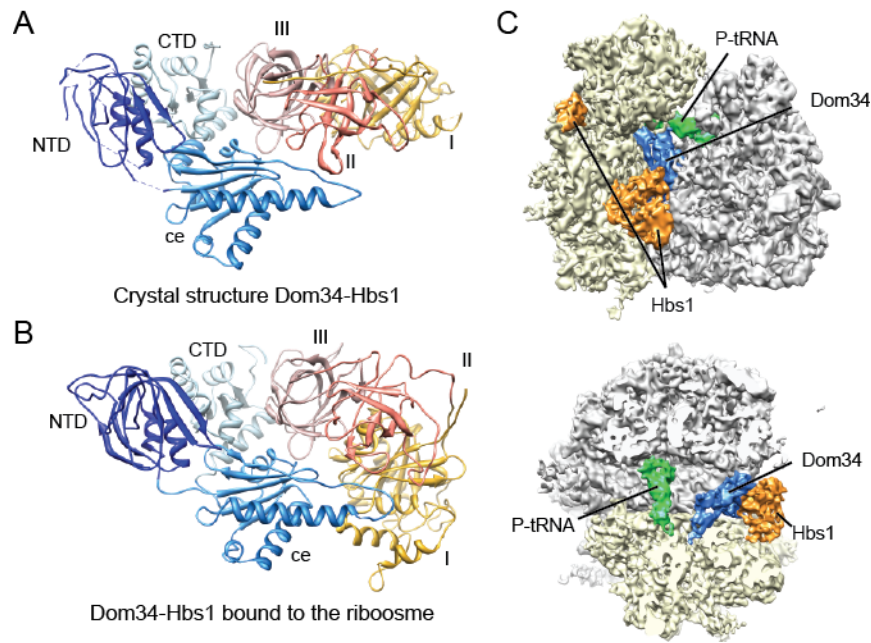
Figure 3: Crystal structure of Dom34-Hbs1 and cryo-EM structure of Dom34-Hbs1 bound to SL-RNCs. (**A**) Crystal structure of Dom34-Hbs1 (Chen et al., 2010). (**B**) Dom34-Hbs1 model in the ribosome bound form, based on the cryo-EM map shown in (**C**) (Becker et al., 2011). The N-terminus of Hbs1 is not displayed in the model. Colors indicate domain architecture of the proteins (**A, B**) or ligands of the ribosome (**C**).

Recently, a cryo-EM structure of Dom34 and Hbs1 bound to SL-RNCs provided insight into the mechanism of NGD (Fig. 3, B and C) (Becker et al., 2011). Hbs1 binds to the ribosome within the canonical translation factor-binding site and positions Dom34 in the ribosomal A site. As observed in the crystal structure of Dom34 and Hbs1 the central domain of Dom34 is in close contact with Hbs1 (Fig. 3, A, B) (Chen et al., 2010). The NTD of Hbs1 could be localized at the mRNA entry site of the small ribosomal subunit. It was hypothesized that the binding of Dom34 and Hbs1 interferes with the codon-anticodon interaction within the ribosome (Fig. 3, C) (Becker et al., 2011).

Functional studies in yeast with dipeptidyl 80S termination complexes revealed that Dom34 and Hbs1 can split the ribosome at low Mg^{2+}-levels and release the peptidyl-tRNA independent of the codon of the mRNA in the A site (Shoemaker et al., 2010). In contrast, experiments performed with purified human Pelota and Hbs1 revealed that the ABC-type ABCE1 is essential for splitting in mammals (Pisareva et al., 2011). ABCE1 - also known as RNase L inhibitor, Rli1 in

yeast or Pixie in Drosophila - is a member of the ATP binding cassette (ABC) transporter family. ABC transporters are involved in many biological processes in all kingdoms of life, mainly transport processes across membranes and DNA repair (Decottignies et al., 1997; Hopfner and Tainer, 2003). In contrast to other subfamilies, the ABCE subfamily with the only member ABCE1 does not contain membrane spanning domains and is therefore unlikely involved in membrane transport (Kerr, 2004; Linton and Higgins, 1998). Other soluble ABC-ATPases are eEF3, Rad50 and ABC50. These ATPases are known to be involved in translation, DNA double strand repair and translation initiation, respectively (Andersen et al., 2006; Hopfner et al., 2000; Paytubi et al., 2009).

Based on the human homologue of ABCE1, PSI-BLAST analysis revealed that the ABCE subfamily is only present in eukaryotes and archaea with usually one homologue per species. No eubacterial homologues were detected (Kerr, 2004). ABCE1 has been shown to be essential in all organisms tested so far (Coelho et al., 2005; Estevez et al., 2004; Winzeler et al., 1999) and is obviously involved in several functions of cellular metabolism: Besides involvement in viral maturation (Klein et al., 2011; Lingappa et al., 2006; Zimmerman et al., 2002) and ribosomal biogenesis (Kispal et al., 2005; Yarunin et al., 2005) it recently became evident that ABCE1 plays an important role in translation regulation as well: *In vivo* and *in vitro* studies revealed that ABCE1 interacts with several initiation factors indicating an involvement in translation initiation (Andersen and Leevers, 2007; Chen et al., 2006; Dong et al., 2004). In addition, it was also shown that ABCE1 interacts with eRF1 and promotes recycling of post-termination complexes in eukaryotes (Khoshnevis et al., 2010; Pisarev et al., 2010). In follow-up experiments the involvement of ABCE1 in the mechanism of NGD was shown; in contrast to Hbs1 having only an auxiliary function, the data revealed that the eRF1 paralog Pelota together with ABCE1 are essential for the process of splitting (Pisareva et al., 2011).

Functional studies with mammalian components revealed that ribosome splitting by ABCE1 and Pelota depends on the length of the remaining nucleotides at the 3'-end of the mRNA (Pisareva et al., 2011): These findings emphasize the importance of an endonucleolytic cleavage of the mRNA in NGD before ribosome recycling can take place. It also suggests that Pelota and ABCE1

should be able to disassemble ribosomes stalled by truncated mRNA as well (Kobayashi et al., 2010).

Altogether, the biochemical data substantiate the important role of ABCE1 in several aspects of translation. But the question that remains is how exactly ABCE1 is able to impact all these processes. Structural data are required to shed light into the detailed interaction of ABCE1 with the ribosome and other factors. This information might help understanding the essential function of ABCE1.

1.2.5. Are there NGD factors in archaea?

Blast analysis, crystallography and biochemical studies have revealed that archaea possess homologues to factors involved in NGD. This indicates an evolutionary conserved mechanism that must have evolved after the separation of bacteria and before the domain separation of archaea and eukaryotes. The following homologues of factors involved in NGD have been identified in archaea:

Archaeal Pelota (aPelota) is app. 20% identical and 40% similar to yeast Dom34 (Davis and Engebrecht, 1998). Even though the homologues are structurally quite conserved there are notable differences. aPelota contains a negatively charged surface patch mimicking the moieties of the tRNA acceptor stem in the central domain which is absent in Dom34 (Kobayashi et al., 2010). This property might be the consequence of aPelota and tRNAs being delivered by only one factor in archaea whereas in eukaryotes a separate protein, Hbs1, is specialized for delivering only Pelota/Dom34: in eukaryotes Pelota/Dom34 is no longer required to mimic the surface charge of a tRNA (Kobayashi et al., 2010).
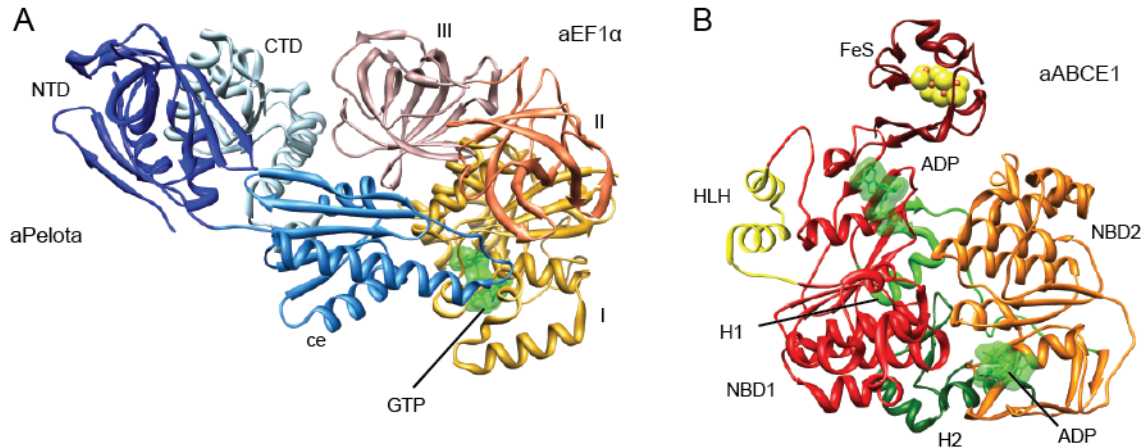
Figure 4: Crystal structures of archaeal homologues involved in NGD. (A) Crystal structure of the aPelota-aEF1α complex (Kobayashi et al., 2010): aPelota with N-terminal domain (NTD) in dark blue, central domain (ce) in blue, C-terminal domain (CTD) in light blue. aEF1α consists of domain I including the GTPase domain in gold, domain II in salmon and domain III in rosy-brown. GTP is highlighted in green. **(B)** Crystal structure of aABCE1 (Karcher et al., 2008): FeS domain in dark red with two iron-sulfur clusters in yellow-brown, nucleotide binding domain I (NBD1) in red with helix-loop-helix motif (HLH) in yellow, hinge regions H1 and H2 in green, nucleotide binding domain 2 (NBD2) in orange. ADPs are colored in green.

Notably, no Hbs1 homologue was identified in archaea. Recent studies suggested that the archaeal EF1α homologue (aEF1α) acts as a universal transporter for tRNA and A-site factors like aPelota and aRF1 (Kobayashi et al., 2010; Saito et al., 2010). A crystal structure of the aPelota-aEF1α complex revealed a similar interaction of the proteins as observed in the Dom34-Hbs1 crystal (Chen et al., 2010; Kobayashi et al., 2010). The CTD and central domain of aPelota or Dom34 are tightly packed against domain II and III of aEF1α or Hbs1, respectively (Fig. 4, A). In contrast to the yeast structure, the domain I of aEF1α is moved closer towards and the central domain of aPelota and also contacting it. The arrangement resembles the cryo-EM map of Dom34 and Hbs1 bound to the ribosome (Fig. 3, B) (Becker et al., 2011).

ABCE1 is highly conserved across the eukaryotic and archaeal domain. Archaeal ABCE1 (aABCE1) shares 45-50% sequence identity with eukaryotic homologues (Karcher et al., 2005). In 2007 the crystal structure of ABCE1 from *Pyrococcus abyssii* has been determined to 2.8 Å resolution (Fig. 4, B) (Karcher et al., 2008). ABCE1 contains two N-terminal iron-sulfur clusters of the $[4Fe-4S]^{2+}$ sub-type of ferredoxins and two nucleotide binding domains (NBDs) in a head to

tail conformation. The domains are separated by two hinge domains and a helix-loop-helix motif (HLH) that interrupts NBD 1. The orientation of the two NBDs allows ABC proteins to conduct a tweezer-like power stroke depending on the nucleotide-bound state (Rees et al., 2009). Recent studies have revealed that archaeal ABCE1 is also involved in recycling, similarly to its eukaryotic counterpart (Barthelme et al., 2011):

The presence of NGD factors and aABCE1 in archaea indicates the existence of an ancient mRNA surveillance mechanism. The challenging question is now how does NGD work in archaea and eukaryotes and what is the order of events that finally leads to ABCE1 induced recycling of the ribosomes.

1.3. Structural analysis of biological complexes

1.3.1. Solving structures of biologically relevant molecules

The structural analysis of biological molecules can be done using X-ray crystallography, nuclear magnetic resonance (NMR) spectroscopy or cryo-EM. Each of these methods has its advantages and disadvantages and can be used to address different aspects of a biological problem: NMR is suitable for the structural analysis of small molecules up to 100 kDa, but mg amounts of sample are needed and the sample preparation is quite laborious. Also in X-ray crystallography the amount of sample is comparatively high and the purity and stability of the protein is essential for generation of crystals. However, in contrast to NMR, the structures of large molecular assemblies, like ribosomes, can be solved.

Cryo-EM - on the other hand - requires only small amounts of sample (µg range) and the size of suitable biological complexes ranges from 150 kDa to several MDa. The major advantage of this technique is that complexes consisting of several components can be assessed in a nearly native environment and buffer system. The homogeneity of the sample is also important for cryo-EM, but the method allows later computational correction of eventual conformational or sample specific heterogeneity. The disadvantage of cryo-EM is the lacking resolution of atomic details compared to X-ray and NMR at least for asymmetric particles such as the ribosome.

To completely analyze and understand complex biochemical processes in the cell, it is advantageous to combine the information of all techniques: The maps obtained by cryo-EM provide a scaffold for docking molecular models based on existing X-ray or NMR structures. This way, a high fidelity interpretation of biochemical complexes can be done at a molecular level.

1.3.2. Cryo-EM and single-particle analysis

The sample for cryo-EM is transferred to a copper grid coated with a thin holey carbon film and subsequently flash frozen in liquid ethane (Adrian et al., 1984). The high cooling rate of more than 100.000 °C/s prevents the formation of ice crystals. With this method the molecules are randomly oriented and distributed across the grid. Data is collected on a nitrogen-cooled transmission electron microscope at low dose conditions around 20 $e^-/Å^2$ (Dubochet et al., 1983; Lepault et al., 1983) and digitized using a CCD camera. Utilizing different software programs, the particles on the micrographs are identified and their orientation is determined (Chen and Grigorieff, 2007; Frank et al., 1996). The information derived from the 2D-projections is then used to calculate 3D-reconstructions. Improvement of the resolution is achieved by iteratively realigning the particles to the newly obtained reconstruction and using this information for a corrected backprojection of the molecule. In the case of ribosomes, structures are available that allow reference-based alignment techniques like projection matching (Penczek et al., 1994).

The resolution in cryo-EM is directly dependent on the homogeneity of the sample and the number of particles. Since the signal to noise ratio of a single particle is quite low, averaging of thousands of perfectly aligned identical particles is required in order to achieve structural details at subnanometer resolution. Even under ideal conditions a certain degree of heterogeneity can be expected in the sample: Domains of a molecule can be found in different conformations; in the case of ribosomes the position of the small subunit in relation to the large subunit can differ. Other reasons for heterogeneity can be observed in complexes consisting of several components. Depending on the on- and off-rate of some components, the composition of the complexes will differ. It is also quite likely that the single components contain intrinsic conformational variability. The alignment is then based only on the largest invariable part of the particle and due to averaging, densities representing flexible parts of the structure will be comparatively weaker and less detailed (Penczek et al., 2006). The problem can be addressed by computational sorting of the dataset.

In this work sorting is performed semi-supervised. In contrast to refinement as described above, two or more references are offered for alignment. All particles are compared with these references and classified according to their cross-correlation value. After classification independent backprojections are generated for each sub-dataset and a new round of sorting is started. In every following round of sorting the backprojections obtained in the previous round are used as references. The sorting is halted, when the particle distribution becomes stable. The method allows sorting for conformational heterogeneity. The initial references have to be chosen carefully to avoid introduction of bias (Spahn and Penczek, 2009). The problem of bias introduction can be minimized by using a reconstruction obtained during an earlier round of refinement as additional reference. In the beginning the optimal cross-correlation and therefore the assignment of the particles to one sub-dataset might be based on random differences of the reference maps. In the following rounds substantial heterogeneities of the dataset will become apparent and finally lead to a stable assignment of particles to each sub-dataset.

Unlike in X-ray crystallography, there is no physically based resolution criterion available for cryo-EM. Therefore, the resolution of cryo-EM maps is determined as follows: The dataset is divided into two random half-sets and the independent reconstructions of each half-set are compared along shells in 3D Fourier space. The Fourier shell correlation (FSC) describes the degree of correlation between the two reconstructions as a function of spatial frequency in Fourier space. The cut-off value is set at 0.5 FSC which is equivalent to a signal to noise ratio of 1. Over the last years a steady improvement of the resolution of biological structures could be observed, whereas particles with high intrinsic symmetry like viruses (< 4 Å) are leading the way (Yu et al., 2011). So far the best resolution obtained for a ribosome is 5.5 Å (Armache et al., 2010a, b). Improving technical equipment and computational power might soon allow atomic detail also for asymmetric particles as the ribosome (Henderson, 2004).

2. Aims of the study

Several aspects of eukaryotic translation are highly conserved and can be found in a simplified version in archaea as well. The analysis of translation associated processes in archaea allows insights into the evolutionary conserved principle behind these mechanisms and provides a better understanding about later duplication and functional diversification of homologues in eukaryotes.

In first part of this PhD thesis an archaeal model shall be established to structurally analyze translation associated processes. This involves the establishment of an archaeal *in vitro* translation system suitable for the generation and purification of ribosome-nascent chain-complexes. These complexes are the prerequisite to address diverse translation associated questions.

In archaea homologues of factors involved in no-go decay have been identified and partially characterized. The no-go decay mechanism targets ribosomes that are stalled on the mRNA during translation and leads to ribosome recycling and degradation of the mRNA. Even though structural data has been obtained revealing the recognition step in the process of no-go decay, the exact mechanism of ribosome recycling is not yet understood. Especially the role of the highly conserved, essential ABC-type ATPase ABCE1 remains to be elucidated.

In the second part of this thesis the interplay of the archaeal no-go decay factors is functionally and structurally analyzed to gather further insight into the mechanism behind. In comparison with known structures from eukaryotes the question is addressed how no-go decay is happening in archaea and whether there is a conserved universal mRNA surveillance mechanism.

3. Material and Methods

All chemicals used for the experiments were obtained from Roth, Sigma-Aldrich, Merck, Invitrogen, VWR and Fluka except when stated otherwise.

3.1. General methods of molecular biology

3.1.1. Polymerase chain reaction

The polymerase chain reaction (PCR) was used for the amplification of specific double stranded DNA fragments. Except stated otherwise, the Phusion Flash High-Fidelity Master Mix (Finnzymes) was used according to the manufacturer's protocol. The concentrations of template and primers in the reaction were 0.2 - 1 ng/µl and 0.3 µM (each), respectively. Cycling conditions were chosen depending on the fragment length and primer composition.

The primers used in this work were synthesized by Metabion and are listed in Table 1. Depending on the application primers were designed accordingly: For cloning primers were used that introduced a restriction site at the 5'- and 3'-end of the fragment. This allowed directional ligation into plasmids adding a tag for detection or purification in frame. The name of the primer provides information about the construct and the respective restriction site. Primers specific for the plasmid backbone allowed the generation of a DNA template suitable for later T7 run-off transcription (see 2.4.5.) or colony PCR (see 2.2.6.) independent on the construct. Finally mutagenesis primers were used to alter an existing construct by inserting or deleting up to 20 oligonucleotides by site directed mutagenesis (see 2.3.1.).

Table 1: Primer

Name	Sequence (5'- 3')	Project
HisNac_for (BamHI)	CGC <u>GGA TCC</u> ATG ATG CCA ATG AAC CCA AAA CAG CTC	Generation of constructs for *in vitro* translation (see 3.3.1)
HisNac_rev (XhoI)	CCG <u>CTC GAG</u> CTA AGG AGA GCC TTC AGT AAG CTT TAG TAT CGC	
NacHis_for (PagI)	AAA A<u>TC ATG A</u>TG CCA ATG AAC CCA AA CAG CTC	
NacHis_rev (XhoI)	AAA A<u>CT CGA G</u>AG GAG AGC CTT CAG TAA GCT TTA GTA TC	
Nac_HA rev	CTA AGC GTA ATC TGG AAC ATC GTA TGG GTA AGG AGA GCC TTC AGT AAG CTT TAG TAT C	
RBS-E for (XbaI)	AAA G<u>TC TAG A</u>CG CAG ATT ACC GAA ATG AG	
RBS-E rev (NcoI)	TTT T<u>CC ATG G</u>AT GCC ACC TCA TTT CGG	
SecF100-his rev (XhoI)	TAT <u>CTC GAG</u> TCC ACT AAC GCT GGT	Generation of stalling constructs (see 3.3.1)
HASecF100-his for (NcoI)	AAA <u>CCA TGG</u> CCT ACC CAT ACG ATG TTC AGA TT	
His-muta_for	TCC AGA TTA CGC TCA CCA CCA CCA CCA CAA GGG TAA AAC TC	Site directed mutagenesis introducing His-tag (see 3.3.1)
His-muta_rev	GAG TTT TAC CCT TGT GGT GGT GGT GGT GGT GAG CGT AAT CTG GA	
Strep Muta blunt for	AGC GCG TGG AGC CAC CCG CAG TTC GAA AAG GGT AAA ACT CAA AAG CC	Site directed mutagenesis introducing Strep-tag (see 3.3.1)
Strep Muta blunt rev	AGC GTA ATC TGG AAC ATC G	
bMut	ACC TCC GCT CTT TTC GAA CTG CGG GTG GCT CCA	Site directed mutagenesis introducing multiple Strep-tags (see 3.3.1, Fig. 5)
HAStrep3SecF rev	CGC GCT TCC GCT TCC CTT TTC GAA CTG CG	
T7 for	TAA TAC GAC TCA CTA TAG G	Colony PCR, DNA template for transcription (see 3.1.5, 3.2.6)
T7 term_rev	TAT GCT AGT TAT TGC TCA G	Colony PCR (see 3.2.6)
aPel_for (NcoI)	AGTA<u>CCATGG</u>AGATACTCGAAGAAAAG	Cloning of aPIelota
aPel_rev (XhoI)	AAT T<u>CT CGA G</u>CT TCA CCC TGA AC	
aIF6+ for	AGG TTG TCG TTG AGG AGA GC	Cloning of aIF6
aIF6+ rev	GTA CCC TTG ACG CGG AAA AC	
aIF6_for (Nco)	TATA<u>CCATGG</u>ACATAGAGAGACTCG	
aIF6_rev (XhoI)	AAT T<u>CT CGA G</u>ACCAAGGAAGC	
aEF1α_for (BamHI)	ATG T<u>GG ATC C</u>AT GGC TAA GGA GA	Cloning of aEF1α
aEF1α_rev (HindIII)	TAT T<u>AA GCT T</u>CA GTC GGC GTT C	
aRF1_for (NcoI)	AGT A<u>CC ATG G</u>CT CAC AAG TCT G	Cloning of aRF1
aRF1_rev (XhoI)	AAT T<u>CT CGA G</u>CT GAA TCT TGT ACC T	

Underlined sequences indicate restriction sites specified in primer name

Cloning procedures involving the restriction site *Nco*I, lead to an alteration of the amino acid in the second position to glutamic acid in all constructs.

3.1.2. PCR purification

The obtained DNA fragment was purified with the QIAquick PCR purification Kit (Qiagen) according to the manufacturer's protocol and eluted in 40 µl EB buffer.

3.1.3. Enzymatic digestion of DNA

Purified PCR fragments and plasmids were digested with the appropriate restriction enzyme(s) (NEB) to linearize plasmids or to generate complementary ends for ligation. The primers listed in Table 1 (see 3.1.1.) specify the respective restriction enzyme. Digestion was performed according to the manufacturer's recommendations at 37°C for 2-5 h. Reactions were set up in a total volume of 50 µl with 2-5 µg DNA and 20 units of enzyme in the appropriate buffer. After digestion the sequences were purified as described in 3.1.2.

3.1.4. Ligation

Digested PCR fragments and plasmids were ligated with T4 DNA Ligase (Metabion) according to the manufacturer's protocol over night at 16°C. Reactions were set up in a total volume of 10 µl and included variable amounts of purified insert and backbone, 1 × reaction buffer and 1 µl T4 DNA Ligase.

3.1.5. T7 run-off transcription

RNA was generated by run-off transcription of linearized plasmids or PCR products containing a T7 promoter using T7 RNA polymerase purified by technicians. 2.5 µg DNA, ca 8 mM ATP, 8 mM CTP, 8 mM UTP, 8 mM GTP, 5 mM DTT, T7 buffer (40 mM Tris, pH 7.9, 2,5 mM spermidine, 26 mM $MgCl_2$, 0.01% (v/v) Triton X-100) and 4 µl T7 Polymerase were incubated at 37°C for 120 min. The RNA was precipitated with 0.8 M LiCl at -20°C for at least 2h. The RNA was pelleted using a pre-cooled Eppendorf Centrifuge 5417 R at 20.000 × g for 30 min. The pellet was washed with 1 ml 70% Ethanol and centrifuged again at 20.000 × g for 10 min. The supernatant was completely removed with a pipette and 20µl water was added immediately. The solubility of the pellet was improved by quickly heating the sample to 65°C for 1 min. RNA was stored at -20°C.

3.1.6. Agarose gel electrophoresis

The length and purity of DNA and RNA fragments was validated by agarose gel electrophoresis. Gels were prepared with 1.5 % agarose in TAE buffer (40 mM Tris/HCl pH 8.0, 20 mM acetic acid, 1 mM EDTA) and were run for 25 min at 130 V using the PerfectBlue Gelsystem Mini (Peqlab). Before the run DNA and RNA were mixed with 6 × Gel Loading Dye (NEB) and GelRed™ (Biotium) according to the manufacturer's recommendations. The gel was digitized at 300 nm using the Intas Gel Documentation System. The 100 bp and 1 kb DNA ladder Plus from NEB were used for size comparison.

3.1.7. Protein precipitation

Diluted protein solutions were precipitated to obtain smaller volumes suitable for SDS-PAGE (see 3.1.8.). The protein solution was diluted with H_2O to a final volume of 800 µl and then precipitated with 100 µl 72 % trichloroacetic acid and 100 µl 0.15 % sodium desoxycholate. The reaction was incubated at -20°C overnight. Then the protein was pelleted at 20.000 × g at 4°C for 40 min (Centrifuge 5417 R Eppendorf). The pellet was washed with 1 ml pre-cooled 100 % acetone, dried and finally suspended in 10 µl 1x sample buffer.

3.1.8. SDS-polyacrylamide gel electrophoresis

Proteins were separated by size using denaturing discontinuous SDS-polyacrylamide gel electrophoresis (SDS-PAGE) (Laemmli, 1970). Samples mixed with 4 × sample buffer (200 mM Tris/HCl pH 6.8, 8% (w/v) SDS, 0.4% (w/v) bromphenol blue, 40% (v/v) glycerol, 400 mM DTT) and loaded on a 15% polyacrylamide gel. Electrophoresis was performed at 230 V for 40 min in Mini-Protean II electrophoresis cells (Bio-Rad). The running buffer contained 25 mM Tris, 192 mM glycine and 0.1 % SDS.

3.1.9. Staining of protein gels

- Coomassie staining

After the electrophoresis the gel was fixed and stained using Coomassie Blue staining solution (0.25% (w/v) Coomassie Blue R 250, 50% (v/v) ethanol, 10% (v/v) acetic acid). Excess staining was removed by repeated washing steps with destain solution (40% (v/v) ethanol, 10% (v/v) acetic acid). The gel was digitized using a standard flat bed scanner.

- SYPRO® orange staining

If the estimated amount of protein was below 0.2 µg/band SDS-gels were stained with SYPRO® Orange (Sigma-Aldrich). After SDS-PAGE, the gel was quickly washed with H_2O and stained in 7.5 % acetic acid with 1:5000 SYPRO® Orange for 1 h in the dark. Excess stain was removed by one washing step with 7.5 % acetic acid (45 sec) and three further washings steps with H_2O (2 min each). Gels were digitized using a Typhoon 9400 scanner (Amersham) at 480 nm excitation wavelength and 580 nm emission filter.

3.1.10. Western blot

Western blotting and subsequent immunostaining allowed the qualitative identification of tagged proteins. After SDS-PAGE, proteins were blotted on nitrocellulose (strep-tagged proteins) or polyvinylidenfluoride membranes (GE Healthcare) using a standard semi-dry blotting apparatus (Bio-Rad) for 55 min at 60 mA per gel. The blotting buffer consisted of 20% (v/v) methanol, 48 mM Tris, 39 mM glycine and 0.037% (w/v) SDS. Successful protein transfer was validated by amido black staining (0.1% (w/v) Naphtol Blue Black, 7.5% (v/v) acetic acid, 20% (v/v) ethanol). The membrane was digitized and destained. The membranes were blocked for 1h at RT with 7.5 % milk in TBS buffer (20 mM Tris/HCl pH 7.6 and 150 mM NaCl) for HA-probe (F-7) mouse antibody (Santa Cruz Biotechnology) and His-tag monoclonal mouse antibody (Applied Biological Materials). Blocking was performed with 3% (w/v) BSA, 0.5% (v/v) Tween 20 in PBS buffer (4 mM KH_2PO_4, 1.6 mM Na_2HPO_4, 11.5 mM NaCl pH 7.4) for Strep-Tactin® HRP conjugate (IBA). αHA antibody was diluted 1:1000 in 3 % (w/v) BSA in TBS buffer, αHis antibody 1:2500 in 7.5 % milk in TBS buffer and incubated for 2 h RT or 4°C overnight with shaking. Excess primary antibody was removed by 3 washing steps with TBS buffer (3 × 10 min) and an additional 10 min washing step with TBS-T (TBS buffer, 0.1% Tween). The secondary antibody was goat anti-mouse IgG-HRP (Santa Cruz Biotechnology) and it was used 1:3000

diluted in 7.5 % milk in TBS (2h at RT). Membranes were then washed four times with TBS-T buffer to remove excess secondary antibody.

In the case of the Strep-Tactin antibody, the horse reddish peroxidase (HRP) was already coupled to the primary antibody. Membrane decoration and washing steps were done according to the manufacturer's protocol.

Signals were visualized using the Chemiluminescent Detection Kit (AppliChem) and fluorography films (Amersham Hyperfilm ECL, GE Healthcare) according to the manufacturers' protocols.

3.1.11. Concentration determination of nucleic acids and proteins in solution

Concentration of proteins, DNA and RNA molecules were determined by photometric measurements using the Nanodrop 1000 Spectrometer (Thermo Scientific). DNA and RNA were measured at A_{260} using the according settings. Proteins were measured at A_{280} and the concentration was calculated using the Protein Calculator software (http://www.mrc-lmb.cam.ac.uk/ms/methods/proteincalculator.html). The concentration of ribosomes was determined using the approximation that 1 A_{260} correlates with 23 pmol 70S ribosomes (Youngman and Green, 2005).

3.2.   Expression and purification of archaeal proteins in *E. coli*

3.2.1. Expression vector

The expression plasmids pET28a(+) (Novagen/Merck) and pET28-mod were used for all constructs. The first vector allows the expression of recombinant proteins with a C-terminal His-tag under the control of a T7 promoter. The second vector is a modified pET28a vector that allowed the expression of recombinant proteins with an N-terminal His-tag followed by a TEV cleavage site. This allows the removal of the His-tag after purification. The plasmids provide the resistance marker kan^r for kanamycine resistance.

3.2.2. *E. coli* strains

For amplification of the plasmids the *E. coli* XL1-blue strain with the genotype *recA1 endA1 gyrA96 thi-1 hsdR17 supE44 relA1 lac* [F′ *proAB lacI*qZΔM15 Tn*10* (Tetr)] (Stratagene) was used; for heterologous expression the *E. coli* Rosetta^{TM} (DE3) strain with the genotype F$^-$ *ompT hsdS*$_B$(r$_B^-$ m$_B^-$) *gal dcm* (DE3) pRARE (Cam^R) (Merck). This strain contains the additional plasmid pRARE which codes for rarely used tRNAs.

3.2.3. Media

E. coli cells were grown in liquid LB medium or on LB plates. LB medium consists of 10 g/l Bacto^{TM} Peptone (BD Bionutrients), 10 g/l NaCl, 5 g/l Bacto^{TM} Yeast Extract (BD Bionutrients) and in case of plates 15 g/l Bacto^{TM} Agar (BD Bionutrients). The medium was autoclaved at 121°C for 20 min. The appropriate antibiotic was added 1:1000 prior to use. The stock solutions for antibiotics were kanamycine 50 mg/ml (in H_2O) and chloramphenicol 34 mg/ml (in ethanol).

3.2.4. Preparation of competent cells

- Chemically competent cells

LB was inoculated 1:200 overnight culture and grown at 37°C until 0.6 OD_{600}. The culture was then cooled on ice for 15 min and the cells were harvested by centrifugation in sterile centrifuge beakers. The pellet was suspended in 0.1 M $CaCl_2$ and kept on ice for 30 min. The cells were pelleted again and finally resuspended in 0.1 M $CaCl_2$ + 15% glycerin. Aliquots of chemically competent cells were frozen in liquid nitrogen and kept at -80 °C.

- Electro-competent cells

Cells were grown and harvested as described above. In contrast to chemically competent cells, the cell pellet was washed four times with 100 ml ice cold H_2O. Then the pellet was washed two times with 10 ml 10% glycerol in H_2O. Finally the pellet was resupended in 10% glycerin. Aliquots were frozen in liquid nitrogen and kept at -80°C.

3.2.5. Transformation of *E. coli*

- Transformation of chemically competent cells

This method was used for retransformation of purified plasmids: 100 µl chemical competent cells were mixed with 40-100 ng purified plasmid DNA and incubated on ice for 20 min. After a heat shock at 42°C for 45 sec, the cells were kept on ice for additional 2 min. Then 1 ml LB was added and the cells were recovered at 37 °C for 45 min in a shaking incubator at 600 rpm (Thermomixer comfort, Eppendorf). 100- 200 µl transformed cells were plated on LB plates containing the appropriate antibiotics for overnight growth at 37°C.

- Electroporation

Electroporation was used to transform *E. coli* with newly circularized plasmids. 80 µl electro-competent cells were mixed with 1 µl ligation reaction in pre-cooled *E. coli* pulser cuvettes (Biorad) with 0.1 cm electrodes. Cells were then electroporated at 1.8 kV. Immediately after electroporation 1 ml LB was added and cells were recovered as described above. In contrast to transformation of chemically competent cells, the whole reaction was plated on one plate.

3.2.6. Colony PCR

The presence of a fragment in the plasmid was verified by colony PCR after transformation of the *E. coli* cells. Using a toothpick, single colonies were picked from the plated cells after overnight incubation and transferred into 0.2 ml tubes. A 20 µl PCR mastermix was added including the respective primers (see 3.1.1, Table 1). The plasmid DNA was released from the cells by an initial denaturation step at 95°C for 5 min. The Taq polymerase (prepared by lab technicians) was used as DNA polymerase for these reactions. The PCR was performed with T7 for and T7 term rev primers (see 3.1.1, Table 1). dNTPs were added at 0.25 mM final concentration. The 10x buffer contained 100 mM Tris/HCl pH 8.8, 500 mM KCl, 0.8% (v/v) Triton X-100, 15 mM $MgCl_2$. Only colonies yielding in DNA fragments with the expected length were further considered for sequencing.

3.2.7. Isolation of plasmids and sequencing

Single colonies were selected based on the result of the colony PCR (2.2.6) and inoculated in 5-10 ml LB containing the appropriate antibiotic at 37 °C over night. The next day the DNA was

isolated using the QIAprep®Spin Miniprep Kit (Qiagen) according to the manufacturer's protocol. 1.5 µg purified plasmid was sent for sequencing to Eurofins MWG.

3.2.8. Protein expression

6 l LB containing the appropriate antibiotics were inoculated with 1/200 overnight culture and incubated at 37°C with shaking (New Brunswick Scientific Co., New Jersey). Expression was induced with 1 mM IPTG at 0.6 - 0.7 OD_{600} for 2 h at 37°C. Cells were harvested and once washed with 200 ml pre-cooled Buffer A (50 mM Tris/HCl pH 8.0, 500 mM NaCl, 1 mM DTT). Finally the cells were suspended in 50 ml Buffer A, frozen in liquid nitrogen and kept at -80°C.

3.2.9. Protein purification

Frozen cells from protein expression were thawed at room temperature and 6 µg/ml DNAseI, 0.1 mM PMSF (in ethanol) and a Complete Protease Inhibitor Cocktail tablet (Roche) were added. The cells were mechanically disrupted using a microfluidizer (Microfluidics) at 15,000 psi for three rounds. The cell lysate was cleared in a subsequent centrifugation (SS34, Sorvall, 13.000 rpm, 15 min, 4°C) and ultracentrifugation step (70Ti, Beckmann Coulter, 30.000 rpm, 30 min, 4°C).

Soluble expressed protein was then purified by affinity chromatography using 1 ml HisTrap HP columns (GE Healthcare) in an Äkta system using Buffer A (see 3.2.8.). The protein was bound in the presence of 20 mM imidazole to reduce background binding. Elution was performed with a 15 ml gradient from 20 – 500 mM imidazole and 0.5 ml fractions were collected. These fractions were analyzed by SDS-PAGE and fractions with high amount of the desired protein were pooled.

Protein expressed in inclusion bodies was resuspended in 50 mM Tris/HCl pH 8.0, 2 M NaCl, 0.5 % Triton, 0.5 % CHAPS, 8 M Urea. Insoluble particles were removed by centrifugation (SS34, Sorvall, 13.000 rpm, 20 min). The protein was purified via 3 ml Ni-NTA Agarose (Qiagen). Four washing steps (4 × 5 ml) were done with 7 M Urea, 20 mM Tris/HCl, 200 mM NaCl at pH 8.0 and two washing steps (2 × 5 ml) at pH 6.3. The protein was then refolded on the column by gradually changing the buffer over 30 ml to 50 mM Tris/HCl pH 8 and 500 mM NaCl. The protein was eluted with 500 mM imidazole in Buffer A.

Remaining imidazole was removed by dialysis against Buffer A or by buffer exchange using Amicon Ultra Centrifugal Filter Units (Milipore). If the protein was expressed with a cleavable His-tag, the tag was removed with TEV protease over night at 4°C in a buffer containing 50 mM Tris/HCl pH 8.0, 200 mM NaCl, 1 mM DTT, 1 mM EDTA. His-tagged TEV protease and cleaved His-tags were then removed by subsequently affinity chromatography using Ni-NTA Agarose. The flow through contained the purified protein in Buffer A.

In case of strong contaminations by *E. coli* proteins a heat denaturation step was performed at 55°C for 10 min. Finally the protein was concentrated, frozen in liquid nitrogen and kept at -80°C.

3.2.10. Reconstitution of the ABCE1 [4Fe-4S]$^{2+}$ cluster

The FeS cluster of aABCE1 from *P. furiosus* was reconstituted as described previously using an anaerobic glove box (Coy laboratory) (Karcher et al., 2008). The protein was kept under nitrogen atmosphere and frozen in liquid nitrogen. To minimize oxidation damage, the aliquots were double-bagged for storage at -80°C.

3.3. *In vitro* translation and functional tests in archaea

3.3.1. Generation of DNA templates

The respective sequence was amplified by PCR and cloned into the standard expression vector. The bacterial ribosomal binding site (RBS) was exchanged against an archaeal RBS of the glutamate dehydrogenase gene derived from published data (Rahman et al., 1998). The change of the 5' UTR reads as follows: 5'-<u>AAG GAG</u> ATA TAC C**AT G**-3' → 5'-TGA GGT GGT ATA C**AT G**-3'. The bacterial RBS is underlined and the start codon is marked. The sequence was further modified by introduction of various tags at the N-terminus of the coding sequence via site-directed mutagenesis following the protocol of the QuickChange II XL Site Directed Mutageneis Kit (Invitrogen) or the Phusion Site-Directed Mutagenesis Kit. Differing from the QuickChange protocol, Phusion High-Fidelity DNA Polymerase (Finnzymes) was used and cycling temperatures were adapted accordingly. The PCR product of 50 µl reaction was digested with *Dpn*I and used for chemical transformation in *E. coli*.
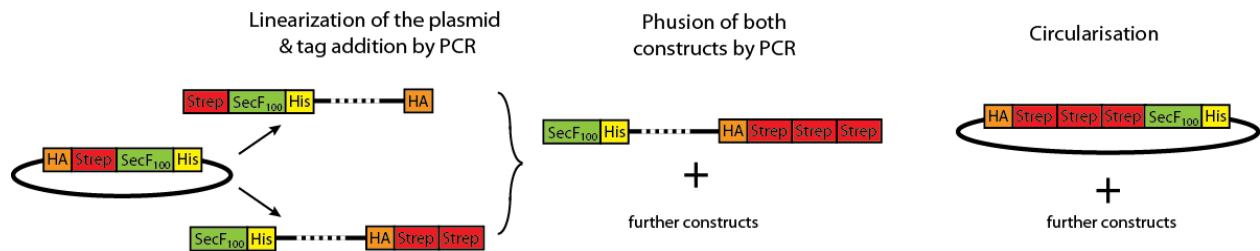
Figure 5: Generation of a multiple Strep-tagged construct using PCR.

For the synthesis of the multiple Strep-tagged constructs a different approach was used (Fig. 5). The plasmid template was linearized in a PCR using primers that included the coding sequences of additional tags at the 5'- or 3'-end of the product. Both products were mixed and used as template for a PCR without primers. This way several linear constructs ranging from one to

three Strep-tags in a row should be generated. The products were then circularized by blunt-end ligation and transformed into chemical competent *E. coli*.

The resulting constructs were validated by sequencing. Primers for mutagenesis are listed in Table 1 (see 3.1.1.).

3.3.2. Generation of translating cell extracts

Frozen cells of early log-phase *Thermococcus kodakarensis* cells were kindly provided by Prof. Michael Thomm (Universität Regensburg). The preparation of translating extracts was derived from published protocols (Endoh et al., 2007; Endoh et al., 2006). Frozen cells were mixed with 1.4 × excess of S30 buffer (10 mM Tris/HOAc pH 7.4, 14 mM Mg(OAc)$_2$, 60 mM KOAc, 1 mM DTT) under liquid nitrogen. Pre-cooled mortar and pestle were used to break the cells and homogenate the mixture under liquid nitrogen. The homogenate was quickly thawed at room temperature and insoluble cell debris was removed by centrifugation using a RP80AT rotor (Sorvall) for 20 min at 30.000 rpm and 20 min at 35.000 rpm. Aliquots were frozen in liquid nitrogen and kept at -80°C.

3.3.3. *In vitro* translation

Based on published data (Endoh et al., 2007; Endoh et al., 2006) a protocol was established for *in vitro* translation. The reaction contained 60% crude cell extract, 80 µM (each) amino acid mix, 3% RNAsin (Ambion), 0.2 µg/µl RNA, 3 mM ATP, 1 mM (each) GTP-UTP-CTP mix, 56 mM Tris/HOAc pH 8.0, 260 mM KOAc, 80 mM NH$_4$OAc, 3 mM EDTA, 0.2 mg/ml spermidine, 0.1 mg/ml tRNA, 0.2% PEG 8000. The reaction was incubated at 65°C using a MJ Minicycler with

heated lid for 20-60 min. For programming ribosomes, truncated mRNA was provided in the reaction. Translation was stopped on ice after 20 min.

3.3.4. Purification strategies of ribosome nascent chain complexes

- His-tag based affinity purification

The protocol for purification of ribosome nascent chain complexes (RNC) via Talon metal affinity resin (Clontech) was derived from the protocol for purification of wheat germ RNCs and modified accordingly (Halic et al., 2004). After translation, the ribosomes are pelleted through 600µl high salt sucrose cushion (105.000 rpm, 60 min, 4°C, RP120AT, Sorvall). The high salt sucrose cushion contained 10 mM Tris/HCl pH 7.0, 60 mM KOAc, 500 mM NH_4OAc, 14 mM $Mg(OAc)_2$, 1 M Sucrose, 10 mM DTT, 0.1 % Nikkol and 0.1% Complete Protease Inhibitor Cocktail (Roche). The ribosomes were resupended in Buffer 250 and bound to 750 µl Co^{2+}-matrix (Talon, Invitrogen). Buffer 250 was changed according to the salt concentration observed in the extract and no cycloheximide was added (56 mM Tris/HOAc pH 7.0, 250 mM KOAc, 80 mM NH_4OAc, 10 mM $Mg(OAc)_2$, 250 mM sucrose, 2.1% Nikkol, 0.1 % Complete Protease Inhibitor Cocktail (Roche), 5 mM β-mercaptoethanol). Eight washing steps were performed with 7 × 1 ml Buffer 250 and 1 × 1 ml Buffer 500. The composition of Buffer 500 was essentially the same as the 250 Buffer, except that the KOAc concentration was reduced to 60 mM and the NH_4OAc concentration was raised to 450 mM. Elution was done with Buffer 250 containing 100 mM imidazole. The RNCs were subsequently pelleted through a high salt sucrose cushion and resuspended in Grid buffer (20 mM Tris/HOAc pH 7, 100 mM KOAc, 10 mM $Mg(OAc)_2$, 1 mM DTT, 125 mM Sucrose, 0.05% Complete Protease Inhibitor Cocktail (Roche), 0.2 U/µl RNAsin (Ambion)). From all steps aliquots (1/100) were collected for later SDS-PAGE and western blot analysis.

The protocol was modified for the usage of Co^{2+}-coated magnetic beads (Dynabeads Talon, Invitrogen). The composition of Buffer 250 was identical and Buffer 500 differed from Buffer 250 by 250 mM KOAc and 250 mM NH_4OAc. Elution was done with 400 mM imidazole in Buffer 250. After centrifugation through a sucrose cushion, the ribosomes were resuspended in Buffer 250. 30 µl Dynabeads were equilibrated with Buffer 250 and unspecific binding was saturated with an excess of tRNA. The programmed ribosomes were bound to the beads at 18°C for 20 min with shaking. The flow through was removed and four low salt (4 × 300 µl) and two high salt (2 × 300 µl) washing steps were performed. Elution was done at 18°C for 20 min with shaking. 1/100 of all fractions was collected and used for later SDS-PAGE and western blot analysis.

- Strep-tag based affinity purification

RNCs based on constructs with Strep-tags were purified as follows: After translation the reaction was pelleted through a sucrose cushion as described above. The pellet was resuspended in Binding Buffer (56 mM Tris/HOAc pH 7.0, 100 mM KOAc, 180 NH4OAc, 10 mM Mg(OAc)2, 250 mM sucrose, 0.1% Nikkol, 0.1% Protease Inhibitor Cocktail (Roche), 5 mM DTT. 100 µl Strep-Tactin Superflow (IBA) was equilibrated with 3 ml Binding Buffer. Programmed ribosomes were bound to the matrix at 15°C for 60 min with shaking. The flow through was removed and eight washing steps (8 × 500 µl) were performed with Binding Buffer. The sample was eluted with Binding Buffer containing 2.5 mM d-Desthiobiotin. The elution was applied on a sucrose cushion and pelleted as described before. The RNCs were resuspended in Grid Buffer. 1/100 of all fractions was collected and used for later SDS-PAGE and western blot analysis.

The protocol was modified for the usage of Strep-Tactin Magnetic Beads (Qiagen). After translation 30 µl beads were equilibrated with Binding Buffer and directly added to the reaction. Binding was performed at 20°C for 20 min with shaking. Four washing steps (4 × 200 µl) with Binding Buffer were performed. Elution was done at 20°C for 10 min with shaking. 1/100 of all fractions was collected and used for later SDS-PAGE and western blot analysis.

3.3.5. Purification of ribosomes

Ribosomes were purified from frozen *P. furiosus/T. kodakarensis* cells, courtesy of Prof. M. Thomm (Universität Regensburg). Cell pellets were suspended in 1.3 × volume S30 buffer (10 mM Tris/HOAc pH 7.4, 60 mM KOAc, 14 mM $Mg(Cl)_2$) over night at 4°C. The homogenous lysate was disrupted with a microfluidizer (Microfluidics). Cell debris was removed by centrifugation at 14.000 rpm at 4°C (Centrifuge 5417 R, Eppendorf). The supernatant was decanted and ribosomes pelleted through a high salt sucrose cushion (1 M Sucrose, 500 mM NH_4OAc, S30 buffer) at 80.000 rpm (RP80AT, Sorvall) for 60 min. The ribosomal pellet was suspended in buffer TrB25 (56 mM Tris/HCl pH 8.2, 250 mM KOAc, 80 mM NH_4OAc, 25 mM $Mg(Cl)_2$, 1 mM DTT). The ribosomes were then gradient purified (10 – 40 % sucrose, 10 mM Tris/HOAc pH 7.4, 60 mM KOAc, 14 mM $Mg(Cl)_2$) at 19.000 rpm (SW40, Beckmann Coulter) for 16h at 4°C. Fractions were collected using a Gradient Station (Biocomp) with an Econo UV Monitor (Biorad) and a FC203B Fraction Collector (Gilson). Fractions containing 70S ribosomes were washed with S30 buffer and concentrated using a 100 kDa Amicon Ultra Centrifugal Filter Unit (Millipore). S30 and TrB25 buffer are based on published data (Endoh et al., 2008; Endoh et al., 2006). TrB25 was derived from the translation buffer.

3.3.6. Reconstitution of 70S-ligand complexes

Archaeal ribosomal complexes were reconstituted in buffer TrB50 (56 mM Tris/HOAc pH 8.2, 250 mM KOAc, 80 mM NH_4OAc, 50 mM $Mg(Cl)_2$, 1 mM DTT) with 2mM ADPNP. Ligands were added in 5-10 × excess and incubated for 25 min at 30°C. In case of ABCE1 reconstitution was performed under anaerobic conditions (glove box, Coy Laboratories) in degassed buffers.

Complexes designated for electron microscopy were diluted to 4.0 A_{260} and kept at RT under anaerobic conditions until vitrification.

In the case of ligand binding assays the reactions (20 μl) were applied on 150 μl 1 M sucrose cushion and centrifuged for 45 min at 70.000 rpm in a TLA100 rotor (Beckmann Coulter). Immediately afterwards, the upper 50 μl of the reaction were collected as supernatant, 100 μl were discarded and the remaining 20 μl were collected as pellet fraction. The fractions were precipitated (see 2.1.7.) and analyzed by SDS-PAGE (see 2.1.8.).

3.3.7. Splitting of 70S ribosomes

15 pmol ribosomes *(T. kodakarensis)* were incubated with 2.5 × excess of ligands under anaerobic conditions in Buffer TrB25. ATP was added to a final concentration of 2 mM. The reaction was incubated for 25 min at 25°C. Splitting of the ribosomes was evaluated by separation on a 15 - 40 % sucrose gradient (56 mM Tris/HOAc pH 8.2, 250 mM KOAc, 80 mM NH$_4$OAc, 50 mM Mg(Cl)$_2$, 1 mM DTT), at 40.000 rpm (SW-60, Beckmann Coulter) for 3 h at 4°C. The gradients were analyzed using a Gradient Station (Biocomp) with an Econo UV Monitor (Biorad) and a FC203B Fraction Collector (Gilson). Splitting efficiency was evaluated by height comparison of 30S, 50S and 70S peaks.

3.4.   Cryo-electron microscopy and computational analysis

3.4.1. Cryo-electron microscopy

Freshly prepared sample was applied to 2 nm pre-coated Quantifoil R3/3 holey carbon supported grids and vitrified using a Vitrobot Mark IV (FEI Company).

The 70S-aABCE1-aPelota sample was visualized on a Titan Krios TEM (FEI Company) at 200 keV under low dose conditions (20 e$^-$/Å^2) at a nominal magnification of 75,000 ×. Data was collected on a TemCam F416 camera (4096 x 4096 pixel, 15.6 μm pixel size, 1 sec/full frame, TVIPS GmbH) leading to a final magnification of 148,721 × at the plane of the CCD camera resulting in a image pixel size of 1.049 Å (object scale). The nominal defocus was set between -1 μm and -3.5 μm. The 70S-aEF1α-aPelota sample was visualized at 300 keV and data was collected using a Eagle 4k × 4k CCD camera (4096 x 4096 pixel, 15 μm pixel, 5 sec/full frame, FEI Company) leading to a final magnification of 128,200 × at the plane of CCD resulting in a image pixel size of 1.119 Å (object scale).

Data collection was done semi-automatically using the software EM-TOOLS (TVIPS). After manual selection of appropriate grid meshes and holes, the acquisition run automatically performed re-centering, drift and focus correction before the final spot scan series were taken. EM-TOOLS also corrected automatically long-term TEM instabilities like beam shift, astigmatism and coma.

3.4.2. Single particle reconstructions

Preprocessing the dataset comprises several semi-automated steps using scripts based on the SPIDER software package (Frank et al., 1996): Firstly, micrographs were converted into spider readable files and the contrast transfer function (CTF) was determined using the SPIDER 'TF ED'

command. Visual inspection of power spectra and micrographs was done using JWEB (http://www.wadsworth.org/spider_doc/web/docs/jweb.html). Micrographs showing serious ice contamination or the focus outside the holes were omitted. Also micrographs with high drift or astigmatism were excluded from the dataset. Also a third qualification was done by omitting all micrographs with defocus values below -1 µm or above -4 µm. Coordinates of particles were automatically determined with a modified version of SIGNATURE (Chen and Grigorieff, 2007) using a eukaryotic ribosome as reference. Based on the coordinates the particles were windowed out from each micrograph. The automated learning based algorithm MAPPOS (URL: http://arxiv.org/a/tresch_a_1) was used for classification of ribosomal and non-ribosomal particles like contaminations, noise or carbon edges. The program was trained with manually selected good and non-particles. The remaining ribosomal particles were initially aligned using cross-correlation based projection matching technique with an angular accuracy of 15° (83 reference projections). The initial reference was obtained form an archaeal ribosome. The alignment assigns translational shifts and Euler's angles to every particle of every image.

The organization of the dataset was changed from micrograph-based to defocus-based for refinement. 1500 to 2000 particles from 1500 to 2000 micrographs with similar defocus were merged into one defocus group. This allowed a faster performance of the refinement on the high performance Intel/Opteron computer cluster. In each refinement round all particles were aligned against the volume generated in the previous round. For the first round of refinement the initial reference was used. The input volume was masked and filtered considering the improving resolution of the structure. Independent reconstructions for each defocus group based on the angle and shift values obtained in the alignment were calculated. Then the defocus-dependent reconstructions were CTF-corrected and combined into a single volume. The resolution was calculated by comparing independent reconstructions of all even and odd particles in each defocus group. The Fourier shell correlation (FSC) was calculated and a cut-off at 0.5 FSC indicated the resolution.

Offering up to four slightly distinct reference volumes during the refinement, the particles were separated according to their best cross correlation with one of these references. Based on the

particles assigned to each reference the backprojections were done separately and used as references for the next round of sorting. This was done iteratively until the number of particles in each sub-dataset was steadily assigned. Since only the initial references were provided, the sorting was done semi-supervised minimizing the chance of introducing artifacts.

3.4.3. Modeling and fitting

A homology model for aPelota was generated using the programs HHPRED (Soding et al., 2005) and MODELLER (Eswar et al., 2008) based on the crystal structure of *Aeropyrnum perinx* (Kobayashi et al., 2010) aPelota (PDB-ID 3AGJ). The model for aABCE1 is based on the crystal structure from *P. abyssii* aABCE1 (PDB-ID 3BK7) (Karcher et al., 2008). A model of the *P. furiosus* ribosome was built by J.P. Armache and A. M. Anger as described before (Armache et al., 2010a, b).

Initial rigid body fitting was done using Chimera (Pettersen et al., 2004). The initial models were refined using the programs DireX (Schroder et al., 2007) and the molecular dynamics flexible fitting (MDFF) method (Phillips et al., 2005; Trabuco et al., 2008).

3.4.4. Simulations

Simulations of transitions between different conformational states were done using the Morph Conformations function in Chimera (Pettersen et al., 2004).

4. Results

4.1. *In vitro* programming of archaeal ribosomes

The establishment of an *in vitro* translation system and programming of archaeal ribosomes is the first step for later structural analysis of translation associated processes. RNCs programmed with different mRNAs are a versatile starting point for multiple analyses with possible interaction partners involved in NGD or also archaeal protein targeting and translocation intermediates.

4.1.1. *In vitro* translation

The template for *in vitro* translation and stalling of ribosomes was derived from the coding sequence of SecF (*T. kodakarensis*). SecF is a membrane protein and contains a potential signal anchor sequence at the N-terminus with the membrane spanning helix reaching from position 37 to 52 (SignalP 3.0 Server) (Emanuelsson et al., 2007). Using only the coding sequence of the first 100 amino acids for *in vitro* translation, the signal anchor is supposed to be completely emerged from the ribosomal peptide exit tunnel. Since nothing is known about stalling mechanisms in archaea so far, truncated mRNA that has been successfully applied for RNC generation and purification from bacteria (Frauenfeld et al., 2011) and eukaryotes (Beckmann et al., 2001) was chosen.

In vitro translation was established using C- or N-terminally tagged reporter constructs including a stop codon based on the coding sequences of the archaeal NAC and SecF proteins. Translation efficiency was sufficient to detect the product with tag-specific antibodies (Fig. 6, A). Interestingly, a construct with an N-terminal His-tag was not translated at all. Even with more sensitive detection methods (Met-^{35}S) no product was observable (data not shown). In contrast, an N-terminal HA-tag was translated; also an N-terminal HA-tag followed by a His-tag

was translated successfully. Several combinations of HA-tags and Strep-tags have also been tested. Multiple Strep-tags lead to a reduction of translation efficiency. Only up to three Strep-tags in a row can be translated, but the efficiency was comparably low. A construct with six Strep-tags was no longer translated. Besides the archaeal RBS, the bacterial RBS used in commercially available expression plasmids was also suitable for *in vitro* translation. Based on the western blot signal, the translation of truncated mRNA seemed to be equally efficient to mRNA with stop codon. No signal is observable on the western blot in the absence of mRNA (Fig. 6, A).

4.1.2. Programming archaeal ribosomes with truncated mRNA

Ribosomes have been programmed successfully with truncated mRNA based on the coding sequence of SecF. Tag-specific antibodies revealed several specific signals (Fig. 6, B). At 12 kDa a strong signal represents the free peptide. Around 30 kDa a weaker signal corresponds to the peptidyl-tRNA. The relatively high amount of free peptide can be a consequence of specific enzymatic activity of the extract or a result of the basic pH during translation. For optimal translation, the pH was set at 8.2. In this basic environment the peptide chain can be easily hydrolyzed. Basic hydrolysis of the nascent chain can also occur during the run of the SDS-PAGE. Additional signals could be seen on the blot besides the expected products. A smear was visible above the signal of the peptidyl-tRNA in the range of 35-70 kDa. There was also a distinct band visible running approximately 2-3 kDa above the free peptide.
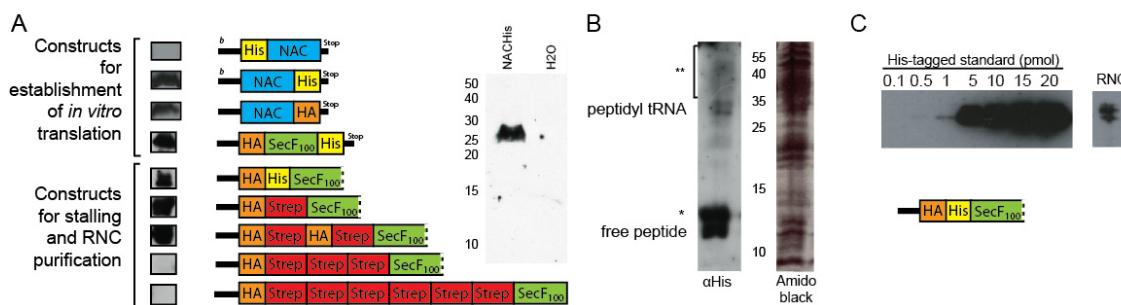
Figure 6: Constructs used for *in vitro* translation and programming of ribosomes. (A) Translation of each construct was validated with a western blot using αHis- or αHA-antibodies. *b* indicates bacterial RBS. Dashed line at the end of the construct indicates truncated mRNA. No background was observable in the negative control without mRNA. **(B)** Stalling of ribosomes with truncated HAHisSecF100 mRNA. The western blot signal and the corresponding amido black staining of the membrane are shown. * indicates 2-3 kDa modification of the free peptide, ** indicates higher molecular weight translation products probably derived from peptidyl-tRNA **(C)** Estimation of programming efficiency by comparison of the peptidyl-tRNA signal derived from a known amount of programmed ribosomes with a His-tagged protein standard on a western blot.

4.1.3. Programming efficiency

To analyze the programming efficiency, *in vitro* translation has been performed using truncated HAHisSecF100 mRNA as template. The reaction was pelleted through a sucrose cushion and resuspended in buffer. The concentration of ribosomes was determined and the amount was calculated using the approximation 1 A_{260} = 23 pmol. The whole sample was now analyzed by SDS-PAGE and Western blot using α-His antibodies. As a reference, a His-tagged protein of known concentration was loaded on the gel ranging from 0.1-20 pmol. Visual inspection revealed a comparable intensity of the translation product between the 1 and 5 pmol protein standards (Fig. 6, C). Comparing the result with the amount of ribosomes in the sample (13.5 pmol) approximately 10-20% of the ribosomes are programmed.

4.1.4. The influence of sparsomycin on translation

Sparsomycin is known to inhibit translation in bacteria and eukaryotes. It binds to the large ribosomal subunit close to the peptidyl-transferase center (PTC) and interacts with the highly conserved base A2602 (*E. coli* numbering, A2717 in *P. furiosus*). This affects the correct positioning of the A-site and P-site tRNAs (Bashan et al., 2003a; Bashan et al., 2003b). In the archaeal *in vitro* translation system, sparsomycin was tested as stabilizer of the peptidyl-tRNA. In the eukaryotic translation systems cycloheximide is added after translation to stabilize the peptidyl-tRNA on the ribosome (Halic et al., 2004). Cycloheximide inhibits the movement of the mRNA and tRNA through the intersubunit space into the E site of the ribosome and thereby translocation.

Interestingly, the addition of sparsomycin before translation reaction did not lead to a translation arrest. In contrast, the signals of peptidyl-tRNA and hydrolyzed peptide obtained by western blot became more defined compared with a negative control. As shown in Fig. 7 increasing amounts of sparsomycin reduced the amount of side products. The higher molecular weight smear and the band running 2-3 kDa above the hydrolyzed peptide were sensitive to sparsomycin addition. Even though the total amount of signal was less then observed in the negative control, the ratio of peptidyl-tRNA signal to other signals was greatly improved.
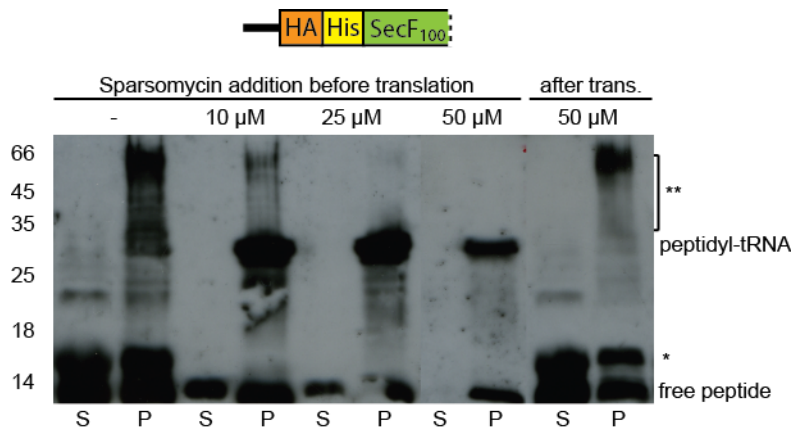
Figure 7: The influence of sparsomycin on *in vitro* translation. Sparsomycin was added before and after *in vitro* translation in increasing amounts. * indicates 2-3 kDa modified free peptide, ** indicates higher molecular weight translation products. S supernatant and P pellet fraction after centrifugation through a sucrose cushion. The addition of sparsomycin led to a reduction of the observed modifications of peptidyl-tRNA and free peptide. αHis-antibodies were used for detection.

No positive effect of sparsomycin regarding the stability of the peptidyl-tRNA ester bond could be detected when added after translation. In contrast, the peptidyl-tRNA signal at the expected size of 30 kDa vanished almost completely and a band at the size of approximately 60 kDa previously hidden in smear emerged.

Unfortunately the experimental results could not be repeated with new extract based on a different charge of cells. It can't be excluded that more factors like protein concentration, growth phase of the cells influence the impact of sparsomycin on *in vitro* translation. In all further experiments sparsomycin inhibited translation already at 5 µM.

4.1.5. Purification attempts of RNCs

Ribosomes were programmed using truncated mRNAs with an N-terminal HA-tag for detection followed by His- or Strep-tags for purification. After translation, the ribosomes were pelleted through a sucrose cushion. After resuspension of the ribosomes, the reaction was incubated on column material. Several column materials and tags have been tested under different buffer conditions and results are described below. Except stated otherwise all buffers had pH 7.0.

The construct HAHisSecF100 was used for trials involving His-tag affinity purification (Fig. 8). The procedure was derived from the published protocol for purification of wheat germ RNCs (Halic et al., 2004). The first purification step consisted of pelleting the ribosomes through a high salt sucrose cushion (see 3.3.4.). Interestingly, after pelleting approximately half of the signal for peptidyl-tRNA could be found in the supernatant (Fig. 8, A: lane SN1). It is possible that this was caused by insufficient centrifugation time or speed, but the ribosomal protein pattern on the stained membrane could only be seen in the pellet fraction (Fig. 8, A: lane R). In comparison, in the 14-25 kDa area where the majority of all the ribosomal proteins are running on SDS-PAGE, only few bands were detectable in the supernatant (Fig. 8, A: lane SN1). The ribosomes in the pellet fraction were then resuspended and bound to Talon metal affinity resin (Co^{2+}-resin). Some unbound hydrolyzed peptide could be found in the flow through (Fig. 8, A: lane FT) and in the first washing step (Fig. 8, A: lane W1). Nothing was eluted from the column in the high salt wash (Fig. 8, A: lane W2). Surprisingly no signal is detectable during the final purification steps: After the final pelleting step, no signal could be seen neither in the supernatant (Fig. 8, A: lane SN2) nor the pellet (Fig. 8, A: lane RNC). The amido black staining of the membrane revealed that there are some minor amounts of ribosomes in the final pellet fraction. However, since there are no western blot signals from the peptide chain visible, these bands might belong to ribosomes that bound unspecific to the Talon material.

It could not be excluded that the Talon-matrix interacted with the nascent chain or the ribosomes and prevented elution. Therefore Dynabeads Talon (Co^{2+}-coated magnetic beads) were tested using comparable buffer conditions. The usage of magnetic beads allowed the usage of smaller volumes and faster handling of the sample: In correspondence to the initial experiment, the ribosomes were pelleted through a sucrose cushion after translation. In the experiment shown in Fig. 8, B, only signal for hydrolyzed peptide could be found in the supernatant. Comparable signal intensities for ribosome-bound and hydrolyzed peptide were obtained before and after pelleting. Ribosomes were resuspended and bound to Dynabeads. In the unbound fraction (Fig. 8, B: lane FT), some ribosome-nascent chain complexes could be detected, but the majority seemed to bind to the matrix. Despite the observed binding to the Dynabeads, no western blot signals could be detected neither in the wash nor the elution

fractions. To exclude the possibility that the RNCs remained bound to the Dynabeads, a second elution step was performed using an excess of EDTA. Subsequently, the Co^{2+}-ions were released from the matrix and protein binding was abolished. No signal was obtained in this fraction as well. Finally the beads were boiled at 95°C in 1x sample buffer to release everything that remained bound to the beads by Co^{2+}-independent interactions. Again this elution steps did not reveal any protein signal on the blot. There were also no additional bands visible on the stained membrane. Compared to the amount of signal found in the pellet fraction (Fig. 8, B: lane R), a substantial amount of the synthesized peptide is missing.

Figure 8: Affinity purification attempts of RNCs using His-tag. 1/100 of all reactions were analyzed by SDS-PAGE and western blot. **(A)** Purification attempt using a Co^{2+} resin: T translation reaction, SN1 supernatant 1, R pelleted ribosomes, FT flow through, W1 and W2 wash steps, SN2 supernatant 2, RNC fraction with ribosome nascent chain complexes. No RNCs were obtained. **(B)** Purification attempt using Co^{2+}-coated magnetic beads: SN supernatant, E elution, EDTA elution with EDTA, B beads boiled in sample buffer. No RNCs could be obtained. **(C)** Purification scheme of released peptides after treatment with puromycin: The released peptide could be purified.

To exclude the possibility that the buffer composition or the biochemical behavior of the peptide chain was incompatible with the purification procedure, the purification of released peptide was tested (Fig. 8, C). The flow through fraction from a purification attempt with

Dynabeads that contained free peptide and RNCs was incubated with 1.5 mM Puromycin to release the remaining nascent peptide chain. The reaction was then mixed with Dynabeads and the pH adjusted to 8.0. The pH was optimized for binding according the manufacturer's protocol. The reaction was washed three times and finally eluted. The western blot revealed a strong signal for the released peptide in the elution fraction. Only minor amounts remained bound to the beads (Fig. 8, C: lane B).

These results attest that the construct is able to bind to Dynabeads Talon. But somehow the ribosome nascent chain complex itself behaves unexpectedly in combination with Talon metal affinity resin or Dynabeads Talon. Perhaps the His-tag is not suitable for purification of archaeal ribosomes. To corroborate this hypothesis the HAHis-tag was exchanged against a HAStrepHAStrep-tag. The buffers were adjusted accordingly and purification trials were done using Strep-Tactin Superflow and Strep-Tactin Magnetic beads.

In the following experiments a double Strep construct (HAStrepHAStrepSecF100) was used (Fig. 9). As mentioned before, the translation reaction was pelleted through a high salt sucrose cushion and ribosomes were resuspended in binding buffer. Interestingly, a large proportion of the signal was again observable in the supernatant (Fig. 9, A: lane SN1). Only a minor proportion of the signal could be found in the pellet (Fig. 9, A: lane R). The resuspended ribosomes were bound to a Strep-Tactin sepharose matrix. In the flow through, only weak signal could be seen for peptidyl-tRNA and released peptide indicating a substantial amount of binding to the column material (Fig. 9, A: lane FT). However, as observed for the His-constructs, nearly no signal could be retrieved from the column. Only a weak band at the size of peptidyl-tRNA is visible in the elution fraction (Fig. 9, A: lane E). Boiling of the sepharose after elution also revealed some signal at the size of the released peptide (Fig. 9, A: lane B). Still, the amount of signal found on all fractions of purification does not sum up to the amount of signal found in the ribosomal pellet.

The same experiment was repeated using Strep-Tactin Magnetic Beads. A substantial amount of signals corresponding to released peptide and peptidyl-tRNA was retrieved in the flow through, indicating limited binding (Fig. 9, B: lane FT). However, in contrast to prior

experiments, RNCs could be released from the column in the elution fraction (Fig. 9, B: lane E) and no signal was found boiling the magnetic beads (Fig. 9, B: lane B). However, even though the signal in the elution fraction indicates the presence of RNCs, the yield was too low for further experiments.
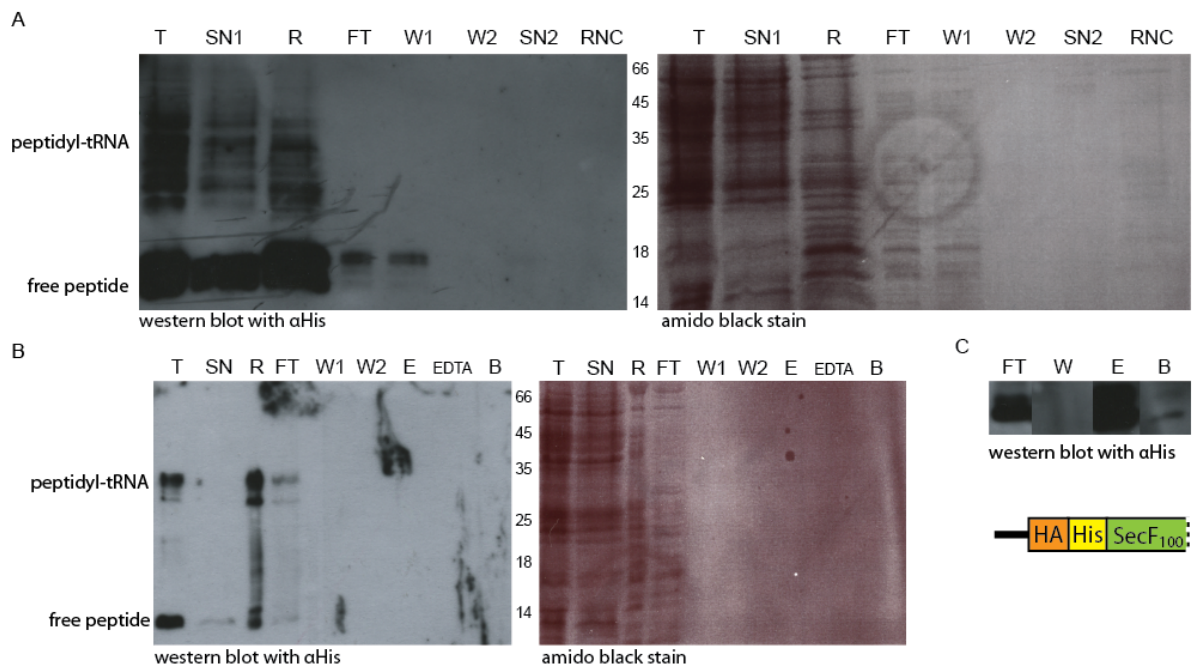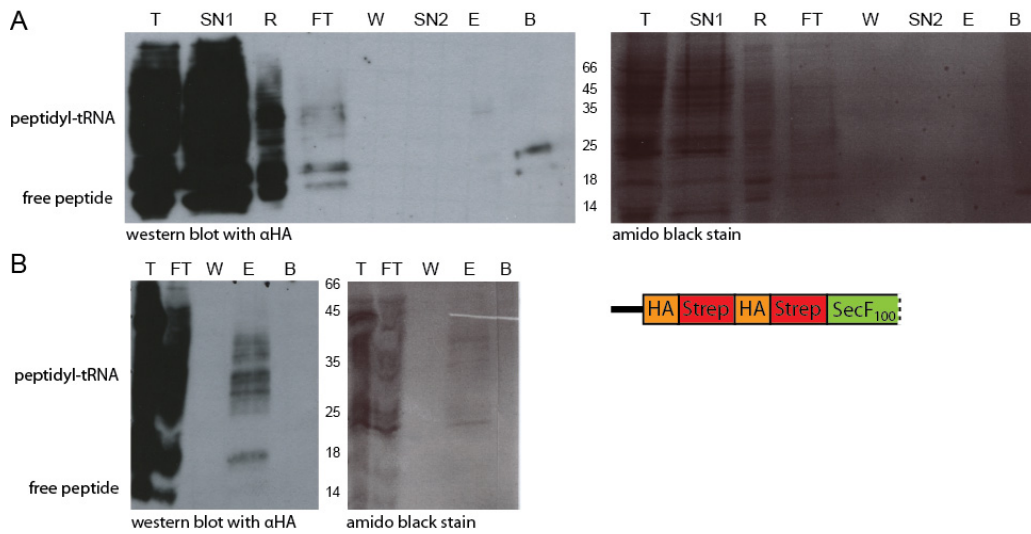

Figure 9: Affinity purification attempts of RNCs using Strep-Tag. 1/100 of all fractions were analyzed by SDS-PAGE and western blot. **(A)** Purification attempt using Strep-Tactin sepharose: T translation reaction, SN1, supernatant 1, R pelleted ribosomes, FT flow through, W wash step, SN2 supernatant 2, E elution, B column material boiled in sample buffer. Only a weak signal for RNCs could be obtained in the elution fraction. **(B)** Purification scheme using Strep-Tactin Magnetic Beads: 1/100 of all reactions were analyzed by SDS-PAGE and western blot. Some RNCs could be obtained in the elution fraction.

Under all chosen conditions no satisfactory binding and concentration of the RNCs was possible. The signal of the peptidyl-tRNA and the hydrolyzed peptide disappeared, as soon as the sample was loaded onto sepharose column or magnetic beads. Neither sepharose nor magnetic beads were responsible for the loss of sample: Boiling of the column material revealed no additional sample. Also changing the reaction tube for low-binding material did not change the outcome (data not shown).

In conclusion, it was possible to establish an archaeal *in vitro* system with extracts prepared from frozen *T. kodakarensis* cells. The extract has been shown to reliably translate many substrate mRNAs on a western blot detection level. However, enrichment of RNCs was not possible due to biochemical obstacles. Further experiments are necessary to identify the requirements for successful purification of RNCs. The most promising candidate for improvement is the HaStrepHaStrepSecF100 constructs using Strep-Tactin Magnetic Beads.

4.2. Purification and *in vitro* reconstitution of archaeal NGD factors

4.2.1. Purification of components and reconstitution of aABCE1

The aPelota, aRF1 and aIF6 proteins were designed with an N-terminal 6 × His-tag, expressed in *E. coli* and purified by affinity chromatography. aEF1α was cloned with a cleavable C-terminal His-tag. The tag was removed after purification. aIF6 was for the most part and aEF1α was only expressed in inclusion bodies. Only the soluble part of aIF6 was purified and used for the experiments. aEF1α was purified from inclusion bodies and refolded on the Ni-NTA column. Most of aRF1 aggregated during concentration; therefore glycerol (1% final concentration) was added. Precipitations were removed by centrifugation. From 6L cells approximately 30 mg aPelota, 30 mg aEF1, 10 mg aRF1 and 0.5 mg aIF6 were obtained.

Purified aABCE1 was kindly provided by Prof. Hopfner (LMU München). Reconstitution was performed as described previously (Karcher et al., 2008). The FeS cluster in aABCE1 is oxygen

sensitive. In an oxidized state the loss of electrons destabilizes the cluster and the catalytic iron ions are no longer coordinated. The FeS synthesis protein IscS from *E. coli* is able reconstitute oxidized FeS clusters. The progress of reconstitution was visualized by a color change of the protein from yellowish brown to dark brown.

4.2.2. Complex formation of aPelota and aEF1α prior binding to ribosomes

The protein aEF1α is a member of EF-Tu like translational GTPases. These GTPases like eEF1, eRF3 and Hbs1 form complexes with the respective A-site factors prior to binding to the ribosome. Consistently, this could be observed for *A. pernix* aEF1α and aPelota and for the yeast homologues Dom34 and Hbs1 *in vitro* (Chen et al., 2010; Kobayashi et al., 2010). Therefore, complex formation of aEF1α and aPelota from *T. kodakarensis* before binding to the ribosome was expected. Since the size of a protein complex is larger than the separate proteins, complex formation can be detected by a change in the migration behavior using gel filtration. Equimolar amounts of purified aEF1α and aPelota were mixed in buffer containing 200 mM NaCl and separated on a Superdex S200 10/30 gel filtration column (Fig. 10). The elution peak of aEF1α alone is located around fraction 32 and has a higher absorption than the elution peak of aPelota around fraction 34. Both proteins together also eluted around fraction 32-33. This implicates that no formation of a complex was achieved under the chosen buffer conditions. Also no difference was observed in the presence of 5 mM GTP or GDPNP. A minor peak was observable around fraction 5-8 originating from aEF1α. This peak corresponds to aggregated proteins due to the preparation from inclusion bodies, but it is negligible compared to the amount of soluble protein.
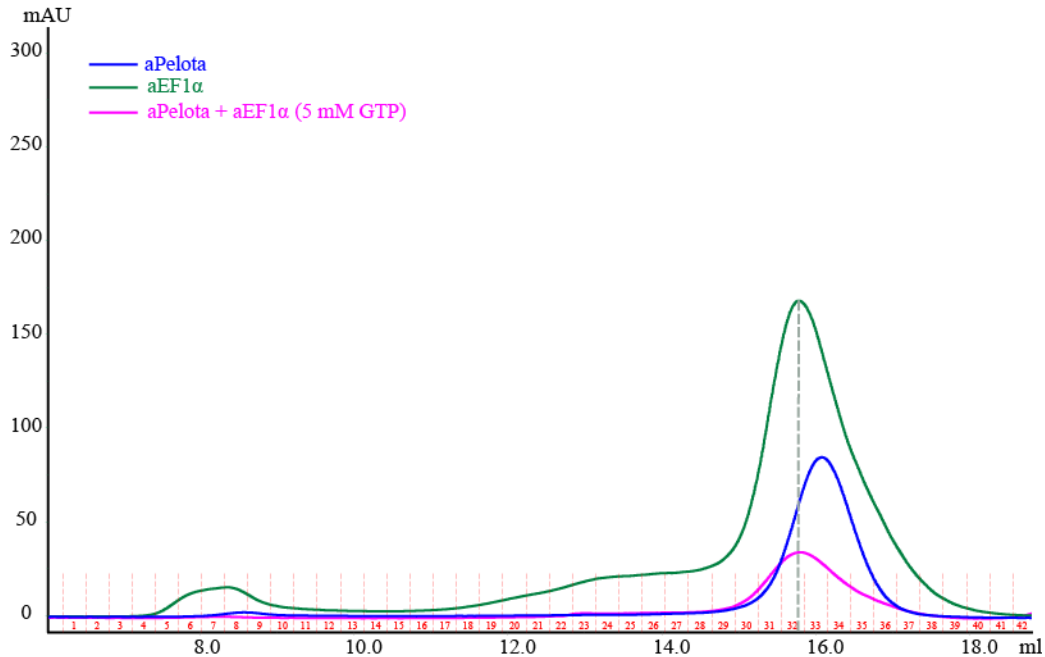
Figure 10: Elution profile of aPelota and aEF1α gel filtration alone and in combination. Blue aPelota alone, green aEF1α alone and pink aPelota and aEF1α together in the presence of 5 mM GTP. aPelota elutes at a slightly higher volume than aEF1α. The elution peak of both proteins corresponds with the elution peak of aEF1α alone, indicated by the dashed line: No complex formation was observable.

4.2.3. *In vitro* reconstitution assays

In vitro reconstitution assays are used to establish buffer conditions that allow complex formation of factors with ribosomes. Purified aPelota, aEF1α and reconstituted aABCE1 were incubated with high-salt purified ribosomes from *P. furiosus* (see 3.3.5) at 30°C under anaerobic conditions. Binding was examined by centrifugation through sucrose cushion. Only proteins binding to ribosomes can be pelleted through the sucrose cushion. The supernatant and pellet fractions were analyzed using SDS-PAGE.

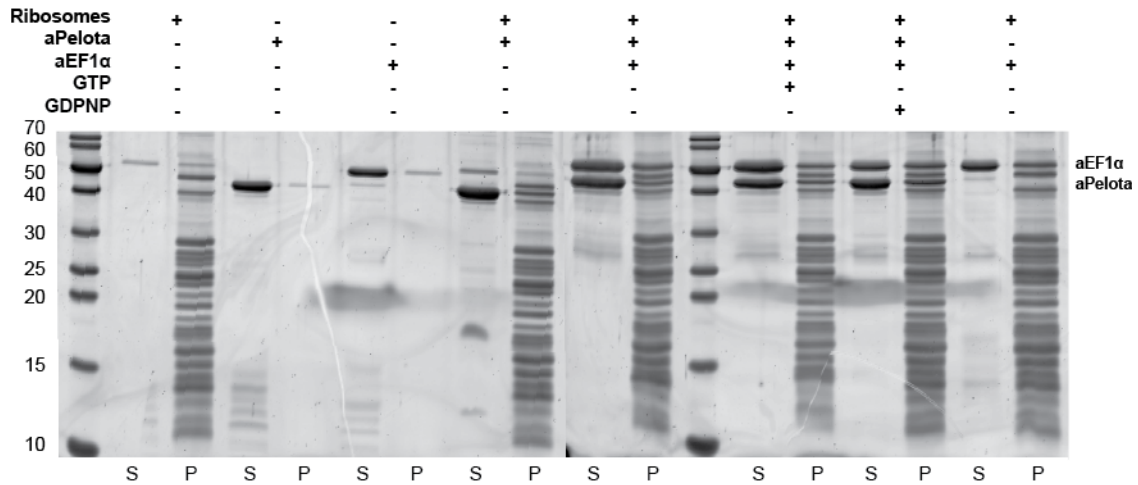- aEF1α and aPelota

Figure 11: *In vitro* ribosome binding of aEF1α and aPelota. Purified aEF1α and aPelota were bound to 70S ribosomes. Reactions were spun through a sucrose cushion. Supernatant S and pellet P fractions were analyzed by SDS-PAGE and stained with SYPRO-Orange. Binding of aPelota and aEF1α alone as well as in combination was detectable.

aEF1α and aPelota bound simultaneously and independently to 70S ribosomes from *P. furiosus* (Fig. 11). The binding of both factors was only marginally affected by the presence or absence of GTP or GDPNP. Minor amounts of aEF1α and aPelota could be found in the pellet fraction in the absence of ribosomes; but the amount was significantly smaller than the amount of proteins found in the pellet fraction in the presence of ribosomes. The intensity of the band on the protein gel indicated stoichiometric binding. In the presence of GDPNP, the binding of aEF1α to the ribosome was slightly enhanced but independent of the presence of aPelota. In contrast, binding of aPelota was favored in presence of aEF1α and GTP or GDPNP.

- aABCE1 and aPelota

Both components - aPelota and aABCE1 - bound independently and simultaneously to ribosomes in virtually stoichiometric amounts (Fig. 12). In the presence of ADPNP the binding of aABCE1 to the ribosome was slightly enhanced. In case of aPelota no difference could be

observed in the presence or absence of aABCE1. Both proteins did not show any signs of aggregation and could be found only in the supernatant in the absence of ribosomes.
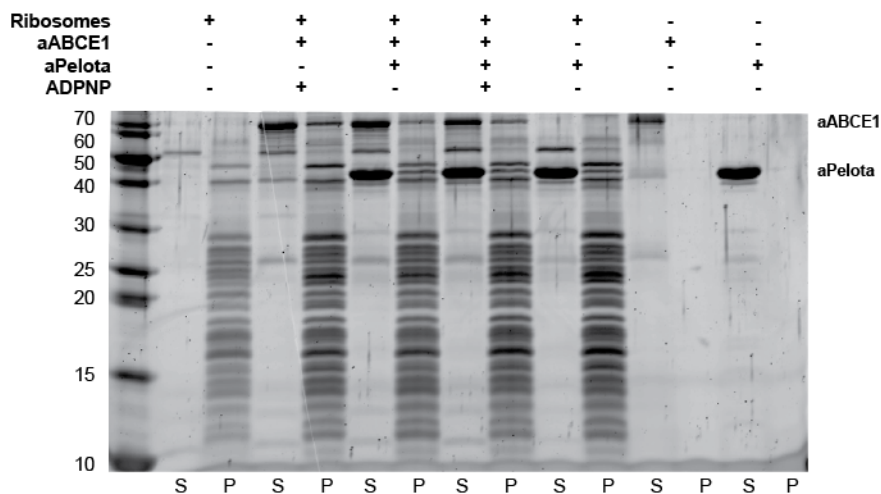
Figure 12: *In vitro* ribosome binding of aABCE1 and aPelota. Purified aPelota and aABCE1 were bound to 70S ribosomes. Reactions were spun through a sucrose cushion. Supernatant S and pellet P fractions were analyzed by SDS-PAGE and stained with SYPRO-Orange. Binding of aPelota and ABCE1 alone as well as in combination was detectable.

Taken together, complexes probably resembling functional NGD intermediates with aPelota and aEF1α and recycling intermediates consisting of aPelota and aABCE1 could be reconstituted and were subsequently subjected to cryo-EM and single particle analysis.

4.2.4. Splitting assays

The activity of the recycling complex in ribosome disassembly was shown in *in vitro* assays using high-salt purified ribosomes (see 3.3.5). All reactions were performed under anaerobic conditions. The readout was done comparing the sum of the heights of the 30S and 50S peaks

with the sum of the heights of the 30S, 50S and 70S peaks (Fig. 13, A, B). For normalization the intrinsic ribosome dissociation of a sample containing only 70S ribosomes was assessed and subtracted from all obtained results. This way, the influence of ligand-independent subunit dissociation could be excluded from the analysis. In all samples aIF6 was added to prevent re-association of the subunits.
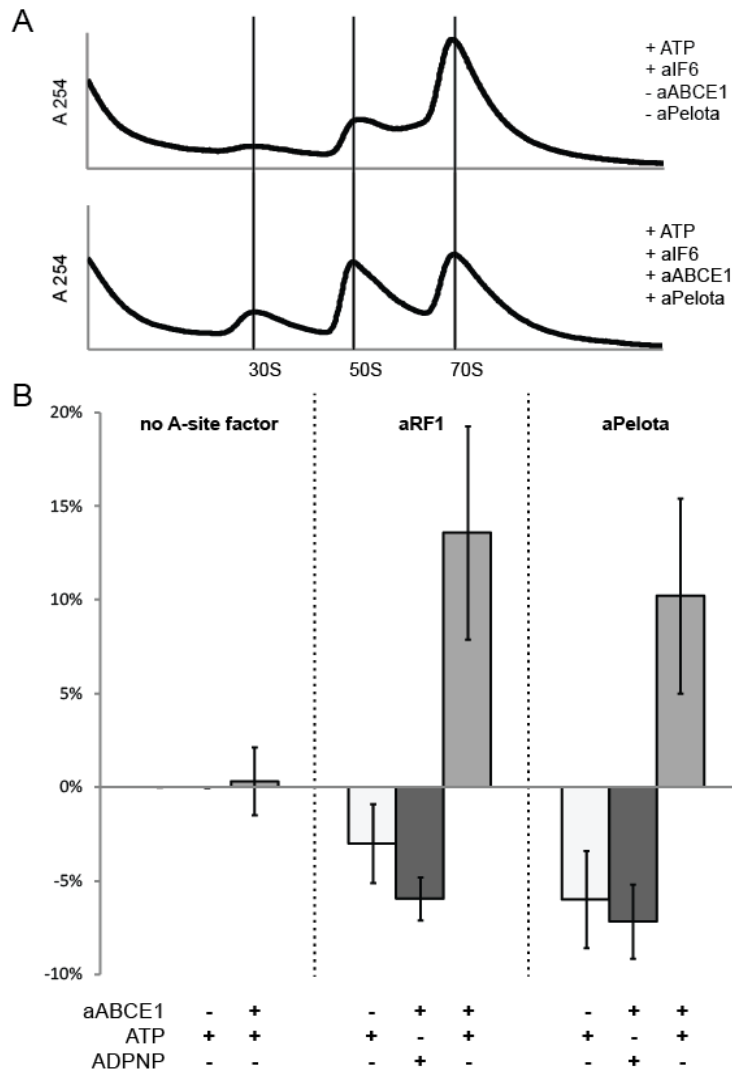
Figure 13: *In vitro* **disassembly of ribosomes. (A)** Dissociation of ribosomes in the presence of aABCE1 and aPelota compared to factor-independent dissociation of 70S ribosomes assayed by sucrose density centrifugation. **(B)** Splitting efficiency of aABCE1, aRF1 and aPelota for archaeal 70S ribosomes using different nucleotides. Error bars indicate +/- standard deviation. aIF6 was added to prevent reassembly of ribosomal subunits.

Significant splitting was observed in the presence of aABCE1 either with aRF1 and ATP or aPelota and ATP (Fig. 13, B). Without aABCE1 the observable amount of splitting was at

background level or even below. There was no significant difference evident comparing the splitting efficiency of aRF1-aABCE1 and aPelota-aABCE1. In contrast to ATP, the non-hydrolysable analog ADPNP did not induce splitting. The ratio of subunits compared to total ribosome signals was actually even below background ratio, at a similar level obtained without aABCE1.

4.3. Cryo-EM reconstructions

Preprocessing of both datasets started with quality assessment of micrographs and calculation of power spectra. Finally, 2496 micrographs were used from the 70S-aEF1α-aPelota dataset and 6441 micrographs from the 70S-aABCE1-aPelota dataset. Particles were isolated and automatically classified into ribosomal and non-ribosomal particles using the MAPPOS algorithm (see 3.4.2). For initial alignment, 368,000 and 472,000 particles respectively were used.

4.3.1. Processing of the 70S-aEF1α-aPelota sample

Even though the particles were automatically classified into ribosomal and non-ribosomal particles before initial alignment, the algorithm is not perfect and a certain number of false positive particles can be expected. The initial backprojection of the 70S-aEF1α-aPelota dataset also revealed a substantial overrepresentation of 50S subunits. Therefore, the false positive

particles and the 50S contamination were eliminated in a first sorting using a noise-derived 3D-reconstruction and a 50S map as additional references. The unexpected amount of 50S subunits was led back to a problem in the ribosome preparation. When the particle distribution became stable, 43% of the 273,000 ribosomal particles (without false positive particles) were found to be attracted by the 50S reference (Fig. 14, 1.I). The corresponding reconstruction contained only density for 50S subunits and some unstructured density at the interface towards the position of the 30S subunit. The second group (Fig. 14, 1.II) attracted 57% of all ribosomal particles. The respective reconstruction contained additional density in the factor binding site and in the A site. Only particles of group 1.II were used for further refinement. The dataset 1.II contained a weak density at the factor binding site, and additional densities in the intersubunit space. A second sorting step was done to reveal any possible conformational heterogeneity of the dataset offering two references. The first sub-dataset 2.I (26%) led to a reconstruction with only vague ribosomal features and no details (Fig. 14, 2.I). Consequently, only the particles of the second sub-dataset 2.II (31%), were further refined. The reconstruction of the sub-dataset 2.II contained an extra density at the factor binding site, P- and E-site tRNA and obviously poorly defined density in the A site.

After a final sorting step two homogenous populations were obtained. The reconstructions differed in the orientation of the 30S subunit towards the 50S (Fig. 14, 3.I and 3.II). A stable particle distribution was achieved allocating 15% of the particles in the group 3.I and 16% of the particles in group 3.II. Both sub-datasets were independently refined.
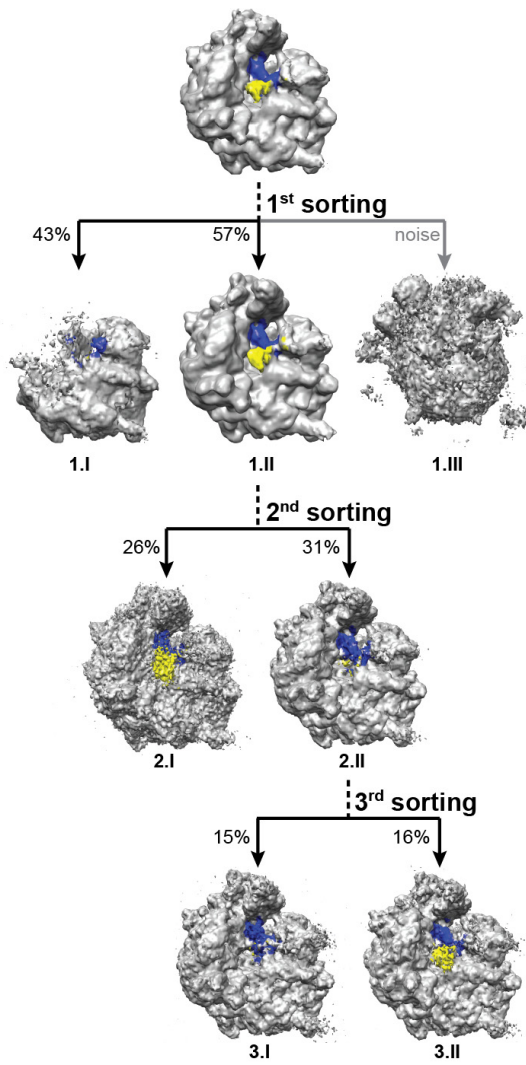
Figure 14: Sorting scheme of the 70S-aEF1α-aPelota dataset. Three sorting steps were performed in order to obtain homogeneous sub-datasets. In the first sorting, a 50S contamination and false positive particles were removed from the dataset (1.I, 1.III). In the second step particles were eliminated that lead to a ribosome reconstruction with only vague ribosomal features (2.I). Finally, the third sorting discriminated between a ratcheted and an unratcheted conformation of the 30S subunit.

For final improvement of the resolution in both sub-datasets, particles were classified according to their cross-correlation values. During refinement, the cross-correlation between particle and projection increases. However, is has been observed that the cross-correlation value for some particles does not increase as expected. Based on visual inspection of the particle-cross-correlation distribution, particles with a cross-correlation value less than 8000 were omitted from the dataset.
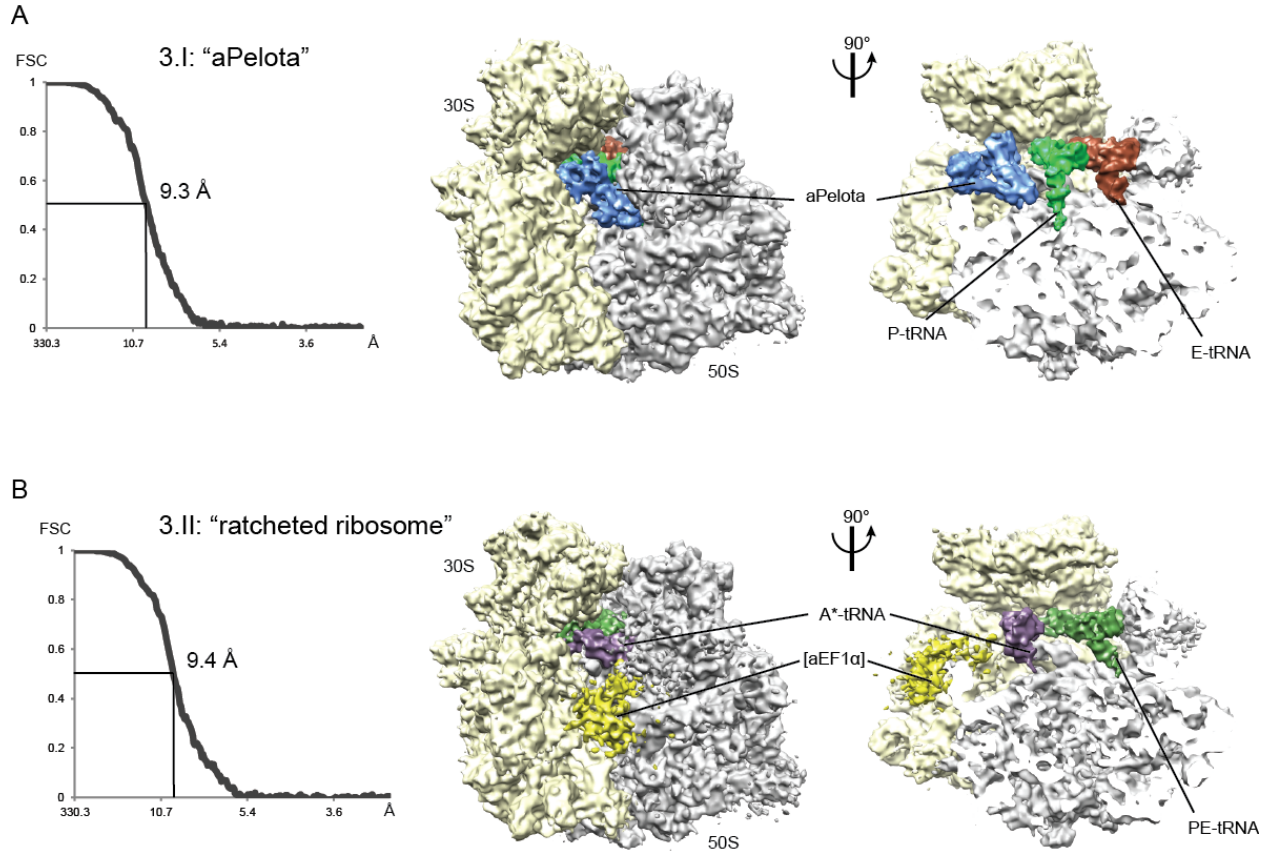
Figure 15: Cryo-EM reconstructions and resolution of the 70S-aEF1α-aPelota dataset.
(A) The cryo-EM map of sub-dataset 3.I contained additional density for aPelota in the A site and P- and E-site tRNA at a resolution of 9.3 Å, according to a FSC cutoff value of 0.5. **(B)** The cryo-EM map of sub-dataset 3.II revealed additional density for tRNAs in the A site and in a P-/E-hybrid state at a resolution of 9.4 Å. The 30S subunit is in a ratcheted conformation. Weak density is visible at the factor binding site and most likely caused by flexibly bound aEF1α (indicated by [aEF1α]).

Sub-datasets 3.I (13% of all particles) and 3.II (13% of all particles) were refined separately to a final resolution of 9.3 and 9.4 Å, respectively. The sub-dataset 3.I revealed additional densities for aPelota, P- and E-site tRNA, but no density in the canonical factor binding site (Fig. 15, A). Sub-dataset 3.II revealed a ribosome with a ratcheted 30S subunit (Fig. 15, B). Consequently, in the intersubunit space tRNA in a PE-hybrid state was found. Notably, a second tRNA could be allocated in A-site position regarding the orientation towards the 30S and 50S subunit. The structure also showed a small additional density in the factor binding site that was most likely contributed by aEF1α. Since the density was too small to accommodate the molecular model of

aEF1α and didn't reveal any reliable structural details, no modeling and molecular interpretation was possible.

4.3.2. Recalculation of the pixel size

Between the data collection of the 70S -aPelota-aEF1α and the 70S-aPelota-aABCE1 dataset, the original Eagle 4k × 4k CCD camera was exchanged against a TemCam 416F CMOS camera. This led to a change in the pixel size, since the pixel size is directly dependent on the magnification of the Titan Krios microscope, the properties of the camera and the position of the camera in the microscope. The new pixel size had to be determined experimentally.

Processing of the 70S-aABCE1-aPelota dataset was done using the old pixel size of 1.119 Å/p valid for the Eagle 4k × 4k CCD camera as starting point. After a few rounds of refinement, the size of the volume differed from the original reference, indicating a disparity of the pixel size. The correct pixel size was now determined by comparison of the cryo-EM map with a calculated map of defined pixel size. The molecular model of the 23S rRNA was chosen as reference. The Spider command 'CP FROM PDB' generated a density map with a given pixel size of 1.0 Å/p and a box size of 368 pixels. A script was used to interpolate the size of the EM-map in a given range and to calculate the cross-correlation of the interpolated map with the reference. The highest cross correlation was determined at an interpolated box size of 351 pixels resulting in a new pixel size of 1.0489 Å/p. This value was used for processing of the 70S-aABCE1-aPelota dataset.

4.3.3. Processing of the 70S-aABCE1-aPelota sample

In the first sorting step the false positive particles were removed from the dataset as described before resulting in 370,000 ribosomal particles. Additional sorting was performed to differentiate between conformational and ligand-induced heterogeneity. Therefore four

differently filtered *P. furiosus* ribosomes were offered as references for alignment. Particle distribution became stable assigning 16% to the first group (Fig. 16, 1.I). The corresponding reconstruction showed a reduced and distorted 30S density, but a valid density representing the 50S subunit. The second group (Fig. 16, 1.II) attracted 39% of all particles. Clear ribosomal features are recognizable for the small and large subunit and additional density in the factor binding site. In the intersubunit space, densities for P-site tRNA and a mixture of aPelota and A-site tRNA as observed in the 70S-aPelota-aEF1α dataset were visible. The third sub-dataset (Fig. 16, 1.III) revealed a map with only vague ribosomal features. In the forth group (Fig 16, 1.IV), 13% of all particles were gathered. The map represented an idle 70S ribosome with no extra densities.
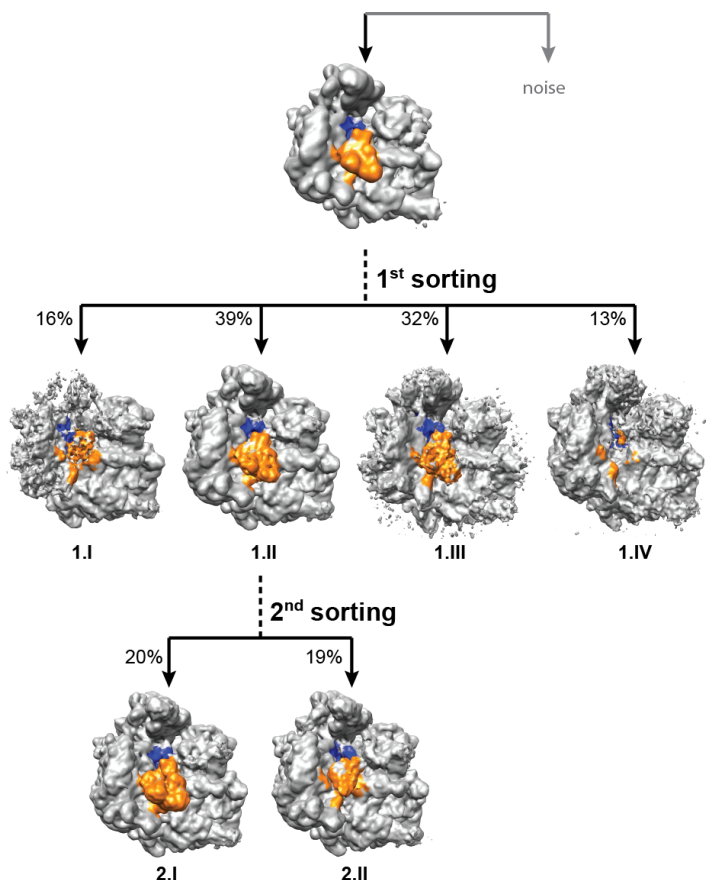
Figure 16: Sorting scheme of the 70S-aABCE1-aPelota dataset. Two successive sorting steps were performed in order to obtain homogeneous sub-datasets. In the first sorting particles were eliminated from the dataset that corresponded to ribosomes with a delocalized 30S subunit (1.I), led to a reconstruction with only vague ribosomal features (1.III) or belonged to ribosomes without bound factors (1.IV). In the second sorting step the remaining particles of 1.II were further sorted with resepect to aPelota (2.I) or tRNA (2.II) in the A-site position. The initial sorting for false positive particles (noise) is not shown.

Particles of group 1.II were further refined. A second sorting step was performed to distinguish between aPelota and A-site tRNA. As expected, sorting resulted in a separation of the dataset

64

into two populations: the first one containing aPelota and aABCE1 (Fig 16, 2.I) and the second with A-site tRNA and an undefined density at the translational GTPases factor binding site (Fig. 16, 2.II). Particles belonging to sub-dataset 2.I and 2.II were independently refined.

To improve the resolution, all particles of group 2.I and group 2.II were now classified according to the cross-correlation values. Based on visual inspection, a cut-off value of 9000 was chosen for the 2.I dataset and 8000 for the 2.II dataset. All particles with a lower cross-correlation value were omitted from the dataset. The final reconstructions were based on 14% of all ribosomal particles initially present in the data for sub-dataset 2.I and 15% of all ribosomal particles for sub-dataset 2.II.
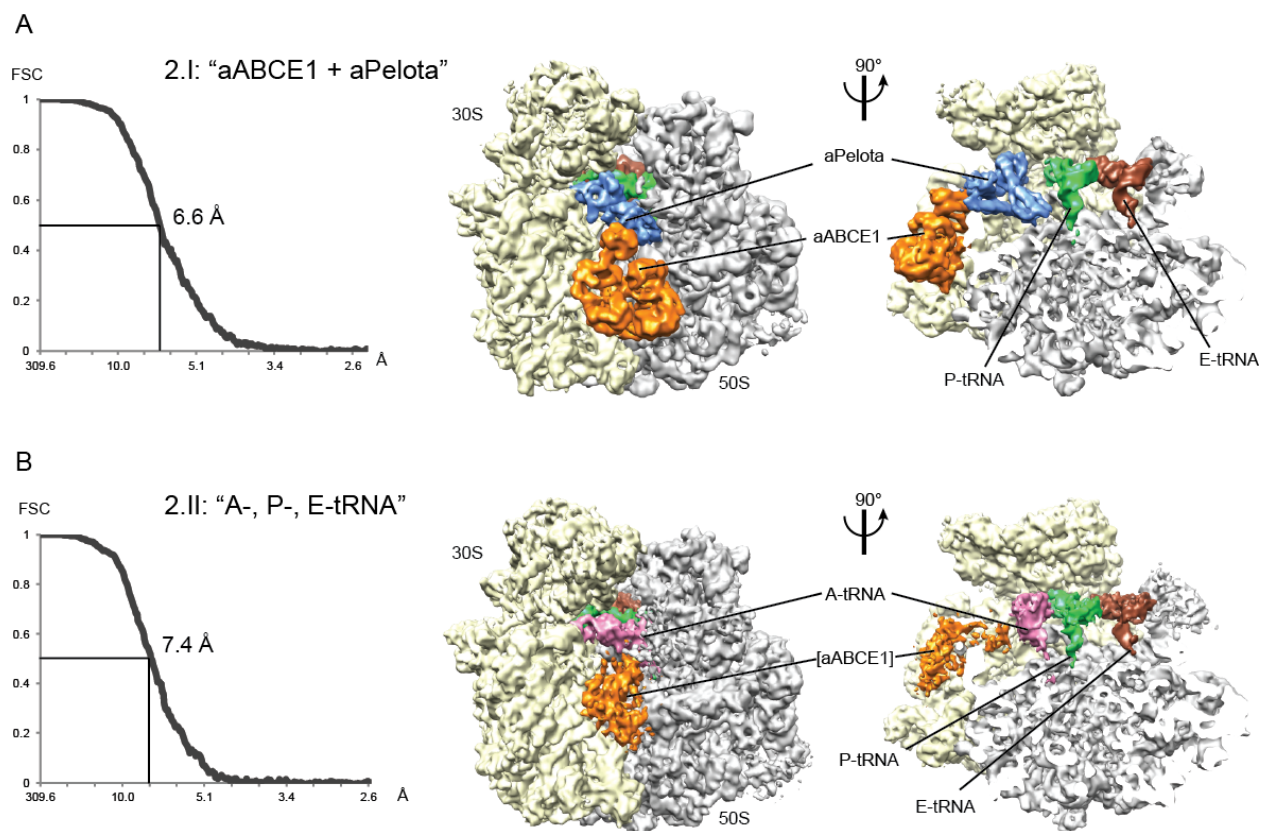
Figure 17: Cryo-EM reconstructions and resolution of the 70S-aABCE1-aPelota dataset. **(A)** The cryo-EM map of sub-dataset 2.I with additional density for aABCE1 at the factor binding site, aPelota in the A site and P- and E-site tRNA at a resolution of 6.6 Å, according to a FSC cutoff value of 0.5. **(B)** The cryo-EM map of sub-dataset 2.II contained additional density for tRNA in the A, P and E site at a final resolution 7.4 Å. Additional density at the factor binding site is most likely caused by flexibly bound aABCE1 indicated by [aABCE1].

The sub-datasets 2.I and 2.II were refined to a final resolution of 6.6 and 7.4 Å, respectively (Fig. 17). In the first reconstruction densities for aPelota in the ribosomal A site, aABCE1 in the factor binding site, and for tRNA in the P and E sites could be observed. Using available crystal structures, individual domains of aPelota and aABCE1 could be assigned and positioned unambiguously (Fig. 17, A, Fig. 19, A-C).

In the second reconstruction (Fig. 17, B), densities for tRNAs in the A, P and E sites were observed. An un-interpretable density without structural details could be found at the factor binding site. This density might correspond to aABCE1 but due to lack of details no interpretation was possible.

4.3.4. Validation of resolution determination

The resolution of all datasets was determined at the 0.5 FSC criterion. The resolution of the aABCE1-aPelota map was calculated to be 6.6 Å. This resolution was validated by comparison with maps generated from pdb-models and filtered to the desired resolution (Fig. 18, C). Fig. 18 shows the cryo-EM map of 70s-aPelota-aABCE1 at two different contour levels in comparison with calculated maps filtered to 5, 6 and 7 Å. Since the phosphates in the rRNA backbone under cryo-EM conditions provide a better signal compared to the amino acids of the proteins, two different contour levels are necessary to assess the details of both components. The backbone of the LSU rRNA helix H25 reveals separation of phosphate groups as seen in the 6 Å map. The details observable in the density representing protein L32e also points towards a resolution around 6 Å. This is in good agreement with the calculated FSC resolution.
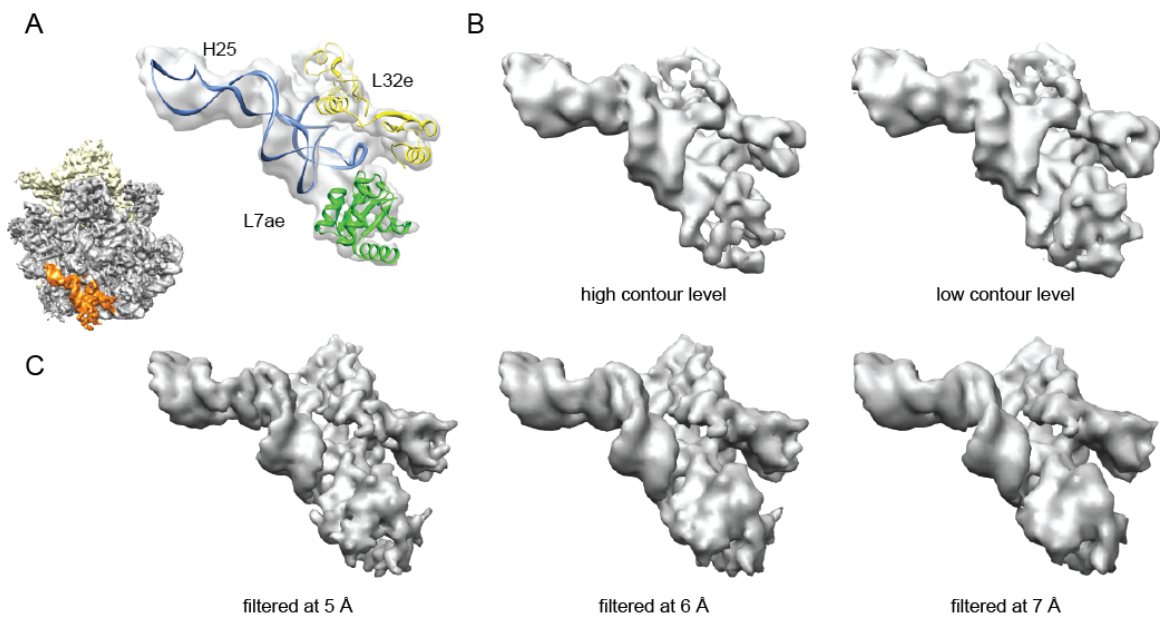
Figure 18: Comparison of the cryo-EM map of the 70S-aABCE1-aPelota structure with calculated density maps of the according pdb-models. **(A)** Docking of the molecular model of H25, L32e and L7ae in the according density. The view is indicated by a thumbnail. **(B)** Isolated density derived from the cryo-EM map shown at higher and lower contour levels to present details of rRNA and protein. **(C)** Calculated density maps of pdb-models filtered at 5, 6 and 7 Å resolution. The details observable on the cryo-EM map correspond to the 6.6 Å resolution determined by 0.5 FSC.

4.4. Structural interpretations

The reconstructions of archaeal 70S ribosome with aPelota and aEF1α or aABCE1 were among the first successful cryo-EM structures based on Titan Krios data in our lab. The data was interpreted by docking of molecular models in the cryo-maps. A homology model of aPelota was generated based on the aPelota-aEF1α crystal structure (Kobayashi et al., 2010). The model of *P. furiosus* aABCE1 was derived from the crystal structure of *P. abysii* aABCE1 (Karcher et al., 2008). A ribosomal homology model was generated for *P. furiosus* (see 3.4.3). Data interpretation was done based on these models.
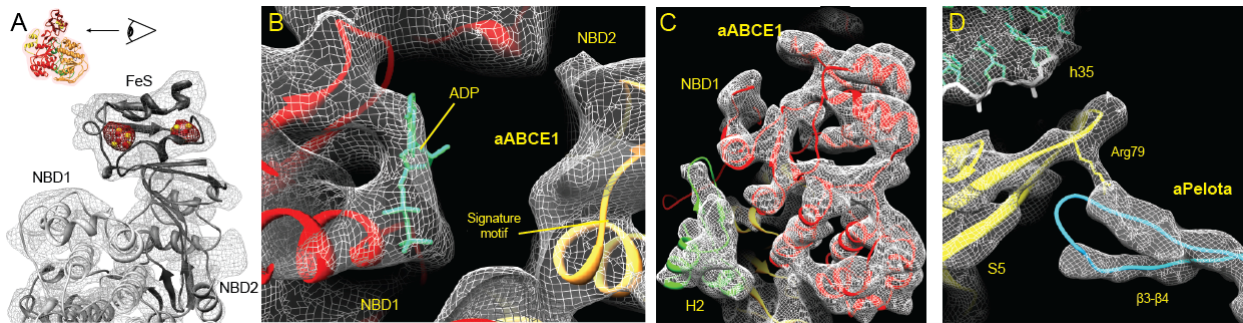
Figure 19: Fitting of molecular models in the 70S-aABCE1-aPelota cryo-EM map. **(A)** Zoom on the FeS domain of aABCE1. The density for the two $[4Fe-4S]^{2+}$ is displayed in red mesh at higher contour level. **(B, C)** Crystal structure of aABCE1 fitted into isolated cryo-EM density (NBD1 red, hinge 2 domain green, NBD2 yellow). **(D)** Homology models for *T. kodakarensis* aPelota, rRNA and ribosomal protein S5 fitted into isolated cyro-EM densities showing the contact between aPelota and S5 formed by Arg79 (NTD blue, S5 yellow, rRNA green-white).

The resolution of the 70S-aPelota-aABCE1 map was sufficient to unambiguously dock molecular models in the electron densities for ribosomal proteins, rRNA and ligands: The two electron dense $[4Fe-4S]^{2+}$ clusters of aABCE1 can be clearly resolved as distinct spheres at high contour levels (Fig. 19, A). In Fig. 19 B and C more examples are given that validate the quality of the map and the positioning of the crystal structure of aABCE1. In some parts of the map, amongst others the contacts sites of aPelota and the ribosome, it was even possible to resolve individual side chains as shown in Fig. 19, D.

4.4.1. Interaction of aABCE1 and the ribosome

aABCE1 binds to the archaeal ribosome in the intersubunit space, where canonical translational GTPases such as EF-TU and EF-G in bacteria and eEF2 and Hbs1 in eukaryotes also interact with the ribosome (Becker et al., 2011; Gao et al., 2009; Schmeing et al., 2009; Spahn et al., 2004; Taylor et al., 2007). Similar to these GTPases, the ATPase aABCE1 contacts the small ribosomal subunit, specifically rRNA helices h5, h8, h14, h15 (Fig. 20, C, Suppl. Table). The h5-h15 region interacts with domain II of the translational GTPases, whereas the h8-h14 junction is the most proximal region the GTPase switch regions (Connell et al., 2007; Villa et al., 2009). Interestingly, the same regions are contacted by aABCE1 via two specific, up to now unexplained, structural features of ABCE1-type ABC-ATPases. The HLH motif of aABCE1 contacts the h5-h15 junction, whereas the hinge region establishes extensive contacts to the h8-h14 junction.
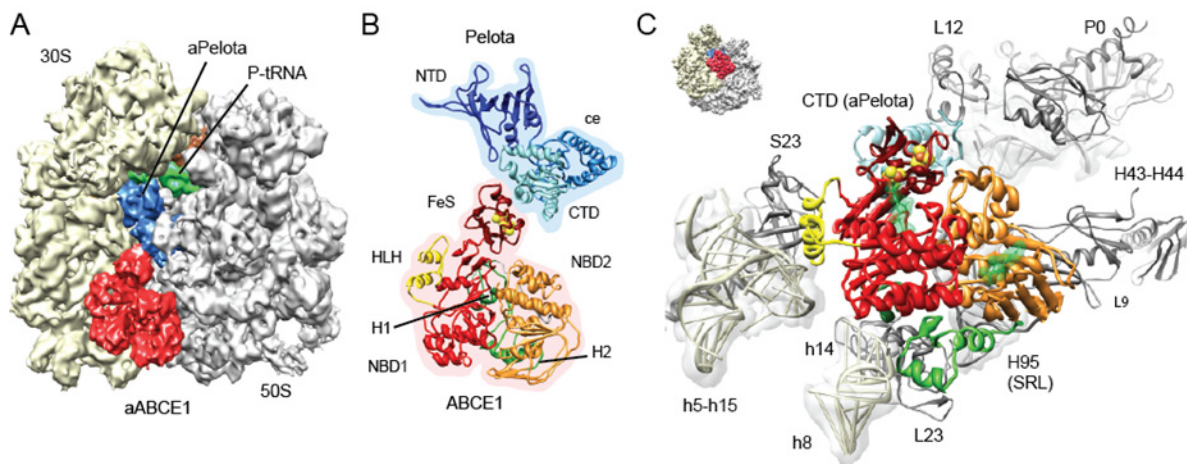
Figure 20: aABCE1 interactions with the ribosome and aPelota. aPelota CTD (light blue), NTD (dark blue), central domain ce (blue), FeS (dark red), hinge domains H1, H2 (green), HLH motif (yellow), red NBD1, orange NBD2, green spheres ADP. (**A**) Cryo-EM map of aABCE1 and aPelota bound to the ribosome. (**B**) Homology model for Pelota and ABCE1 indicating the arrangement of both proteins. Same view as seen in (A). (**C**) Interactions of aABCE1 with the ribosome. The view is indicated by a thumbnail.

In contrast to translational GTPases that engage in close interaction with the sarcin-ricin-loop of H95 (SRL), contacts of aABCE1 to the large subunit are essentially limited to L9. The FeS cluster

domain does not contact the ribosome directly but only interacts with the C-terminal domain of aPelota (Fig 20, A and B).

4.4.2. Interaction of aPelota and the ribosome

aPelota binds to the archaeal ribosome in the A-site position in the presence and absence of aABCE1, as shown before in the SL-RNC-Dom34-Hbs1 cryo-EM map (Becker et al., 2011). The ribosomal subunits are unratcheted as observed in the post-state (see also Fig. 22).
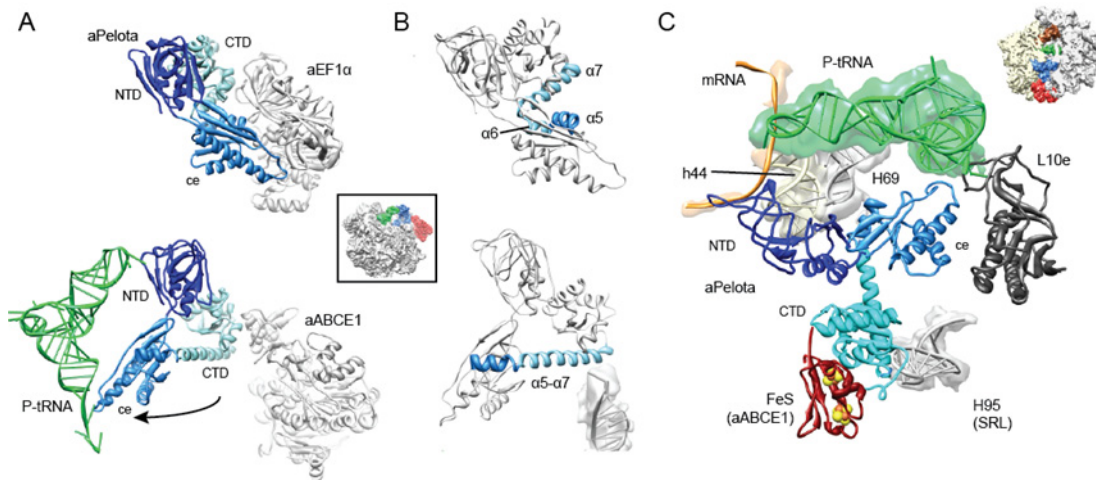
Figure 21: Domain movement in aPelota. (A) Comparison of the aPelota-aEF1α crystal structure (Kobayashi et al., 2010) with the ribosome-bound aPelota in complex with aABCE1. The central domain of aPelota swings towards the P-site tRNA. CTD C-terminal domain, NTD, N-terminal domain, ce central domain. **(B)** Helices α5-α7 refold into a long α-helix during movement of the central domain. **(C)** Interactions of the aPelota NTD and central domain within the ribosome with P-site tRNA, L10e and H69 of the large ribosomal subunit and h44 of the small ribosomal subunit.

The N-terminal domain (NTD) of aPelota is located in the A site contacting rRNA helices h18, h28, h31, h34 and h44 (Suppl. Table). The β3-β4 loop reaches deeply into the A site and contacts the ribosomal protein S5. Compared to the crystal structure of *A. pernix* aPelota-aEF1α and the yeast structure of Dom34-Hbs1 bound to the ribosome, the central domain and the C-terminal domain (CTD) of aPelota undergo large rearrangements (Becker et al., 2011; Kobayashi

et al., 2010) (Fig. 21, A): in the crystal structure and the EM-map the central domain of aPelota/Dom34 is tightly packed against aEF1α/Hbs1 (Becker et al., 2011; Kobayashi et al., 2010); however, without GTPase present, the central domain of aPelota is rotated approximately 140 degrees towards the P-site tRNA. In this conformation it establishes new contacts to rRNA, involving helices H69, H72 and H89 (Suppl. Table). The positively charged loop β10-α3 directly contacts the P-site tRNA acceptor stem and the ribosomal protein L10e (Fig. 21, C). The CTD of aPelota is positioned on top of the ribosomal SRL and a strong contact is established. The helices α5, α6 and α7 that link the central domain and the CTD of aPelota establish one long alpha helix with a kink between α5 and α6 that reaches from the SRL deeply into the A site (Fig. 21, B). The CTD of aPelota establishes the only contact site to aABCE1 via the FeS cluster domain (Fig. 20, B).

4.4.3. Conformational changes upon aABCE1 and/or aPelota binding to the ribosome

Difference maps were generated comparing the map containing aABCE1 and aPelota with the only aPelota-bound map and the map containing A-, P- and E-site tRNAs (Fig. 22). The difference maps were calculated with filter values corresponding to the resolution. In Fig. 22, A the differences in the presence and absence of aABCE1 (red and blue, respectively) are highlighted. The binding of aABCE1 induced a slight outwards rotation of the body of the 30S subunit. A movement of aPelota was also observable. Upon binding of aABCE1, the CTD and NTD of aPelota moved downwards by 2 Å towards the PTC.

In the second map (Fig. 22, B) the differences between aABCE1 together with aPelota (red) and a ribosome with only tRNAs bound (blue) are highlighted. Comparison of both reconstructions revealed that the positions of the large subunit and tRNAs in the ribosomal P and E site were basically identical. The position of the A-site tRNA and aPelota confirmed that only one factor can bind at a time.
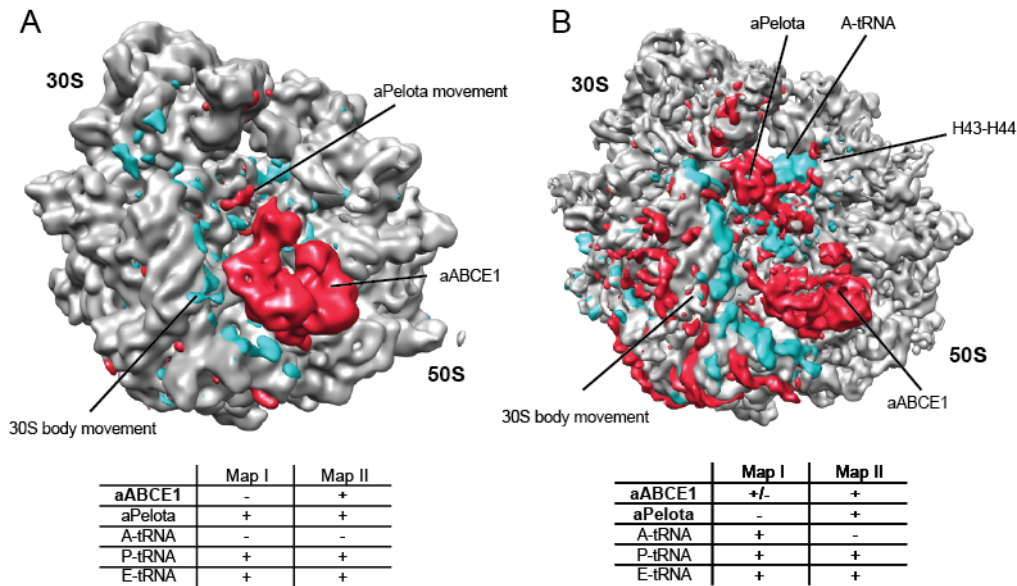
Figure 22: Difference maps of aABCE1 and aPelota binding to the ribosome. The difference maps were calculated comparing the cryo-EM map of 70S-ABCE1-aPelota (red) with the cryo-EM maps with only aPelota (blue) **(A)** or with A-site tRNA (blue) **(B)** filtered at 10 Å and 7 Å, respectively. The body of the 30S subunit is rotated downwards upon binding of aPelota and ABCE1. aPelota is moving towards the PTC upon binding of aABCE1.

There was an even more prominent movement of the 30S body in the +/- aABCE1-aPelota map compared to the +/- aPelota map (Fig. 22, A, B). Obviously the binding of aPelota required or induced a rotation of the 30S subunit contrary to ratchet movement. Also a small movement of H43-H44 was observable upon aPelota and aABCE1 binding. The helices were moving towards aPelota by approximately 4 Å. There was no complete density representing aABCE1 since the reconstruction with the A-, P- and E-site tRNA contained also a small unstructured density of flexibly bound aABCE1 at this position.

4.4.4. Comparison with NGD and recycling intermediate structures from yeast

In yeast two structures of NGD intermediates are available. Firstly the SL-RNC-Dom34-Hbs1 structure published this year (Becker et al., 2011) and secondly a not yet published structure also generated by Thomas Becker consisting of yeast Rli1 and Dom34 bound to SL-RNCs.

The comparison of the archaeal 70S-aPelota-aABCE1 structure with the yeast homologues Dom34 and Rli1 bound to SL-RNCs, revealed a remarkable similarity concerning conformation of the factors and interaction with the ribosome (Fig. 23, A). The only major difference was the additional E-site tRNA in the archaeal map. Docking of molecular models confirmed the similarity. Only a few additional contacts were present in the yeast complex: Rli1 contacted additionally rpS6e and rpS24e in the small subunit and rpP0 and a small region of the SRL (Fig. 23, B). Dom34 established additional contacts to rpS30. As observed in archaea, the FeS cluster of Rli1 only interacted with the CTD of Dom34, but not with the ribosome (Fig. 23, A, Fig. 20, B).
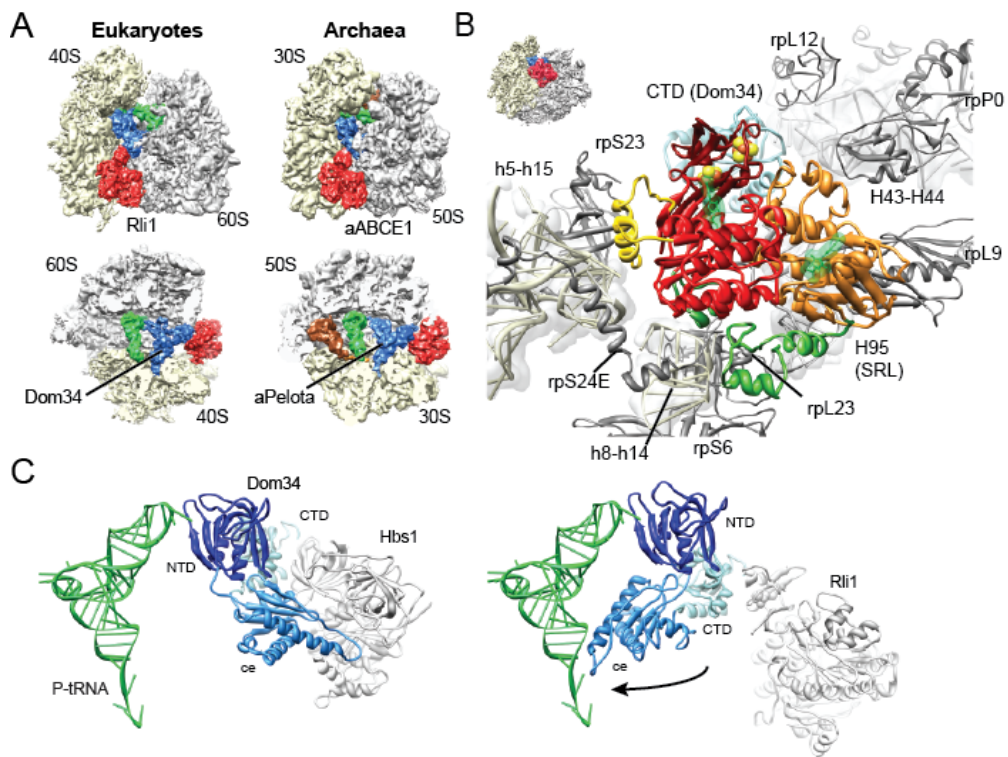
Figure 23: Cryo-EM map of yeast SL-RNC-Rli1-Dom34. (A) Cryo-EM maps of yeast SL-RNC-Dom34-Rli1 and archaeal 70S-aPelota-aABCE1. **(B)** Interactions of yeast Rli1 with the ribosome. The view is indicated by a thumbnail. The color code is as in Fig. 20, B. **(C)** Movement of the Dom34 central domain upon binding of Rli1.

As observed in archaea, the central domain of Dom34 is swung towards the P-site tRNA upon binding of Rli1. The overall conformation seemed extremely similar to aPelota in the ABCE1-

bound conformation. Interestingly, in yeast the formation of a long α-helix connecting the CTD and the central domain was not observed (Fig. 23, C, Fig. 21, B).

In summary, in both species the interaction mode of ABCE1 and Pelota with the ribosome is highly conserved. The presence of ABCE1 stabilizes Pelota in a conformation where the central domain reaches through the A site to contact the P-site tRNA (Fig. 21, C).

4.4.5. Comparison of ribosome-bound aABCE1 with crystal structures

To analyze the mechanochemical function of ABCE1 in ribosome splitting, the ribosome-bound conformation of aABCE1 was compared with an open ADP-bound form as observed in several crystal structures (Barthelme et al., 2011; Karcher et al., 2005; Karcher et al., 2008) and with a model for the closed ATP-bound state. The model for the closed state is derived from superimposition of the NBDs of aABCE1 with NBDs of the MJ0796 ABC-ATPase crystallized in the ATP bound state (Smith et al., 2002). Interestingly, neither the open nor the closed model can be easily modeled into the electron density neither in archaea, nor in yeast (Fig. 24). Instead, an intermediate, half-open state of the two NBDs was observed: NBD2 rotated by approximately 17 degrees towards NBD1 and the FeS cluster domain. However, an additional upward movement by 8 Å of NBD2 would be required in order to obtain the fully closed conformation where the signature motif of one NBD domain contacts the nucleotide binding domain pocket of the other NBD domain. Notably, in the observed half-open state of ABCE1 a contact between the NBD2 domain and the FeS cluster domain can be seen. This feature differs from the crystal structures of the open state. Adoption of the fully closed ATP-bound conformation would therefore require a substantial shift of the FeS cluster domain, also by approximately 8 Å in order to avoid a sterical clash. While the limited resolution of the reconstruction did not allow for any conclusions regarding the nature of the bound nucleotide, the conformations of the individual lobes within the NBD1 and NBD2 domains resembled more closely those of the ADP-bound X-ray structures. Binding to the ribosome induced an allosteric

change in ABCE1, perhaps related to allosteric control of ABC transporter by substrate binding (Locher, 2009).
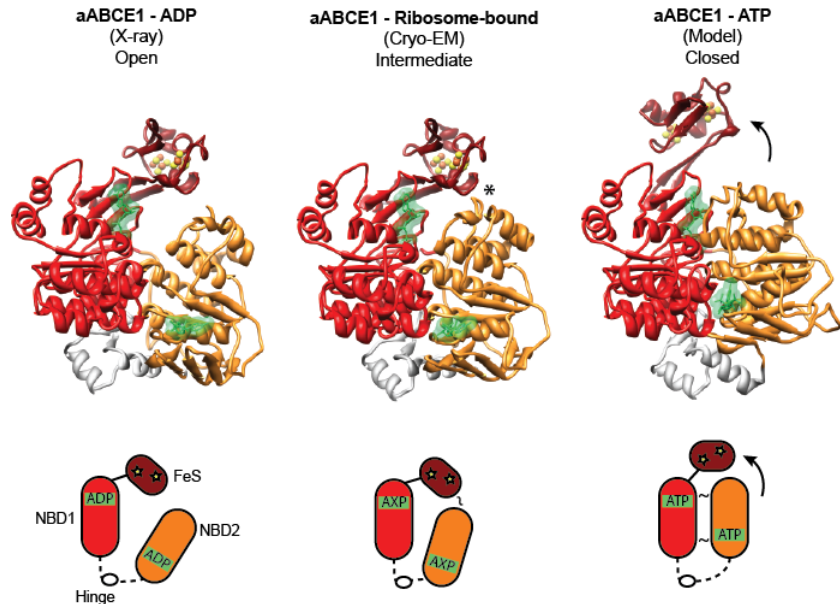
Figure 24: aABCE1 conformations: NBD1 red, NBD2, orange, FeS dark red. Crystal structure of open (ADP-bound) aABCE1 (Karcher et al., 2008), the ribosome-bound aABCE1 model derived from the cryo-EM structure and a homology model of closed (ATP-bound) aABCE1. An asterisk indicates the contact between NBD2 and the FeS domain of aABCE1. Schematic drawings emphasize conformational changes of the FeS-domain and NBD2 relative to NBD1 upon domain closure.

4.4.6. Comparison of ratcheted and classic state ribosomal reconstructions

The reconstructions of the archaeal 70S-aPelota-aEF1α dataset differed in ratcheting of the 30S subunit. aPelota was only found binding to the classic state ribosome. The same observation was true for the 70s-aPelota-aABCE1 reconstruction. Upon binding of aABCE1 the body of the 30S subunit showed an additional outward movement, contrary to ratchet movement, providing space to accommodate the ABC ATPase in the canonical factor binding site.

In contrast, the two maps without aPelota illustrated different time points of 30S movement relative to the large subunit. The difference map was calculated comparing the map containing canonical A-, P- and E-site tRNAs (Fig. 25, red) with the map of the ratcheted ribosome (Fig. 25, blue). The ratchet movement of the 30S subunit illustrates an upward movement of the body and a head swiveling toward the 50S subunit. In the intersubunit space the most dramatic

rearrangement can be seen for the P- and E-site tRNAs. In the ratcheted conformation only one tRNA can be found in a hybrid state contacting the 30S subunit in the P site and the 50S subunit near the E site. The position of the A-site tRNA is not essentially altered. The tRNA is still occupying the A-site position on both subunits, but the anticodon arm is slightly shifted towards the P site compared to the canonical A site tRNA position.

Since the L1 stalk is involved in correct positioning of the tRNA at the exit site, it is turned inwards in the ratcheted conformation and is in contact with the elbow of the PE-hybrid state tRNA.
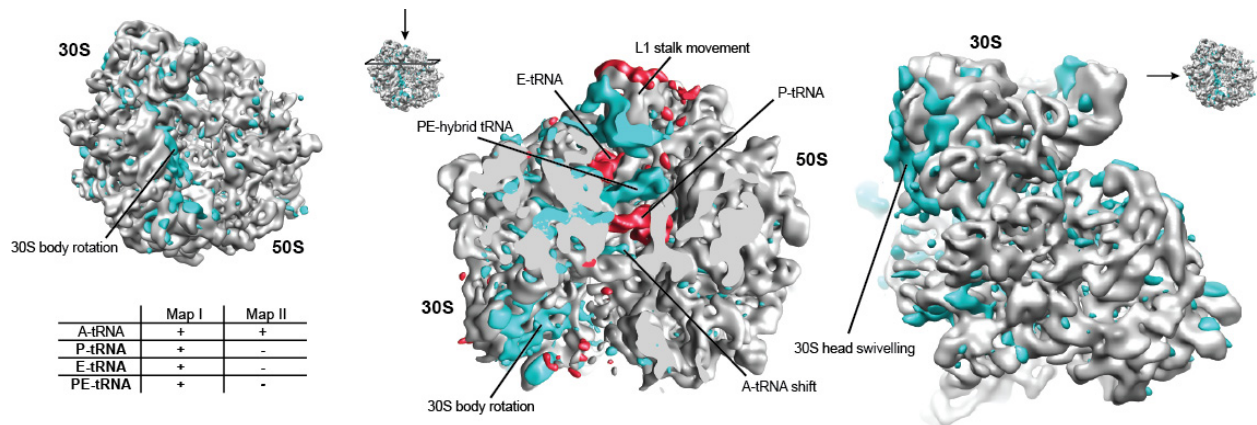
Figure 25: Difference maps of classic and ratcheted ribosomal states. Cryo-EM map of the 70S reconstruction with A-, P- and E-site tRNA (red) overlaid with the difference map of the ribosome in the ratcheted conformation (blue) filtered at 10 Å. In the ratcheted conformation, the body of the 30S subunit is rotated upwards. The head is swiveled towards the 50S subunit. The L1 stalk moves inwards contacting the tRNA in the PE-hybrid state. A small shift of the anticodon stem of the A-site tRNA towards the P-site is observable. Views are indicated by thumbnails.

5. Discussion

In this thesis, the usage of archaea as model organisms for the structural analysis of evolutionary conserved translation associated processes was investigated. In the first part, archaeal cell extracts were tested for programming of ribosomes with truncated mRNA and initial experiments were performed to establish possible purification strategies for archaeal RNCs. In the second part, archaeal NGD intermediates were reconstituted and biochemically and structurally analyzed.

5.1.   Observations on translating archaeal extracts

Structural analysis of physiological translation intermediates by cryo-EM requires a homogeneous sample of RNCs with interacting factors. RNCs are commonly generated using *in vitro* translation systems in bacteria and eukaryotes. The mRNAs used for stalling do not contain stop codons at the 3'-end and encode for peptides with N-terminal tags that allow subsequent affinity purification. In archaea, only two *in vitro* translation systems have been reported yet (Endoh et al., 2006; Ruggero et al., 1993). Until now, no details are known about stalling of archaeal ribosomes and subsequent purification of RNCs. For the establishment of archaea as model organism for structural analysis of translation associated processes, protocols were tested for the generation and purification of RNCs.

5.1.1. *In vitro* translation

A protocol was published in 2008 by Endoh and co-workers that described the conditions for *in vitro* translation using early log-phase *T. kodakarensis* cells. The protocol was adapted and extracts prepared from frozen *T. kodakarensis* cells successfully translated mRNA *in vitro*. The translation rate was sufficient to detect the newly synthesized proteins with tag-specific

antibodies. Interestingly, no product was observable when the construct included an N-terminal 6 × His-tag. Apparently, the biochemical properties of the mRNA or the nascent peptide chain are not compatible with archaeal translation. In bacteria and eukaryotes no problems with N-terminal His-tags have been described before. On the contrary, the tag is often used in this position for heterologous expression of proteins or generation of RNCs in yeast, wheat germ, *E. coli* and *Bacillus subtilis* (Becker et al., 2011; Bhushan et al., 2011; Frauenfeld et al., 2011; Nguyen et al., 2005).

The translation problem seemed to be sequence and localization dependent: Using an N-terminal HA-tag, the construct could be translated efficiently. The combination of an N-terminal HA-tag followed by a His-tag was also translatable. In addition, constructs were successfully translated containing a C-terminal His-tag. This observation points towards a problem with translation initiation.

5.1.2. Programming ribosomes with truncated mRNA

The generation of a homogeneous population of translating ribosomes requires mRNA that is able to stop translation at a certain codon. Since no peptide based stalling mechanism has been analyzed in archaea so far, truncated mRNA was tested for *in vitro* translation and stalling of *T. kodakarensis* ribosomes.

Truncated mRNA could be successfully used to stall ribosomes, and peptidyl-tRNA was detectable by western blotting indicating that the peptide is still bound to the P-site tRNA after translation stopped. Besides the signal for peptidyl-tRNA and hydrolyzed peptide, there were further substantial signals on the blot. These signals were specific, since no background signals were detectable in the absence of mRNA. An additional strong band was visible 2-3 kDa larger than the hydrolyzed peptide. It is possible that the second band corresponds to a modification of the peptide chain being the consequence of an archaeal surveillance mechanism targeting erroneous proteins for degradation. Such a system is known in bacteria rescuing ribosomes

stalled by nonstop mRNA: the tmRNA adds a degradation signal to the C-terminus of the nascent chain and releases it (Gillet and Felden, 2001). The signal encoded in the open reading frame of the tmRNA leads to rapid degradation of the released protein. In eukaryotes the ubiquitinylation of a protein serves the same function. It is possible that archaea possess an analogous mechanism that allows targeting of defect proteins already on the ribosome. This theory might also explain the presence of additional weak signals in the range of app. 35-70 kDa. The smear could correspond to different time points of modifications of the peptidyl-tRNA. The modifications seem to be stable enough to stay associated with the peptidyl-tRNA during SDS-PAGE. However, the existence of such a mechanism remains to be proven. Assuming that archaea own a mechanism comparable to the bacterial tmRNA system, it will be difficult to detect it by simple BLAST analysis since already in the bacterial domain the tmRNA sequences can vary in size (Gueneau de Novoa and Williams, 2004) and are hardly conserved (Keiler, 2008). Mass-spec analysis of the free peptide and the 2-3 kDa larger peptide might provide additional insights and direct further investigations.

Based on the observed western blot signal corresponding to peptidyl-tRNA, the programming efficiency was determined by comparison with a His-tagged protein of known concentration. The analysis revealed that approximately 10-20% of all ribosomes were stalled. This is comparable to known programming rates in yeast (Beckmann et al., 2001). This result indicates that the extract preparation and the conditions for *in vitro* translation are suitable for generating a substantial amount of stalled ribosomes for subsequent purification.

5.1.3. The influence of sparsomycin on archaeal translation

In eukaryotes the addition of the antibiotic cycloheximide after translation is known to stabilize the peptidyl-tRNA and has been employed successfully for RNC purification (Halic et al., 2004). Comparably, the universal translation inhibitor sparsomycin also interferes with translation by affecting the correct positioning of the A- and P-site tRNA (Bashan et al., 2003a; Bashan et al.,

2003b). Therefore, sparsomycin was tested in the archaeal system to reveal a potential positive influence on the stability of the peptidyl-tRNA.

First of all, no effect was detectable on the western blot when sparsomycin was added after translation. In contrast, addition before translation did not inhibit translation, but instead led to a reduction of the observed side products: the higher molecular weight smear as well as the band above the free peptide vanished upon addition of 10-50 μM sparsomycin. The data suggests that sparsomycin interferes with components of a mechanism modifying the free peptide and the nascent chain. The modifications that could be observed under normal translation conditions were severely affected with increasing concentrations of the antibiotic. Sparsomycin binds to the peptidyl-transferase center (Bashan et al., 2003a; Bashan et al., 2003b). The proposed degradation mechanism (see 5.1.2.) might therefore act in close proximity to the peptidyl-transferase center.

Unfortunately, the experiment could not be repeated with a new charge of cells. In all follow up experiments no translation was visible in the presence of sparsomycin. It cannot be excluded that the cells were harvested at a different time point compared to the previous batch of cells and therefore the protein composition inside the extract might have varied. Perhaps the interplay of sparsomycin with the ribosome involves other factors as well and therefore is highly sensitive to changing experimental conditions.

It remains to be seen if the exact experimental conditions can be repeated to further analyze the exact effect of sparsomycin on translating archaeal ribosomes. Also additional data are necessary to investigate the existence of a degrading mechanism in archaea that targets nascent peptide chains on stalled ribosomes. A starting point might be a mass-spec analysis of the observed free peptides after translation of truncated mRNA. These peptides differ in size by 2-3 kDa. Identification of the chemical nature of the modification of the peptide could substantiate the speculation about an archaeal translation associated protein degradation mechanism.

5.1.4. Purification attempts of archaeal RNCs

Several protocols have been published that describe purification strategies for RNCs in eukaryotes and bacteria using affinity purification (Beckmann et al., 2001; Bhushan et al., 2011; Halic et al., 2004; Seidelt et al., 2009). Based on these protocols, conditions were tested for the purification of archaeal RNCs via His- or multiple Strep-tags in the N-terminal part of the nascent peptide chain.

Different constructs have been tested to stall archaeal ribosomes *in vitro*. Even though the presence of peptidyl-tRNA was verified by western blot, it was not possible to enrich the fraction of RNCs in the extract after translation. Neither His- nor Strep-tags could be employed successfully for affinity purification. Interestingly, after release of the nascent chain, the peptide could be purified using a His-tag and a Co^{2+}-matrix. The only difference in the purification protocol was the elevated pH (from pH 7.0 to pH 8.0). The RNC purification is generally performed at pH 7.0 to prevent the peptidyl-tRNA from basic hydrolysis. Therefore, it is unlikely that the pH is the reason for the insufficient binding, since Co^{2+}-matrices have been used before to purify RNCs at comparable buffer conditions via His-tag (Bhushan et al., 2011; Halic et al., 2004; Seidelt et al., 2009). So far it is unknown which property of the RNC is actually interfering with the affinity of the tags.

To rule out the possibility that the affinity of one single tag was too low to actually keep a ribosome attached to the column material or that the localization of the tag on the nascent chain prevented binding, repetitive tags and different tag combinations were tested as well. Up to three Strep-tags in a row were could be still translated, even though the translation rate dropped. In contrast, constructs combining several HA- and Strep-tags were translated at comparable amounts. However, a double Strep-tagged construct (HAStrepHAStrepSecF100) was also not suitable for the enrichment of RNCs. Besides the fact that the RNCs could not be bound to the column material, a loss of signal was apparent on the western blot. After incubation of the pelleted ribosomes with the column material, only a small fraction of the expected signal could be observed on the western blot for all the consecutive wash and elution

steps. Unspecific binding of the ribosomes to the column material as reason for the missing peptidyl-tRNA and free peptide signals could be excluded.

So far, there is no explanation where the majority of the peptidyl-tRNA disappeared. It is possible -even though unlikely- that there are some proteases still present in the sample after the pelleting step. These proteases might digest the nascent peptide and by degradation of the tag interfere with binding to the column and detection by antibodies. This scenario is quite unlikely since it was possible to purify peptides released from the ribosome without any signs of degradation.

In conclusion, the combination of Strep-tags and Strep-Tactin coated magnetic beads seemed to be the most promising approach. With the double Strep-tagged construct it was possible to purify a minor amount of RNCs. Nevertheless the protocol needs to be further optimized; under the chosen experimental conditions the binding efficiency was quite low. Therefore the buffer and binding conditions have to be thoroughly analyzed to achieve a higher affinity between tag and matrix.

In conclusion, the extract prepared from *T. kodakarensis* provides a robust system for *in vitro* translation. It allows expression of variously N- and C-terminally tagged proteins under the control of archaeal or bacterial RBS, with the only exception being constructs with an N-terminal His-tag. It was also possible to program a substantial amount of ribosomes with truncated mRNA as prerequisite for RNC purification. However a reliable protocol for the affinity purification and enrichment of archaeal RNCs could not be established yet.

5.2. Biochemical analysis of archaeal NGD and ribosome recycling homologues

The eukaryotic NGD mechanism comprises several factors that are responsible for recognition of the stalled ribosome (Pelota/Dom34, Hbs1) and ribosomal recycling (ABCE1/Rli1). Homologues of these factors have been identified in archaea as well and the existence of a comparable recycling mechanism can be expected. In the second part of the thesis the archaeal NDG factors aPelota, aEF1α and aABCE1 were biochemically and structurally analyzed to obtain new insights into the general mechanism of NGD.

5.2.1. Interaction of aEF1α and aPelota *in vitro*

In archaea, the translational GTPase aEF1α acts as a delivery factor for aa-tRNAs, the recycling factor aRF1 and also the NDG factor aPelota (Kobayashi et al., 2010). This step requires complex formation of the factors before ribosome binding. Consequently, complex formation of *A. pernix* aEF1α and aPelota and their eukaryotic counterparts Hbs1 and Dom34 have been observed *in vitro* (Chen et al., 2010; Kobayashi et al., 2010). Hence, aEF1α and aPelota also are likely to form a complex before binding to the ribosome. However, gel filtration revealed that *in vitro* complex formation of purified aPelota and aEF1α from *T. kodakarensis* was not possible.

Several explanations are imaginable. The aEF1α preparation did not contain any nucleotides since the protein was refolded from inclusion bodies without adding nucleotides. It is conceivable that an additional protein is needed to load aEF1α with GTP before complex formation with aPelota can be established. However, this would be in contrast to the observations based on complexes from *A. pernix;* GTP that was added to the aPelota-aEF1α sample before crystallization and the incorporation of was verified in the later structure (Kobayashi et al., 2010). Also in eukaryotes, complex formation and crystallization of Dom34 and Hbs1 was achieved without adding nucleotides (Chen et al., 2010). Based on these results it is quite unlikely that an additional factor is required.

Another possibility might be that the refolded protein aEF1α is not active. However, this is quite unlikely since gel filtration revealed that aEF1α is mostly soluble and a monomer. No significant amounts of aggregates were observable during gel filtration. That indicates native folding.

In conclusion, it is probable that the affinity of aEF1α and aPelota in general is quite low. Since aEF1α acts as universal delivery factor also for aa-tRNAs and aRF1 (Kobayashi et al., 2010), the cell must be able to discriminate between these factors. So, likely the affinity of aEF1α for tRNAs is higher than for the specialized factors aPelota and aRF1. This might explain why aEF1α and aPelota do not form a complex in solution.

5.2.2. Binding of aEF1α, aPelota and aABCE1 to the ribosome

The generation of NGD intermediates for cryo-EM required the establishment of adequate buffer conditions that allowed complex formation of ribosome and factors. Complex formation was analyzed by pelleting of ribosomes and interacting factors through a sucrose cushion. Only factors bound to the ribosome were able to co-migrate through the cushion as well. aPelota, aEF1α and aABCE1 alone as well as aPelota-aEF1α or aPelota-aABCE1 were shown to bind to high-salt purified 70S ribosomes in approximately stoichiometric manner. Only a minor effect could be observed upon the addition of nucleotides (GTP) or their non-hydrolysable analogues (GDPNP, ADPNP). The binding of the GTPase aEF1α to the ribosome was slightly enhanced upon addition of GDPNP compared to GTP. However the effect was comparably small, therefore the later 70S-aPelota-aEF1α sample was prepared without nucleotide for cryo-EM. The binding of aPelota was positively influenced by aEF1α. This is in agreement with aEF1α acting as delivery factor for aPelota (Kobayashi et al., 2010). However, aPelota is able to bind to ribosomes without delivery factor as well. This observation is also consistent with the results presented by Pisareva et al. (2011) describing the role of Hbs1, the eukaryotic aEF1α paralog, as auxiliary but not essential in NGD.

The binding of aABCE1 to the ribosome was also slightly favored in the presence of ADPNP as observed for ribosome-binding of aEF1α in presence of GDPNP. The binding of aPelota and aABCE1 seems to be unaffected by the binding of the respective other protein. This finding is in agreement with the current model of ribosome recycling after termination: The termination factor eRF1, a Pelota homologue, is delivered by eRF3, an aEF1α paralog, to the ribosome and the peptide is released. The recycling factor ABCE1 binds at a later time point and induces subunit dissociation.

Taken together, the results confirm that both aPelota-aEF1α and aPelota-aABCE1 indeed form a complex on the ribosome which can be stabilized by non-hydrolysable nucleotide analogs.

5.2.3. *In vitro* ribosome disassembly with aABCE1

Compared to bacterial ribosome recycling, insights about the mechanism in eukaryotes have been obtained just recently. The first factor that could be shown to play a role in post-termination recycling of ribosomes was initiation factor eIF3 (Pisarev et al., 2007). eIF3 belongs to the factors that assemble on the small subunit to from the 43S pre-initiation complex. This complex scans along the mRNA for the start codon. In their publication, Pisarev et al. (2007) showed that eIF3 enhanced by other initiation factors is able to promote energy-free subunit dissociation after termination *in vitro* at 2.5 mM Mg^{2+}. Later studies done by the same group revealed that the ATPase ABCE1 is essential for ribosome dissociation at higher Mg^{2+}-levels and also requires eRF1 for its function (Pisarev et al., 2010). The function of ABCE1 in ribosome recycling is not restricted to post-termination complexes only. ABCE1 has also been shown to facilitate ribosome recycling in NGD acting together with the RF1 homologue Pelota (Dom34 in yeast) (Pisareva et al., 2011). In archaea, a comparable role of aABCE1 in recycling of post-termination complexes together with aRF1 was observed (Barthelme et al., 2011). Interestingly, despite the overall similarity of the observed splitting mechanism of ABCE1 in eukaryotes and

archaea, the role of ATP hydrolysis was not yet clear. While in the eukaryotic system the binding and ATP hydrolysis have been shown to promote splitting (Pisarev et al., 2010; Pisareva et al., 2011; Shoemaker and Green, 2011), the binding of ATP to ABCE1 was assumed to be sufficient for splitting in archaea, while the hydrolysis of ATP is only required for the release of ABCE1 from the small subunit after recycling (Barthelme et al., 2011).

To gain further insight in the splitting behavior of aABCE1 and to validate the functionality of the purified components which were used for cryo-EM reconstructions, *in vitro* splitting assays were performed; idle ribosomes were incubated with the archaeal NGD factor aPelota, the termination factor aRF1 and/or aABCE1, and the influence of ATP and the non-hydrolysable ATP analogue ADPNP was evaluated.

aABCE1 was able to split high salt purified ribosomes *in vitro* in concert with aRF1 or aPelota under high Mg^{2+} (25 mM) concentrations. In retrospect, the cryo-EM reconstructions of 70s-aPelota-aABCE1 and 70s-aPelota-aEF1α revealed that a significant amount of ribosomes contained tRNA in the A, P and E site. Therefore it can be assumed that these ribosomes represent different states of translation. Obviously, the archaeal cells that were harvested at late log phase contained a substantial amount of translating ribosomes or ribosomes stalled by aberrant mRNA. The mixture of ribosomes in unknown translation states might also include physiological substrates for aPelota-aABCE1 or aRF1-aABCE1. Observations in the mammalian system as well as in yeast revealed that Pelota, Hbs1 and ABCE1 are able to split efficiently idle ribosomes (Pisareva et al., 2011; Shoemaker and Green, 2011); in contrast, eRF1, eRF3 and ABCE1 did only dissociate post-termination complexes (Pisareva et al., 2011). This observation could not be confirmed here, since no significant difference in the splitting efficiency of aRF1-aABCE1 or aPelota-aABCE1 was apparent. However, since the exact programming state of the ribosomes present in the sample cannot be assessed, no conclusion can be obtained regarding the translation state specificity of aRF1-aABCE1 or aPelota-aABCE1.

In contrast to the eukaryotic system, where splitting was greatly reduced at higher Mg^{2+} levels (only 15% at 20 mM Mg^{2+}), the archaeal system seemed to be more tolerant to high Mg^{2+} levels and ribosomes were split even at 25 mM Mg^{2+}.

Notably, in the splitting experiment, the addition of the A-site factors aPelota or aRF1 alone led to a stabilization of the ribosome and decreased the probability for splitting. With respect to the localization of the factors that was determined in the later cryo-EM structures, aPelota and aRF1 alone act as an additional bridge between the subunits in the A site and reduce the degree of freedom for the movement of one subunit against the other. Therefore the possibility of autonomous splitting is reduced.

Interestingly, a similar observation could be made in the experiment with a sample containing aABCE1, A-site factor and non-hydrolysable ADPNP. The ratio of subunits to ribosomes was below background level and similar to the ratio obtained with A-site factors alone. This outcome is in contrast to the recently proposed model for termination in archaea (Barthelme et al., 2011). The authors suggest that the binding of ATP/ADPNP induces splitting and the hydrolysis is only required to release aABCE1 from the small subunit. This model does not explain the observed results. Assuming that the binding of the ATP-analog would be sufficient for splitting, significant splitting and not stabilization of the ribosomes should be observed. aABCE1 was added in 5 × molar excess in the experiment, therefore the splitting effect should be apparent even under the assumption that aABCE1 remains bound to the 30S subunit after splitting and therefore every aABCE1 molecule can only dissociate one ribosome. Therefore, the results observed here are clearly contradicting the model by Barthelme et al. (2011) and are more in agreement with the model proposed for eukaryotic system where ATP binding and hydrolysis is required for splitting (Pisarev et al., 2010; Pisareva et al., 2011; Shoemaker and Green, 2011).

Closer inspection of the experiment that was performed by Barthelme et al. revealed that an alternative interpretation of the data in agreement with the results obtained here is conceivable; for better comparison, the layout and the results of the respective experiment are depicted in Fig. 26.
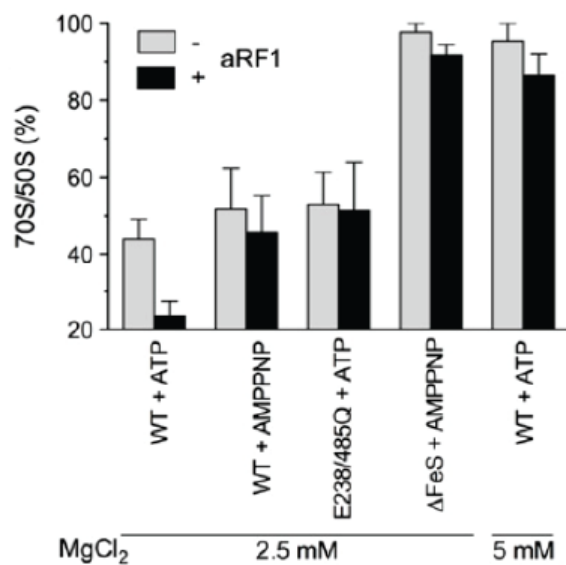
Figure 26: *In vitro* splitting of 70S ribosomes performed by Barthelme et al. (2011). Isolated 70S ribosomes from *T. celer* were incubated with equimolar amounts of aABCE1 in the presence and absence of aRF1 for 4 min at 73°C and different nucleotides. aIF6 was added to prevent re-association of the subunits. Data was analyzed by sucrose density centrifugation. The 70S/50s ratio in the absence of aABCE1 served as control (100%). Experiments were performed in duplicates.

The authors analyzed in the experiment the splitting ability of wild-type aABCE1, a ΔFes-mutant and a NBD-mutant (ABCE1[E238/485Q]) that is permanently in the ATP-occluded closed state in concert with aRF1 using ATP or ADPNP. The ratio of 70S/50S was used for assessing the amount of dissociated ribosomes. Taking the standard deviation into consideration, the only sample that showed a significant difference in the splitting behavior in presence and absence of aRF1 is the sample containing wild type aABCE1 with ATP in a buffer containing 2.5 mM $MgCl_2$ (Fig. 26, "WT + ATP"). The difference in the splitting efficiency added up to approximately 20%. The 70S/50S ratios observed in the other experiments correlated with the ratio observed by using only aABCE1 and ADPNP (Fig. 26, "WT + AMPPNP") or the ratio of the NBD-mutant in the ATP-occluded state (Fig. 26, "E238/485Q + ATP"). In the remaining two set-ups (Fig. 26, "ΔFes + AMPPNP", "WT + ATP (5 mM $MgCl_2$)") the 70S/50S ratio corresponded to the background (without aABCE1) and revealed no significant difference in the absence or presence of aRF1.

Since aABCE1 is only able to split ribosomes in concert with an A-site factor like Pelota or RF1 (Pisarev et al., 2010; Pisareva et al., 2011; Shoemaker and Green, 2011) the only valid readout can be obtained from the "WT + ATP" sample where a significant difference in the splitting efficiency depending on the presence and absence of aRF1 can be seen. Assuming that the readout of the experiment without aRF1 corresponds to the amount of ribosomes that split autonomously, the remaining results do not provide any signs of active splitting by aABCE1.

With this interpretation the experiments do indeed favor a universal splitting mechanism by ABCE1 in eukaryotes and archaea.

In conclusion, the ribosome dissociation experiment indicated clearly that the recycling factors aPelota, aRF1 and aABCE1 are functional and can efficiently split ribosomes. In addition, the results favor a universal recycling mechanism by aABCE1 in archaea and eukaryotes that is dependent on ATP hydrolysis for ribosome dissociation.

5.3. Functional implication of cryo-EM reconstructions of archaeal NGD intermediates

Cryo-EM has been employed successfully to solve the structure of the NGD factors Dom34 and Hbs1 bound to SL-RNCs in yeast (Becker et al., 2011). This provided valuable insights into the recognition state of NGD. Dom34, the yeast homologue of Pelota, is being delivered by the translational GTPase Hbs1 and binds to the ribosomal A site. Hbs1 is located in the factor binding site. Interestingly, both components are in close vicinity to the mRNA path. These contacts might be responsible for the recognition of stalled ribosomes. Now the question remains, what is actually happening between recognition of the stalled ribosome and recycling? Where does ABCE1, which has been shown to be involved in recycling of eukaryotic and archaeal ribosomes, actually bind to the ribosome and how does it promote subunit dissociation? Since archaea do also possess NGD factors and the involvement of aABCE1 in

archaeal ribosome recycling has been shown before (Barthelme et al., 2011), cryo-EM structures obtained from archaea were calculated to gain further insight into the obviously evolutionary conserved process of ribosome recycling.

5.3.1. Cryo-EM reconstructions of archaeal NGD intermediates

The 70S-aPelota-aEF1α and the 70S-aPelota-aABCE1 dataset could be successfully processed revealing four reconstructions differing in ligand occupancy and translational state of the ribosome. In both datasets, the initial data contained particles that weren't ribosomes or of inferior quality. These particles were identified and eliminated by subsequent sorting steps. The non-ribosomal particles comprise ice or ethane blobs on the grid that weren't correctly classified by the particle picking algorithm MAPPOS. The remaining ribosomal particles needed to be sub-sorted for quality reasons. Low quality reconstructions of ribosomes with unstructured surface were obtained during sorting. It is possible that these low quality maps were based on ribosomal particles that suffered from beam damage or that were embedded in thicker ice. The remaining data was refined and resulted in unambiguous reconstructions.

The 70S-aPelota-aABCE1 dataset could be processed to two final ribosomal reconstructions at a resolution of 6.6 and 7.4 Å, respectively. The first reconstruction revealed aABCE1 binding at the canonical factor binding site and aPelota at the ribosomal A site. P- and E-site tRNA could also be modeled unambiguously. The second reconstruction accommodated tRNAs at the A, P and E site of the ribosome. Since all tRNAs are present in this map, the ribosome is most likely in a pre-translocation state. In this state, the ribosome has typically bound A-site and P-site tRNA and the nascent chain is already transferred to the acceptor stem of the A-site tRNA (Agirrezabala et al., 2008; Julian et al., 2008). The location of the peptide chain could not be determined since no additional density was visible. Under the presented experimental conditions, the ribosomes are not programmed with a specific mRNA but rather represent a snapshot of the ongoing cellular translation at the moment of harvesting. The diversity of the

nascent chains might lead to a flexible position inside the exit tunnel, and therefore escape detection at the given resolution. The map also showed a weak density presumably representing aABCE1 at the factor binding site. This density might correspond to aABCE1 binding flexibly or only transiently to the ribosome in the pre-translocation state. This is in good agreement with the fact that ABCE1 only acts on ribosomes together with splitting factors like RF1 or Pelota (Barthelme et al., 2011; Pisarev et al., 2010; Pisareva et al., 2011).

The 70S-aPelota-aEF1α dataset revealed two distinct reconstructions at a resolution of 9.3 and 9.4 Å, respectively. The first reconstruction revealed aPelota in the A site and P- and E-site tRNAs. No additional density was present at the factor binding site. The second reconstruction showed a ratcheted conformation of the 30S subunit and accordingly a hybrid state P-/E-tRNA. Interestingly, the second tRNA was not accommodated in an A-/P-hybrid state, instead it was occupying the canonical ribosomal A site. At the factor binding site, a barely resolved density was observed. This density was interpreted as aEF1α that was flexibly bound to the ribosome.

The analysis of difference maps revealed interesting changes of the ribosome conformation depending on the interacting factors. Obviously, the binding of aPelota and aPelota-aABCE1 required or induced a movement of the 30S body contrary to the ratchet movement which was most obvious when both factors were bound. Neither aABCE1 nor aPelota have been found associated with ratcheted ribosomes. This observation is also valid in the yeast system. In the process of sorting the SL-RNC-Dom34-Hbs1 dataset, a ribosome map with a ratcheted conformation was observed. Likewise, Dom34, the yeast Pelota homologue, was only found on the non-ratcheted ribosome reconstruction (Becker et al., 2011). Biochemical analyses in mammals also confirm these findings. Pelota and ABCE1 can only split ribosomes in the post-translocation state or idle ribosomes, indicating a non-ratcheted orientation of the subunits (Pisareva et al., 2011).

The conformation of the ribosome seemed to affect also the binding of aEF1α. Even though the observed density did not allow any interpretation of the exact interaction of the translational GTPase and the ribosome, the density was observed only on the ratcheted ribosome. The ratcheted 30S subunit seemed to provide a platform that allowed aEF1 to bind to the ribosome

in a flexible manner. Whether the ratcheting of the 30S subunit favored binding of aEF1α compared to ribosomes in the unratcheted state or whether the presence of aPelota in the A site interfered with aEF1α binding cannot be elucidated here. Notably, aPelota and aEF1α, even though they are known to form a complex, were not found to bind at the ribosome at the same time.

In comparison, in the yeast system a reconstruction of Dom34 and Hbs1 bound to SL-RNCs could be obtained and revealed a close interaction of Dom34 and Hbs1 (Becker et al., 2011). Here, the sample contained the GTP analog GDPNP. Even though the reconstitution assays (4.2.3.) did not reveal a substantial difference in aEF1α binding to the ribosome with and without GDPNP, it is quite likely, that the rigid binding of aEF1α requires the presence of a non-hydrolysable nucleotide.

To further analyze the binding behavior of aEF1α regarding the conformation of the ribosome and revealing any interaction with aPelota, a new sample with GDPNP has to be prepared and analyzed.

5.3.2. Ratchet movement of the small subunit

In eukaryotes, only a few structures of ribosomes in the ratcheted state are known so far. A crystal structure of a ratcheted ribosome from yeast does not contain any tRNA molecules (Ben-Shem et al., 2010) and the cryo-EM structure of a ribosome from *Thermomyces lanuginosus* with elongation factor eEF2 bound contains only P-/E-hybrid tRNA (Spahn et al., 2004; Taylor et al., 2007). However, some insights into the dynamics of tRNA in the eukaryotic ribosome can be derived from the cryo-EM structures of mammalian pre-translocation complexes (Budkevich et al., 2011). Besides two distinct classical states, two additional structures were obtained that comprise ratcheted ribosomes. The first structure revealed A-/P- and P-/E-hybrid tRNA, the second A-site and P-/E-hybrid tRNA. Structures of bacterial ribosomes in the ratcheting state are often favoring both tRNAs in hybrid positions

(Agirrezabala et al., 2008; Bhushan et al., 2011) or include a factor that occludes the A site and stabilizes the hybrid conformation of the P-/E-tRNA like the ribosomal recycling factor (RRF) or the bacterial release factor RF3 (Dunkle et al., 2011; Jin et al., 2011). More recently also structures comprising intermediate steps including A-site tRNA in combination with P-/E-hybrid state tRNA have been visualized. The first structure was a cryo-EM structure of a retro-translocation complex. The complex was generated by mixing deacylated tRNA[fMet] with ribosomes that contained P-site tRNA. The deacylated tRNA bound at the E site and induced retro-translocation (Fischer et al., 2010). Another group described a mutation of the P-loop in the PTC which enhanced the probability for the formation of P-/E-hybrid tRNA while simultaneously stabilizing the classical A-site tRNA conformation (Fu et al., 2011).

The dataset comprising 70S ribosomes, aPelota and aEF1α led to an additional reconstruction of a ribosome with a ratcheted 30S subunit. The ratcheting comprises an upward movement of the body and head swiveling towards the 50S subunit. Notably, the map revealed that one tRNA occupied a hybrid P-/E- position while a second tRNA was accommodated in the canonical A site position. A comparison with the cryo-EM structure containing canonical A-, P-, and E-site tRNA revealed that the anticodon loop of the A-site tRNA in the ratcheted ribosome was slightly translocated towards the 30S P site following the movement of the 30S head. The position of the acceptor stem was essentially unaltered.

The observed arrangement is in agreement with the current model of loosely coupled movement of the tRNAs through the ribosome. It is possible that the high Mg^{2+} concentration (50mM) in the sample stabilized the observed conformation. A high Mg^{2+} concentration is known to reduce the rate of tRNA dynamics (Blanchard et al., 2004). It was also observed that high Mg^{2+} concentrations favor the observed classical A- and P-/E- hybrid state in case of the P-loop mutation in *E. coli* (Fu et al., 2011).

Taken together, the structure presents the first archaeal ribosome in a ratcheted conformation. The arrangement of tRNAs in a A- and P-/E-hybrid position as reported from eukaryotic and bacterial ribosomal structures is also valid for archaea under the given experimental conditions.

5.3.3. Comparison with a yeast SL-RNC-Rli1-Dom34 reconstruction

A cryo-EM structure of SL-RNCs with Rli1 and Dom34, the yeast homologues of aABCE1 and Pelota, could be obtained by Thomas Becker at a resolution of 7.2 Å. This allowed a detailed comparison of a NGD intermediate in archaea and eukaryotes. Strikingly, the structures displayed a high similarity. The location of the factors on the ribosome is virtually identical and their interaction with the ribosome for the most part conserved. Only a few additional contacts are visible in the yeast reconstruction and the intrinsic domain arrangement of Dom34 differs slightly from aPelota. This is in agreement with the minor degree of conservation of these proteins compared to ABCE1. However, the loop of the central domain is contacting the acceptor stem of the P-site tRNA in both cases in a comparable manner. This observation supports the theory of a highly conserved NGD mechanism in these two domains of life.

ABCE1 binds to the ribosomes in the factor binding site where also Hbs1 binding was observed in the according SL-RNC-Dom34-Hbs cryo-EM structure (Becker et al., 2011). Therefore, the translational GTPase Hbs1 has to dissociate before binding of aABCE1. The same course of events can be assumed for aEF1α the delivery factor for aPelota and aABCE1 in archaea.

5.3.4. A homology based model for RF1

The ribosome release factor RF1 is a paralogue of Pelota and is present in archaea and eukaryotes. The protein is involved in translation termination and recycling of post-termination complexes together with ABCE1 (Barthelme et al., 2011; Pisarev et al., 2010; Shoemaker and Green, 2011). Based on the cryo-EM structures of Pelota-ABCE1 bound to ribosomes in yeast and archaea and the published yeast SL-RNC-Dom34-Hbs1 structure (Becker et al., 2011), it is tempting to assume a similar rearrangement of the central domain of RF1 on the ribosome depending on the interaction with the delivery factor eRF3 or ABCE1 (Fig. 27, C).
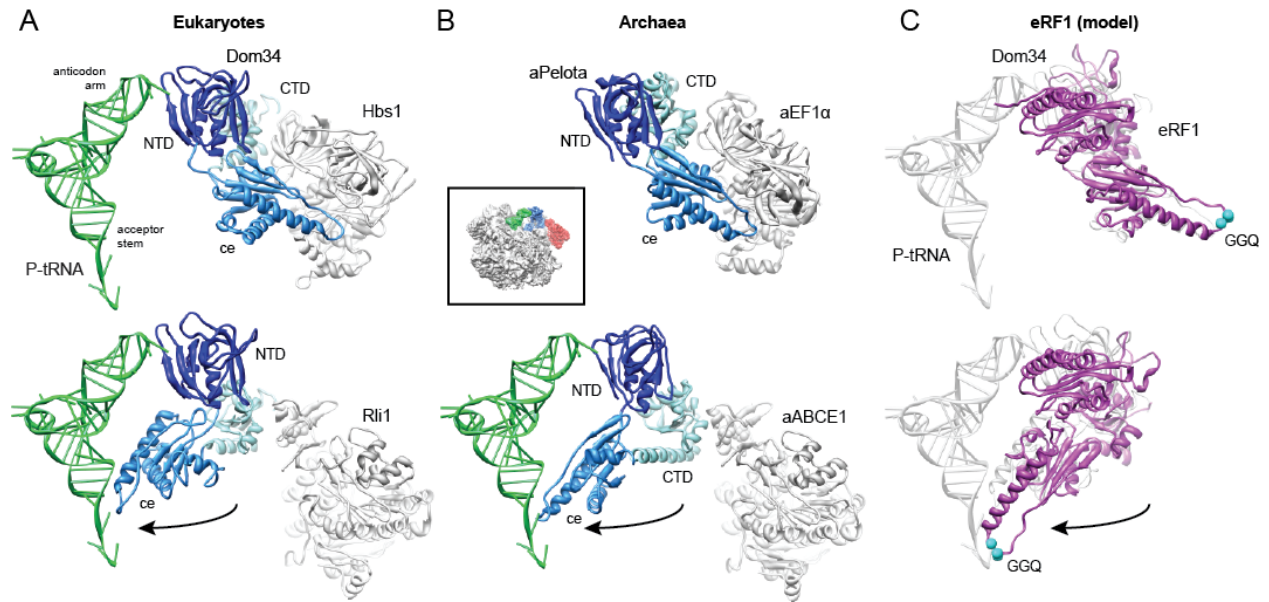
Figure 27: Domain movements in Pelota and eRF1. View is indicated by a thumbnail. (**A**) Comparison of the ribosome-bound Dom34 conformation in complex with Hbs1 (top section) and Rli1 (lower section). (**B**) Comparison of the aPelota-aEF1α crystal structure (Kobayashi et al., 2010) with the ribosome-bound aPelota in complex with aABCE1. In both archaea and eukaryotes, the central domain of Pelota swings out towards the P-site tRNA. (**C**) Models for eRF1 before and after the suggested movement of the central domain.

The central domain of RF1 corresponds to the central domain of Pelota and contains a GGQ motif at the tip of the loop. This motif is essential for catalyzing the hydrolysis of the peptide chain from the peptidyl-tRNA (Frolova et al., 1999; Song et al., 2000). RF1 is delivered to the ribosome by eRF3 in eukaryotes (Frolova et al., 1996) and presumably aEF1α in archaea (Saito et al., 2010). In this state, the central domain and therefore the GGQ motif of RF1 would be interacting with the delivery factor. Upon release of eRF3/aEF1α the central domain would be able to swing towards the PTC as observed in the 70S-aPelota structure. In this position the GGQ motif of RF1 would be ideally positioned to interact with the CCA-end of the P-site peptidyl-tRNA. The binding of ABCE1 then further stabilizes the postulated conformation (Fig. 27, A, B). This model offers an explanation how GTP hydrolysis of eRF3 already promotes termination activity of eRF1 (Alkalaeva et al., 2006) and also ABCE1 further stimulates peptide release *in vivo* and *in vitro* (Khoshnevis et al., 2010; Shoemaker and Green, 2011).

This model still needs to be validated with according cryo-EM structures. In archaea, structures consisting of a 70S-aRF1-aEF1α complex and a 70S-aRF1-aABCE1 complex might provide further insight in peptide release and RF1-dependent recycling of post-termination complexes.

5.3.5. Functional implications for aABCE1-induced splitting

Typically, ABC proteins generate mechanochemical work by nucleotide driven tweezer like motions of the two NBDs: in the apo- or ADP-bound state, NBDs adopt an open conformation often linked to a higher affinity for the given substrate of the ABC enzyme. ATP-binding and subsequent ATP-hydrolysis lead to a "power stroke" that usually causes concomitant conformational changes in connected domains or binding partners.

The archaeal and also yeast cryo-EM reconstructions revealed an intermediate half-open state concerning the arrangement of the two NBDs. The state differs clearly from the ADP-bound crystal structure where the two NBDs of aABCE1 are arranged in an open configuration (Karcher et al., 2008) and a model of an ATP bound closed state. Notably, the conformation of the individual lobes is similar to the crystal structure suggesting that two molecules of ADP and not ADPNP are bound to the respective domains. Since ATP hydrolysis is required for full splitting activity (Pisarev et al., 2010; Pisareva et al., 2011) it is obvious that ABCE1 has to undergo a conversion from the observed half-open pre-splitting conformation to the fully closed ATP state in order to efficiently dissociate ribosomes. In order to investigate how domain closure might induce splitting, the half-open ribosome-bound state of ABCE1 was superimposed with the model for the closed-state. In fact, in the closed conformation ABCE1 would not sterically clash with the ribosomal subunits, indicating no direct affect of ABCE1. Instead, two models are conceivable that explain possible splitting mechanisms. One possibility is that the small and large ribosomal subunits simply follow the trajectory of NBD1 and NBD2 of ABCE1, respectively. In this case, the ribosomal subunits would sufficiently rotate away from each other so as to affect the inter-subunit bridges and, thus, the overall ribosome stability (Fig. 28, A).
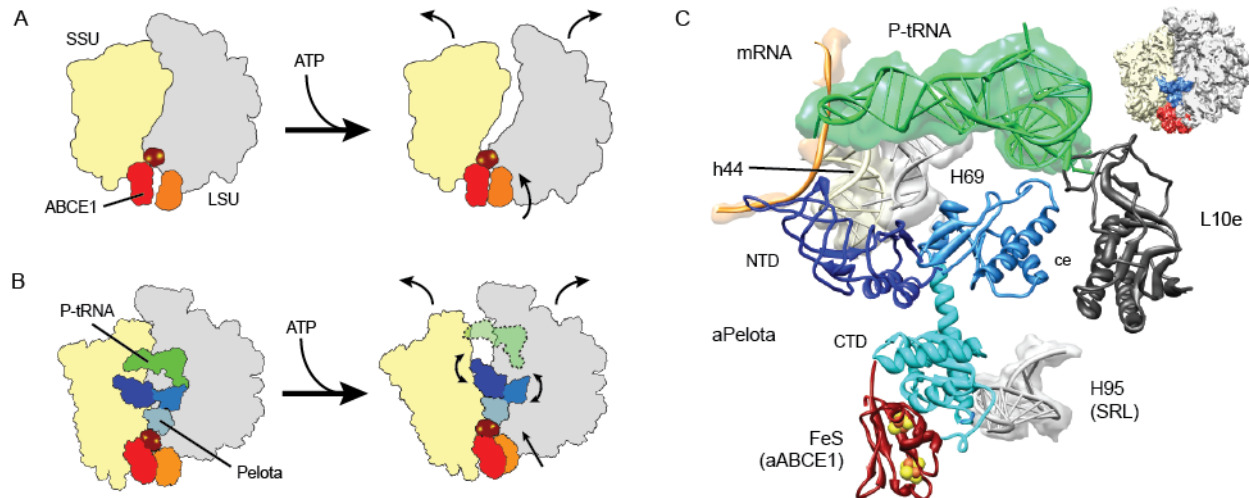
Figure 28: Mechanochemical activity of ABCE1 on the ribosome. (A) Ribosomal subunits may be dissociated by following the trajectory of ABCE1 domain closure upon ATP-binding. **(B)** ABCE1 domain closure could also lead to an allosteric cascade with the FeS domain acting as a bolt on the CTD of Pelota to rearrange the NTD and central domain of Pelota. **(C)** Interactions of aPelota NTD and central domain within the archaeal ribosome with the P-site tRNA, L10e and H69 of the large ribosomal subunit and h44 of the small ribosomal subunit. View is indicated by a thumbnail.

It is more likely, however, that the transition of ABCE1 through the closed conformation triggers an allosteric cascade affecting Pelota: Notably, in the ribosome-bound conformation the FeS cluster domain already establishes a new contact to the NBD2 domain and has to follow the movement of the NBD2 during closure. This conformational change of the FeS cluster domain towards the intersubunit space is likely to be transmitted to Pelota via the close interaction with its CTD. A shift of the CTD would in turn be transmitted to both the NTD and the central domain of Pelota. The Pelota domains establish a network of contacts with the small and the large ribosomal subunit as well as with the P-site tRNA (Fig. 28, B, C). A conformational shift can be easily envisaged to cause dissociation of the ribosome by destabilizing inter-subunit bridges and the P-site tRNA. A function of the FeS cluster domain of ABCE1 as a structural bolt to remodel Pelota by transmitting ATP induced changes from the NBDs is in good agreement with the finding that deletion of this domain abolishes splitting activity (Barthelme et al., 2011) (see Suppl. Table). The second model also takes the active involvement of an A-site factor into account. Several authors and also the biochemical data obtained here demonstrated the importance of an A site factor for ABCE1 induced subunit dissociation (Pisarev et al., 2010;

Pisareva et al., 2011; Shoemaker and Green, 2011). Along these lines, mutation of residues in the NTD and the central domain of Pelota that are involved in ribosomal contacts have been shown to abolish the activity of Pelota (see Suppl. Table).

5.3.6. A model for recycling in eukaryotes and archaea

The cryo-EM and biochemical data obtained in archaea and yeast provided a structural basis and a universal mechanistic model for eukaryotic and archaeal recycling in which ABCE1 actively coordinates rescue (or translation termination) with recycling and re-initiation (Fig. 29).

In the first stage, the recognition stage, the sensing factors Pelota (for rescue) or RF1 (for termination) are delivered to stalled ribosomes or pre-termination complexes by EF-Tu like GTPases. In the next step, the GTPase dissociates. The central domain of the A site factor is able to swing towards the P-site tRNA. ABCE1 interacts with the CTD of Pelota or RF1 to stabilize the extended conformation of the central domain. In the case of translation termination, the GGQ motif of RF1 will be positioned proximal to the CCA-end of the P-site tRNA to catalyze peptide release; in the case of ribosome rescue, the central domain will be tightly accommodated proximal to the PTC. Subsequently, in both cases, ABCE1 triggers ribosome disassembly into subunits by a power stroke upon ATP-dependent NBD domain closure and ATP hydrolysis (Pisareva et al., 2011). This conformational switch could cause either a direct disruption of the ribosomal intersubunit bridges or, more likely, further conformational changes via an allosteric cascade from the ABCE1 FeS cluster domain to the central domain and NTD of Pelota. In the archaeal system ABCE1 remains bound to the small ribosomal subunit after splitting (Barthelme et al., 2011) and it has been also found on the small ribosomal subunit also in eukaryotes (Andersen and Leevers, 2007; Dong et al., 2004). Notably, ribosome recycling is coupled in eukaryotes with re-initiation when initiation factors such as eIF3, eIF1 and eIF1A bind the small ribosomal subunit as recycling is completed (Pisarev et al., 2007). An initial recruitment of eIF3 to the 80S ribosome may even occur directly via ABCE1 interaction with the eIF3 subunit eIF3j

(Hcr1p in yeast), even before recycling is completed (Khoshnevis et al., 2010; Kispal et al., 2005; Yarunin et al., 2005).
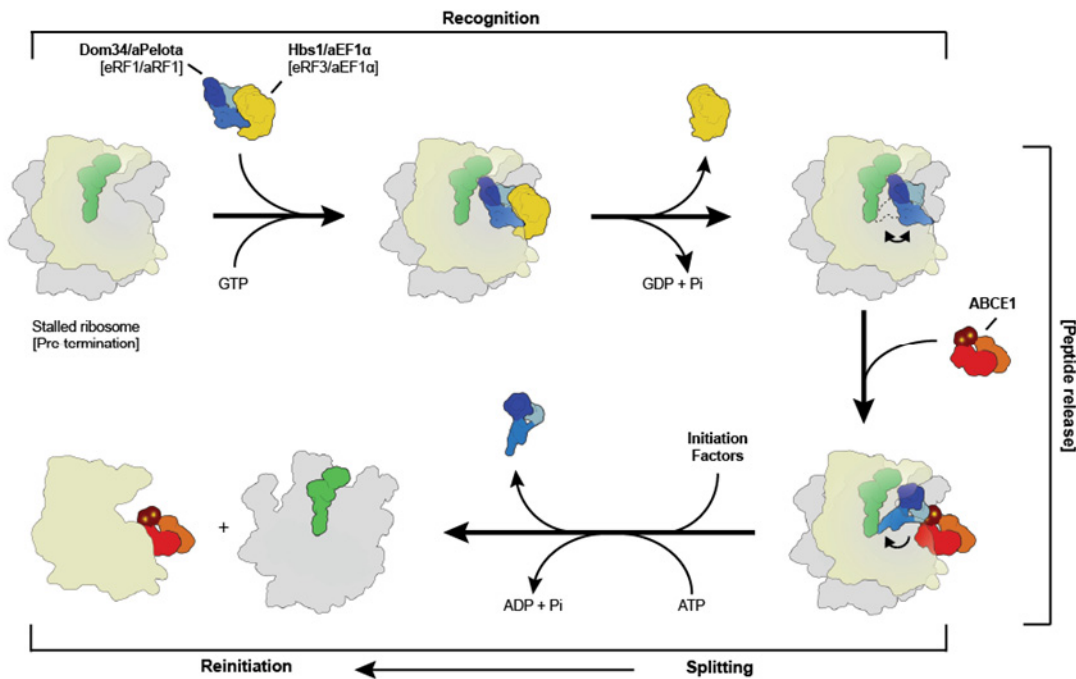

Figure 29: Scheme of archaeal and eukaryotic ribosome recycling bridging termination with re-initiation. A translational GTPAse (Hbs1/ aEF1α/eRF3) delivers the factor which recognizes stalled ribosomes (Pelota) or pre-termination complexes (eRF1/aRF1). After GTP hydrolysis, the GTPase dissociates and ABCE1 can bind. ABCE1 induces or stabilizes the swung out conformation of Pelota (eRF1/aRF1) which would lead to peptide release in case of termination. Ribosome splitting is induced after ATP-binding to ABCE1 and closure of its NBD domains. In eukaryotes, initiation factors can bind during the splitting reaction coupling ribosome recycling with re-initiation. After splitting ABCE1 stays associated with the small ribosomal subunit.

In conclusion, the archaeal and eukaryotic kingdoms have maintained an extremely conserved general ribosome recycling system with an ABC-type ATPase at the core: the mechanochemical properties of ABCE1 are employed through a still enigmatic FeS cluster domain. This domain triggers an allosteric cascade that actively coordinates translation termination or rescue with recycling, and eventually with re-initiation.

5.3.7. Comparison with bacterial recycling

It is interesting to compare the proposed model for eukaryotic and archaeal translation with the mechanism that is known in bacteria. In bacteria not only one, but two A-site factors, RF1 and RF2 which differ in their stop codon specificity, are responsible for termination (Scolnick et al., 1968). RF1 and RF2 are neither sequentially nor structurally related with the eukaryotic or archaeal aRF1. Nevertheless, the mechanism of hydrolysis seems to be conserved since it also involves a conserved GGQ motif (Mora et al., 2003). A homologue of EF-Tu, RF3, is involved in the process, but in contrast to the eukaryotic and archaeal system, RF3 does not deliver RF1 and RF2 but instead accelerates the dissociation of the factors after hydrolysis of the peptidyl-tRNA (Freistroffer et al., 1997). Interestingly, a cryo-EM structure of RF3 bound to the ribosome revealed that the ribosomal subunits are rotated relative to one another and the 30S subunit is found in a ratcheted conformation (Gao et al., 2007). RF1 or RF2 catalyze hydrolysis of the peptidyl-tRNA and dissociate from the ribosome. The factors are not involved in recycling. Recycling is conducted by the bacterial ribosomal recycling factor RRF. RRF binds to the ribosome and also stabilizes the ratcheted conformation. Structural data revealed that RRF binds in the tRNA binding cleft and stabilizes the tRNA in a P-/E-hybrid position (Dunkle et al., 2011). Now EF-G, a translational GTPase, is supposed to promote subunit dissociation inducing a conformational change in RRF. RRF then sterically clashes with the 30S subunit and promotes subunit dissociation (Gao et al., 2005). The participation of initiation factors in bacterial recycling factors is still under debate (Pavlov et al., 2008).

Interestingly, in bacteria there is no tRNA mimicry of factors involved in termination and recycling. The overall shape of RF1 and RF2 evolved differently. Also in bacteria, peptide release and ribosome recycling requires a ratcheted conformation while in the archaeal ribosome data have shown that the non-ratcheted state is required – at least in NGD. Due to the high degree of structural conservation between Pelota and RF1, it is quite likely that the release and splitting mechanism after termination involving RF1 also requires the ribosomal subunits in an unratcheted state. This will be hopefully ascertained in the near future by solving cryo-EM

structures of archaeal ribosomes with aRF1 in complex with the delivery factor aEF1α or the recycling factor aABCE1.

5.3.8. NDG – the earliest form of mRNA surveillance?

The observation that ABCE1 and Pelota can be found from archaea to eukaryotes interacting with the ribosome in a virtually identical manner indicates an evolutionary strongly conserved mechanism. It is suggestive, that the mRNA surveillance mechanism identified as NGD might be the first mRNA surveillance mechanism that evolved in the eukaryotic and archaeal lineage at all (Atkinson et al., 2008). The other eukaryotic mechanisms - NSD and NMD - might have evolved at a later time point. The hypothesis is supported by the structural data obtained in this work and by biochemical evidence: It has been found that the components of NGD can at least partially complement NSD and NMD knock-outs *in vitro* (Doma and Parker, 2006; Kobayashi et al., 2010). Along with these lines, it can be speculated that aABCE1s essential function might actually be its involvement in ribosome recycling.

6. Summary

Translation associated processes in eukaryotes often contain highly conserved core components that can be identified in archaea as well. In this study, archaea were tested as model organisms to biochemically and structurally analyze translation intermediates using cryo-electron microscopy. Since ribosome-nascent chain-complexes are essential for reconstitution of translation intermediate complexes *in vitro*, a translation assay was established that allowed stalling of ribosomes with truncated mRNA. However, a suitable protocol for purification and enrichment of ribosome-nascent chain-complexes could not be obtained.

Nevertheless, cryo-electron microscopy and single particle analysis of idle ribosomes revealed a substantial amount of endogenous programming. Thereby, reconstitution of archaeal translation intermediates was possible without further enrichment of ribosome-nascent chain-complexes.

In the second part of this thesis, the essential ATPase ABCE1 that is present in eukaryotes and archaea has been functionally and structurally analyzed in the archaeal system. ABCE1 has been shown to be involved in recycling of ribosomes after termination and in the no-go decay mRNA surveillance mechanism. As reported in the eukaryotic system, *in vitro* disassembly of archaeal ribosomes requires ATP hydrolysis for the concomitant action of aABCE1 and an A-site factor (aRF1 or aPelota).

Cryo-electron microscopy structures of no-go decay intermediates containing aABCE1 and aPelota bound to 70S ribosomes were generated. These structures allowed the unambiguous docking of molecular models and revealed in concordance with the biochemical data a high degree of conservation between archaea and eukaryotes. These findings allowed proposing a model for a universal recycling mechanism.

7. References

Adrian, M., Dubochet, J., Lepault, J., and McDowall, A.W. (1984). Cryo-electron microscopy of viruses. Nature *308*, 32-36.

Agirrezabala, X., Lei, J., Brunelle, J., Ortiz-Meoz, R., Green, R., and Frank, J. (2008). Visualization of the hybrid state of tRNA binding promoted by spontaneous ratcheting of the ribosome. Mol. Cell *32*, 190-197.

Alkalaeva, E.Z., Pisarev, A.V., Frolova, L.Y., Kisselev, L.L., and Pestova, T.V. (2006). *In vitro* reconstitution of eukaryotic translation reveals cooperativity between release factors eRF1 and eRF3. Cell *125*, 1125-1136.

Allen, G.S., and Frank, J. (2007). Structural insights on the translation initiation complex: ghosts of a universal initiation complex. Mol. Microbiol. *63*, 941-950.

Amrani, N., Ganesan, R., Kervestin, S., Mangus, D., Ghosh, S., and Jacobson, A. (2004). A faux 3'-UTR promotes aberrant termination and triggers nonsense-mediated mRNA decay. Nature *432*, 112 - 118.

Andersen, C., Becker, T., Blau, M., Anand, M., Halic, M., Balar, B., Mielke, T., Boesen, T., Pedersen, J., Spahn, C.*,* Kinzy, T.G., Andersen, G.R., and Beckmann, R. (2006). Structure of eEF3 and the mechanism of transfer RNA release from the E-site. Nature *443,* 663-668.

Andersen, D., and Leevers, S. (2007). The essential drosophila ATP-binding cassette domain protein, Pixie, binds the 40 S ribosome in an ATP-dependent manner and is required for translation initiation. J. Biol. Chem. *282*, 14752-14760.

Armache, J.P., Jarasch, A., Anger, A.M., Villa, E., Becker, T., Bhushan, S., Jossinet, F., Habeck, M., Dindar, G., Franckenberg, S.*,* Marqez, V., Mielke, T., Thomm, M., Berninghausen, O., Beatrix, B., Soding, J., Westhof, E., Wilson, D.N., and Beckmann, R. (2010a). Cryo-EM structure and rRNA model of a translating eukaryotic 80S ribosome at 5.5-Å resolution. Proc. Natl. Acad. Sci. *107*, 19748-19753.

Armache, J.P., Jarasch, A., Anger, A.M., Villa, E., Becker, T., Bhushan, S., Jossinet, F., Habeck, M., Dindar, G., Franckenberg, S.*,* Marqez, V., Mielke, T., Thomm, M., Berninghausen, O., Beatrix, B., Soding, J., Westhof, E., Wilson, D.N., and Beckmann, R. (2010b). Localization of eukaryote-specific ribosomal proteins in a 5.5-Å cryo-EM map of the 80S eukaryotic ribosome. Proc. Natl. Acad. Sci. *107*, 19754-19759.

Atkinson, G., Baldauf, S., and Hauryliuk, V. (2008). Evolution of nonstop, no-go and nonsense-mediated mRNA decay and their termination factor-derived components. BMC Evol. Biol. *8*, 290.

Auer, J., Spicker, G., and Bock, A. (1991). Presence of a gene in the archaebacterium *Methanococcus vannielii* homologous to secY of eubacteria. Biochimie *73*, 683-688.

Avery, P., Vicente-Crespo, M., Francis, D., Nashchekina, O., Alonso, C.R., and Palacios, I.M. (2011). Drosophila Upf1 and Upf2 loss of function inhibits cell growth and causes animal death in a Upf3-independent manner. RNA *17*, 624-638.

Ban, N., Nissen, P., Hansen, J., Capel, M., Moore, P.B., and Steitz, T.A. (1999). Placement of protein and RNA structures into a 5 Å-resolution map of the 50S ribosomal subunit. Nature *400*, 841-847.

Ban, N., Nissen, P., Hansen, J., Moore, P.B., and Steitz, T.A. (2000). The complete atomic structure of the large ribosomal subunit at 2.4 Å resolution. Science *289*, 905-920.

Barthelme, D., Dinkelaker, S., Albers, S.V., Londei, P., Ermler, U., and Tampe, R. (2011). Ribosome recycling depends on a mechanistic link between the FeS cluster domain and a conformational switch of the twin-ATPase ABCE1. Proc. Natl. Acad. Sci. .

Barthelme, D., Scheele, U., Dinkelaker, S., Janoschka, A., Macmillan, F., Albers, S.V., Driessen, A.J., Stagni, M.S., Bill, E., Meyer-Klaucke, W., Schunemann, V., and Tampe, R. (2007). Structural organization of essential iron-sulfur clusters in the evolutionarily highly conserved ATP-binding cassette protein ABCE1. J. Biol. Chem. *282*, 14598-14607.

Bashan, A., Agmon, I., Zarivach, R., Schluenzen, F., Harms, J., Berisio, R., Bartels, H., Franceschi, F., Auerbach, T., Hansen, H.A., Kossoy, E., Kessler, M., and Yonath, A. (2003a). Structural basis of the ribosomal machinery for peptide bond formation, translocation, and nascent chain progression. Mol. Cell *11*, 91-102.

Bashan, A., Zarivach, R., Schluenzen, F., Agmon, I., Harms, J., Auerbach, T., Baram, D., Berisio, R., Bartels, H., Hansen, H.A., Fucini, P., Wilson, D., Peretz, M., Kessler, M., and Yonath, A. (2003b). Ribosomal crystallography: peptide bond formation and its inhibition. Biopolymers *70*, 19-41.

Becker, T., Armache, J.-P., Jarasch, A., Anger, A.M., Villa, E., Sieber, H., Motaal, B.A., Mielke, T., Berninghausen, O., and Beckmann, R. (2011). Structure of the no-go mRNA decay complex Dom34–Hbs1 bound to a stalled 80S ribosome. Nat. Struct. Mol. Biol. *18*, 715-720.

Beckmann, R., Spahn, C.M., Eswar, N., Helmers, J., Penczek, P.A., Sali, A., Frank, J., and Blobel, G. (2001). Architecture of the protein-conducting channel associated with the translating 80S ribosome. Cell *107*, 361-372.

Bell, S.D., and Jackson, S.P. (1998). Transcription and translation in archaea: a mosaic of eukaryal and bacterial features. Trends Microbiol. *6*, 222-228.

Ben-Shem, A., Jenner, L., Yusupova, G., and Yusupov, M. (2010). Crystal structure of the eukaryotic ribosome. Science *330*, 1203-1209.

Bhushan, S., Hoffmann, T., Seidelt, B., Frauenfeld, J., Mielke, T., Berninghausen, O., Wilson, D.N., and Beckmann, R. (2011). SecM-stalled ribosomes adopt an altered geometry at the peptidyl transferase center. PLoS. Biol. *9*, e1000581.

Blanchard, S.C., Kim, H.D., Gonzalez, R.L., Jr., Puglisi, J.D., and Chu, S. (2004). tRNA dynamics on the ribosome during translation. Proc. Natl. Acad. Sci. *101*, 12893-12898.

Bryant, J.A., and Aves, S.J. (2011). Initiation of DNA replication: functional and evolutionary aspects. Ann. Bot. *107*, 1119-1126.

Budkevich, T., Giesebrecht, J., Altman, Roger B., Munro, James B., Mielke, T., Nierhaus, Knud H., Blanchard, Scott C., and Spahn, C.M. (2011). Structure and dynamics of the mammalian ribosomal pretranslocation complex. Mol. Cell *44*, 214-224.

Chamieh, H., Ballut, L., Bonneau, F., and Le Hir, H. (2008). NMD factors UPF2 and UPF3 bridge UPF1 to the exon junction complex and stimulate its RNA helicase activity. Nat. Struct. Mol. Biol. *15*, 85-93.

Chen, J.Z., and Grigorieff, N. (2007). SIGNATURE: a single-particle selection system for molecular electron microscopy. J. Struct. Biol. *157*, 168-173.

Chen, L., Muhlrad, D., Hauryliuk, V., Cheng, Z., Lim, M.K., Shyp, V., Parker, R., and Song, H. (2010). Structure of the Dom34-Hbs1 complex and implications for no-go decay. Nat. Struct. Mol. Biol. *17*, 1233-1240.

Chen, Z.Q., Dong, J., Ishimura, A., Daar, I., Hinnebusch, A.G., and Dean, M. (2006). The essential vertebrate ABCE1 protein interacts with eukaryotic initiation factors. J. Biol. Chem. *281*, 7452-7457.

Clement, S.L., and Lykke-Andersen, J. (2006). No mercy for messages that mess with the ribosome. Nat. Struct. Mol. Biol. *13*, 299-301.

Coelho, C.M., Kolevski, B., Bunn, C., Walker, C., Dahanukar, A., and Leevers, S.J. (2005). Growth and cell survival are unevenly impaired in pixie mutant wing discs. Development *132*, 5411-5424.

Condo, I., Ciammaruconi, A., Benelli, D., Ruggero, D., and Londei, P. (1999). Cis-acting signals controlling translational initiation in the thermophilic archaeon Sulfolobus solfataricus. Mol. Microbiol. *34*, 377-384.

Connell, S.R., Takemoto, C., Wilson, D.N., Wang, H., Murayama, K., Terada, T., Shirouzu, M., Rost, M., Schuler, M., Giesebrecht, J., Dabrowski, M., Mielke, T., Fucini, P., Yokoyama, S. and Spahn, C.M. (2007). Structural basis for interaction of the ribosome with the switch regions of GTP-bound elongation factors. Mol. Cell *25*, 751-764.

Danson, M.J., and Hough, D.W. (1992). The enzymology of archaebacterial pathways of central metabolism. Biochem. Soc. Symp. *58*, 7-21.

Davis, L., and Engebrecht, J. (1998). Yeast Dom34 mutants are defective in multiple developmental pathways and exhibit decreased levels of polyribosomes. Genetics *149*, 45 - 56.

Decottignies, A., Goffeau, A., and Balzi, E. (1997). Genetic purification of yeast ABC proteins. Folia Microbiol. (Praha) *42*, 260.

DeLong, E. (1998). Archaeal means and extremes. Science *280*, 542-543.

Dmitriev, S.E., Stolboushkina, E.A., Terenin, I.M., Andreev, D.E., Garber, M.B., and Shatsky, I.N. (2011). Archaeal translation initiation factor aIF2 can substitute for eukaryotic eIF2 in ribosomal scanning during mammalian 48S complex formation. J Mol Biol *413*, 106-114.

Doma, M., and Parker, R. (2006). Endonucleolytic cleavage of eukaryotic mRNAs with stalls in translation elongation. Nature *440*, 561 - 564.

Doma, M.K., and Parker, R. (2007). RNA quality control in eukaryotes. Cell *131*, 660-668.

Dong, J., Lai, R., Nielsen, K., Fekete, C.A., Qiu, H., and Hinnebusch, A.G. (2004). The essential ATP-binding cassette protein RLI1 functions in translation by promoting preinitiation complex assembly. J. Biol. Chem. *279*, 42157-42168.

Dridi, B., Raoult, D., and Drancourt, M. (2011). Archaea as emerging organisms in complex human microbiomes. Anaerobe *17*, 56-63.

Dubochet, J., McDowall, A.W., Menge, B., Schmid, E.N., and Lickfeld, K.G. (1983). Electron-microscopy of frozen-hydrated bacteria. J. Bacteriol. *155*, 381-390.

Dunkle, J.A., Wang, L., Feldman, M.B., Pulk, A., Chen, V.B., Kapral, G.J., Noeske, J., Richardson, J.S., Blanchard, S.C., and Cate, J.H. (2011). Structures of the bacterial ribosome in classical and hybrid states of tRNA binding. Science *332*, 981-984.

Dvorak, H.F., Brockman, R.W., and Heppel, L.A. (1967). Purification and properties of two acid phosphatase fractions isolated from osmotic shock fluid of *Escherichia coli*. Biochemistry *6*, 1743-1751.

Eberhart, C., and Wasserman, S. (1995). The pelota locus encodes a protein required for meiotic cell division: an analysis of G2/M arrest in Drosophila spermatogenesis. Development *121*, 3477 - 3486.

Egea, P.F., Napetschnig, J., Walter, P., and Stroud, R.M. (2008). Structures of SRP54 and SRP19, the two proteins that organize the ribonucleic core of the signal recognition particle from *Pyrococcus furiosus*. PLoS ONE *3*, e3528.

Egea, P.F., and Stroud, R.M. (2010). Lateral opening of a translocon upon entry of protein suggests the mechanism of insertion into membranes. Proc. Natl. Acad. Sci. *107*, 17182-17187.

Emanuelsson, O., Brunak, S., von Heijne, G., and Nielsen, H. (2007). Locating proteins in the cell using TargetP, SignalP and related tools. Nat. Protoc. *2*, 953-971.

Endo, Y., and Sawasaki, T. (2004). High-throughput, genome-scale protein production method based on the wheat germ cell-free expression system. J. Struct. Funct. Genomics *5*, 45-57.

Endoh, T., Kanai, T., and Imanaka, T. (2007). A highly productive system for cell-free protein synthesis using a lysate of the hyperthermophilic archaeon, *Thermococcus kodakaraensis*. Appl. Microbiol. Biotechnol. *74*, 1153-1161.

Endoh, T., Kanai, T., and Imanaka, T. (2008). Effective approaches for the production of heterologous proteins using the *Thermococcus kodakaraensis*-based translation system. J. Biotechnol. *133*, 177-182.

Endoh, T., Kanai, T., Sato, Y.T., Liu, D.V., Yoshikawa, K., Atomi, H., and Imanaka, T. (2006). Cell-free protein synthesis at high temperatures using the lysate of a hyperthermophile. J. Biotechnol. *126*, 186-195.

Estevez, A.M., Haile, S., Steinbuchel, M., Quijada, L., and Clayton, C. (2004). Effects of depletion and overexpression of the *Trypanosoma brucei* ribonuclease L inhibitor homologue. Mol. Biochem. Parasitol. *133*, 137-141.

Eswar, N., Eramian, D., Webb, B., Shen, M.Y., and Sali, A. (2008). Protein structure modeling with MODELLER. Methods Mol. Biol. *426*, 145-159.

Fischer, N., Konevega, A.L., Wintermeyer, W., Rodnina, M.V., and Stark, H. (2010). Ribosome dynamics and tRNA movement by time-resolved electron cryomicroscopy. Nature *466*, 329-333.

Frank, J., Radermacher, M., Penczek, P., Zhu, J., Li, Y., Ladjadj, M., and Leith, A. (1996). SPIDER and WEB: processing and visualization of images in 3D electron microscopy and related fields. J. Struct. Biol. *116*, 190-199.

Frauenfeld, J., Gumbart, J., Sluis, E.O., Funes, S., Gartmann, M., Beatrix, B., Mielke, T., Berninghausen, O., Becker, T., Schulten, K.*,* and Beckmann, R. (2011). Cryo-EM structure of the ribosome-SecYE complex in the membrane environment. Nat. Struct. Mol. Biol. *18*, 614-621.

Freistroffer, D.V., Pavlov, M.Y., MacDougall, J., Buckingham, R.H., and Ehrenberg, M. (1997). Release factor RF3 in *E.coli* accelerates the dissociation of release factors RF1 and RF2 from the ribosome in a GTP-dependent manner. EMBO J. *16*, 4126-4133.

Frolova, L., Le Goff, X., Rasmussen, H., Cheperegin, S., Drugeon, G., Kress, M., Arman, I., Haenni, A., Celis, J., and Philippe, M. (1994). A highly conserved eukaryotic protein family possessing properties of polypeptide chain release factor. Nature *372*, 701 - 703.

Frolova, L., Le Goff, X., Zhouravleva, G., Davydova, E., Philippe, M., and Kisselev, L. (1996). Eukaryotic polypeptide chain release factor eRF3 is an eRF1- and ribosome-dependent guanosine triphosphatase. RNA *2*, 334 - 341.

Frolova, L., Seit-Nebi, A., and Kisselev, L. (2002). Highly conserved NIKS tetrapeptide is functionally essential in eukaryotic translation termination factor eRF1. RNA *8*, 129 - 136.

Frolova, L., Tsivkovskii, R., Sivolobova, G., Oparina, N., Serpinsky, O., Blinov, V., Tatkov, S., and Kisselev, L. (1999). Mutations in the highly conserved GGQ motif of class 1 polypeptide release factors abolish ability of human eRF1 to trigger peptidyl-tRNA hydrolysis. RNA *5*, 1014 - 1020.

Fu, J., Munro, J.B., Blanchard, S.C., and Frank, J. (2011). Cryoelectron microscopy structures of the ribosome complex in intermediate states during tRNA translocation. Proc. Natl. Acad. Sci. *108*, 4817-4821.

Gandhi, R., Manzoor, M., and Hudak, K.A. (2008). Depurination of Brome mosaic virus RNA3 *in vivo* results in translation-dependent accelerated degradation of the viral RNA. J. Biol. Chem. *283*, 32218-32228.

Gao, H., Zhou, Z., Rawat, U., Huang, C., Bouakaz, L., Wang, C., Cheng, Z., Liu, Y., Zavialov, A., Gursky, R.*,* Sanyal, S., Ehrenberg, M., Frank, J., and Song, H. (2007). RF3 induces ribosomal conformational changes responsible for dissociation of class I release factors. Cell *129*, 929-941.

Gao, N., Zavialov, A.V., Li, W., Sengupta, J., Valle, M., Gursky, R.P., Ehrenberg, M., and Frank, J. (2005). Mechanism for the disassembly of the posttermination complex inferred from cryo-EM studies. Mol. Cell *18*, 663-674.

Gao, Y.G., Selmer, M., Dunham, C.M., Weixlbaumer, A., Kelley, A.C., and Ramakrishnan, V. (2009). The structure of the ribosome with elongation factor G trapped in the posttranslocational state. Science *326*, 694-699.

Gatfield, D., Unterholzner, L., Ciccarelli, F.D., Bork, P., and Izaurralde, E. (2003). Nonsense-mediated mRNA decay in Drosophila: at the intersection of the yeast and mammalian pathways. EMBO J. *22*, 3960-3970.

Ghosh, S., Ganesan, R., Amrani, N., and Jacobson, A. (2010). Translational competence of ribosomes released from a premature termination codon is modulated by NMD factors. RNA *16*, 1832-1847.

Gillet, R., and Felden, B. (2001). Emerging views on tmRNA-mediated protein tagging and ribosome rescue. Mol. Microbiol. *42*, 879-885.

Graille, M., Chaillet, M., and van Tilbeurgh, H. (2008). Structure of yeast Dom34: a protein related to translation termination factor eRF1 and involved in No-Go decay. J. Biol. Chem. *283*, 7145 - 7154.

Gueneau de Novoa, P., and Williams, K.P. (2004). The tmRNA website: reductive evolution of tmRNA in plastids and other endosymbionts. Nucleic Acids Res. *32*, D104-108.

Hainzl, T., Huang, S., Merilainen, G., Brannstrom, K., and Sauer-Eriksson, A.E. (2011). Structural basis of signal-sequence recognition by the signal recognition particle. Nat. Struct. Mol. Biol. *18*, 389-391.

Halic, M., Becker, T., Pool, M.R., Spahn, C.M., Grassucci, R.A., Frank, J., and Beckmann, R. (2004). Structure of the signal recognition particle interacting with the elongation-arrested ribosome. Nature *427*, 808-814.

Henderson, R. (2004). Realizing the potential of electron cryo-microscopy. Q. Rev. Biophys. *37*, 3-13.

Henrich, B., Lubitz, W., and Plapp, R. (1982). Lysis of *Escherichia coli* by induction of cloned phi X174 genes. Mol. Gen. Genet. *185*, 493-497.

Hentze, M.W., and Kulozik, A.E. (1999). A perfect message: RNA surveillance and nonsense-mediated decay. Cell *96*, 307-310.

Hopfner, K.P., Karcher, A., Shin, D.S., Craig, L., Arthur, L.M., Carney, J.P., and Tainer, J.A. (2000). Structural biology of Rad50 ATPase: ATP-driven conformational control in DNA double-strand break repair and the ABC-ATPase superfamily. Cell *101*, 789-800.

Hopfner, K.P., and Tainer, J.A. (2003). Rad50/SMC proteins and ABC transporters: unifying concepts from high-resolution structures. Curr. Opin. Struct. Biol. *13*, 249-255.

Isken, O., and Maquat, L.E. (2007). Quality control of eukaryotic mRNA: safeguarding cells from abnormal mRNA function. Genes Dev. *21*, 1833-1856.

Ito-Harashima, S., Kuroha, K., Tatematsu, T., and Inada, T. (2007). Translation of the poly(A) tail plays crucial roles in nonstop mRNA surveillance via translation repression and protein destabilization by proteasome in yeast. Genes Dev. *21*, 519-524.

Janda, C.Y., Li, J., Oubridge, C., Hernandez, H., Robinson, C.V., and Nagai, K. (2010). Recognition of a signal peptide by the signal recognition particle. Nature *465*, 507-510.

Jin, H., Kelley, A.C., and Ramakrishnan, V. (2011). Crystal structure of the hybrid state of ribosome in complex with the guanosine triphosphatase release factor 3. Proc. Natl. Acad. Sci. *108*, 15798-15803.

Julian, P., Konevega, A.L., Scheres, S.H., Lazaro, M., Gil, D., Wintermeyer, W., Rodnina, M.V., and Valle, M. (2008). Structure of ratcheted ribosomes with tRNAs in hybrid states. Proc. Natl. Acad. Sci. *105*, 16924-16927.

Karcher, A., Buttner, K., Martens, B., Jansen, R.P., and Hopfner, K.P. (2005). X-ray structure of RLI, an essential twin cassette ABC ATPase involved in ribosome biogenesis and HIV capsid assembly. Structure *13*, 649-659.

Karcher, A., Schele, A., and Hopfner, K.-P. (2008). X-ray structure of the complete ABC enzyme ABCE1 from *Pyrococcus abyssi*. J. Biol. Chem. *283*, 7962-7971.

Kates, M., Kushner, D.J., and Matheson, A.T. (1993). The biochemistry of archaeae (*Archaebacteria*). Elsevier Science Ltd..

Keiler, K.C. (2008). Biology of trans-translation. Annu. Rev. Microbiol. 62, 133-151.

Kerr, I.D. (2004). Sequence analysis of twin ATP binding cassette proteins involved in translational control, antibiotic resistance, and ribonuclease L inhibition. Biochem. Biophys. Res. Commun. *315*, 166-173.

Khoshnevis, S., Gross, T., Rotte, C., Baierlein, C., Ficner, R., and Krebber, H. (2010). The iron-sulphur protein RNase L inhibitor functions in translation termination. EMBO Rep. *11*, 214-219.

Kispal, G., Sipos, K., Lange, H., Fekete, Z., Bedekovics, T., Janaky, T., Bassler, J., Aguilar Netz, D.J., Balk, J., Rotte, C.*,* and Lill, R. (2005). Biogenesis of cytosolic ribosomes requires the essential iron-sulphur protein Rli1p and mitochondria. EMBO J. *24*, 589-598.

Klein, K.C., Reed, J.C., Tanaka, M., Nguyen, V.T., Giri, S., and Lingappa, J.R. (2011). HIV gag-leucine zipper chimeras form ABCE1-containing intermediates and RNase-resistant immature capsids similar to those formed by wild-type HIV-1 gag. J. Virol. *85*, 7419-7435.

Kobayashi, K., Kikuno, I., Kuroha, K., Saito, K., Ito, K., Ishitani, R., Inada, T., and Nureki, O. (2010). Structural basis for mRNA surveillance by archaeal Pelota and GTP-bound EF1α complex. Proc. Natl. Acad. Sci. *107*, 17575-17579.

Komine, Y., Kitabatake, M., Yokogawa, T., Nishikawa, K., and Inokuchi, H. (1994). A tRNA-like structure is present in 10Sa RNA, a small stable RNA from *Escherichia coli*. Proc. Natl. Acad. Sci. *91*, 9223-9227.

Kozak, M. (1990). Evaluation of the fidelity of initiation of translation in reticulocyte lysates from commercial sources. Nucleic Acids Res. *18*, 2828.

Krab, I.M., and Parmeggiani, A. (1998). EF-Tu, a GTPase odyssey. Biochim. Biophys. Acta *1443*, 1-22.

Laemmli, U.K. (1970). Cleavage of structural proteins during the assembly of the head of bacteriophage T4. Nature *227*, 680-685.

Lee, H.H., Kim, Y.S., Kim, K.H., Heo, I., Kim, S.K., Kim, O., Kim, H.K., Yoon, J.Y., Kim, H.S., Kim do, J.*,* Lee, S.J., Yoon, H.J., Kim, S.J., Lee, B.G., Song, H.K., Kim, V.N., Park, C.M. and Suh, S.W. (2007). Structural and functional insights into Dom34, a key component of no-go mRNA decay. Mol. Cell *27*, 938-950.

Lepault, J., Freeman, R., and Dubochet, J. (1983). Electron-beam induced vitrified ice. J. Microsc. *132*, RP3-RP4.

Lingappa, J.R., Dooher, J.E., Newman, M.A., Kiser, P.K., and Klein, K.C. (2006). Basic residues in the nucleocapsid domain of Gag are required for interaction of HIV-1 gag with ABCE1 (HP68), a cellular protein important for HIV-1 capsid assembly. J. Biol. Chem. *281*, 3773-3784.

Linton, K.J., and Higgins, C.F. (1998). The *Escherichia coli* ATP-binding cassette (ABC) proteins. Mol. Microbiol. *28*, 5-13.

Liu, D.V., Zawada, J.F., and Swartz, J.R. (2005). Streamlining *Escherichia coli* S30 extract preparation for economical cell-free protein synthesis. Biotechnol. Prog. *21*, 460-465.
Locher, K.P. (2009). Review. Structure and mechanism of ATP-binding cassette transporters. Philos. Trans. R. Soc. Lond. B. Biol. Sci. *364*, 239-245.

Lykke-Andersen, J., Shu, M.D., and Steitz, J.A. (2000). Human Upf proteins target an mRNA for nonsense-mediated decay when bound downstream of a termination codon. Cell *103*, 1121-1131.

Matthaei, J.H., and Nirenberg, M.W. (1961). Characteristics and stabilization of DNAase-sensitive protein synthesis in *E. coli* extracts. Proc. Natl. Acad. Sci. *47*, 1580-1588.

Mora, L., Heurgue-Hamard, V., Champ, S., Ehrenberg, M., Kisselev, L.L., and Buckingham, R.H. (2003). The essential role of the invariant GGQ motif in the function and stability *in vivo* of bacterial release factors RF1 and RF2. Mol. Microbiol. *47*, 267-275.

Morikawa, M., Izawaka, Y., Rashid, N., Hoaki, T., and Imanaka, T. (1994). Purification and characterization of a thermostable thiol protease from a newly isolated hyperthermophilic *Pyrococcus sp*. Appl. Environ. Microbiol. *60*, 4559-4566.

Nagy, E., and Maquat, L.E. (1998). A rule for termination-codon position within intron-containing genes: when nonsense affects RNA abundance. Trends Biochem. Sci*. 23*, 198-199.

Negrutskii, B.S., and El'skaya, A.V. (1998). Eukaryotic translation elongation factor 1 alpha: structure, expression, functions, and possible role in aminoacyl-tRNA channeling. Prog. Nucleic. Acid. Res. Mol. Biol. *60*, 47-78.

Nguyen, H.D., Nguyen, Q.A., Ferreira, R.C., Ferreira, L.C., Tran, L.T., and Schumann, W. (2005). Construction of plasmid-based expression vectors for *Bacillus subtilis* exhibiting full structural stability. Plasmid *54*, 241-248.

Noren, C.J., Anthony-Cahill, S.J., Griffith, M.C., and Schultz, P.G. (1989). A general method for site-specific incorporation of unnatural amino acids into proteins. Science *244*, 182-188.

Passos, D., Doma, M., Shoemaker, C., Muhlrad, D., Green, R., Weissman, J., Hollien, J., and Parker, R. (2009). Analysis of Dom34 and its function in no-go decay. Mol. Biol. Cell *20*, 3025-3032.

Pavlov, M.Y., Antoun, A., Lovmar, M., and Ehrenberg, M. (2008). Complementary roles of initiation factor 1 and ribosome recycling factor in 70S ribosome splitting. EMBO J. *27*, 1706-1717.

Paytubi, S., Wang, X., Lam, Y.W., Izquierdo, L., Hunter, M.J., Jan, E., Hundal, H.S., and Proud, C.G. (2009). ABC50 promotes translation initiation in mammalian cells. J. Biol. Chem. *284*, 24061-24073.

Penczek, P.A., Grassucci, R.A., and Frank, J. (1994). The ribosome at improved resolution: new techniques for merging and orientation refinement in 3D cryo-electron microscopy of biological particles. Ultramicroscopy *53*, 251-270.

Penczek, P.A., Yang, C., Frank, J., and Spahn, C.M. (2006). Estimation of variance in single-particle reconstruction using the bootstrap technique. J. Struct. Biol. *154*, 168-183.

Pettersen, E.F., Goddard, T.D., Huang, C.C., Couch, G.S., Greenblatt, D.M., Meng, E.C., and Ferrin, T.E. (2004). UCSF Chimera - a visualization system for exploratory research and analysis. J. Comput. Chem. *25*, 1605-1612.

Phillips, J.C., Braun, R., Wang, W., Gumbart, J., Tajkhorshid, E., Villa, E., Chipot, C., Skeel, R.D., Kale, L., and Schulten, K. (2005). Scalable molecular dynamics with NAMD. J. Comput. Chem. *26*, 1781-1802.

Pisarev, A.V., Hellen, C.U., and Pestova, T.V. (2007). Recycling of eukaryotic posttermination ribosomal complexes. Cell *131*, 286-299.

Pisarev, A.V., Skabkin, M.A., Pisareva, V.P., Skabkina, O.V., Rakotondrafara, A.M., Hentze, M.W., Hellen, C.U.T., and Pestova, T.V. (2010). The Role of ABCE1 in eukaryotic posttermination ribosomal recycling. Mol. Cell *37*, 196-210.

Pisareva, V.P., Skabkin, M.A., Hellen, C.U., Pestova, T.V., and Pisarev, A.V. (2011). Dissociation by Pelota, Hbs1 and ABCE1 of mammalian vacant 80S ribosomes and stalled elongation complexes. EMBO J. *30*, 1804-1817

Poole, A.M., and Penny, D. (2007). Evaluating hypotheses for the origin of eukaryotes. Bioessays *29*, 74-84.

Pulak, R., and Anderson, P. (1993). mRNA surveillance by the *Caenorhabditis elegans* smg genes. Genes Dev. *7*, 1885-1897.

Rahman, R., Fujiwara, S., Takagi, M., and Imanaka, T. (1998). Sequence analysis of glutamate dehydrogenase (GDH) from the hyperthermophilic archaeon *Pyrococcus sp*. KOD1 and comparison of the enzymatic characteristics of native and recombinant GDHs. Mol. Gen. Genet. *257*, 338-347.

Rees, D.C., Johnson, E., and Lewinson, O. (2009). ABC transporters: the power to change. Nat. Rev. Mol. Cell. Biol. *10*, 218-227.

Ruggero, D., Creti, R., and Londei, P. (1993). *In vitro* translation of archaeal natural mRNAs at high temperature. FEMS Microbiol. Lett. *107*, 89-94.

Saito, K., Kobayashi, K., Wada, M., Kikuno, I., Takusagawa, A., Mochizuki, M., Uchiumi, T., Ishitani, R., Nureki, O., and Ito, K. (2010). Omnipotent role of archaeal elongation factor 1 alpha (EF1α) in translational elongation and termination, and quality control of protein synthesis. Proc. Natl. Acad. Sci. *107*, 19242-19247.

Schmeing, T.M., Voorhees, R.M., Kelley, A.C., Gao, Y.G., Murphy, F.V.t., Weir, J.R., and Ramakrishnan, V. (2009). The crystal structure of the ribosome bound to EF-Tu and aminoacyl-tRNA. Science *326*, 688-694.

Schroder, G.F., Brunger, A.T., and Levitt, M. (2007). Combining efficient conformational sampling with a deformable elastic network model facilitates structure refinement at low resolution. Structure *15*, 1630-1641.

Scolnick, E., Tompkins, R., Caskey, T., and Nirenberg, M. (1968). Release factors differing in specificity for terminator codons. Proc. Natl. Acad. Sci. *61*, 768 - 774.

Seidelt, B., Innis, C.A., Wilson, D.N., Gartmann, M., Armache, J.P., Villa, E., Trabuco, L.G., Becker, T., Mielke, T., Schulten, K., Steitz, T.A., and Beckmann, R., (2009). Structural insight into nascent polypeptide chain-mediated translational stalling. Science *326*, 1412-1415.

Shoemaker, C.J., Eyler, D.E., and Green, R. (2010). Dom34:Hbs1 promotes subunit dissociation and peptidyl-tRNA drop-off to initiate no-go decay. Science *330*, 369-372.

Shoemaker, C.J., and Green, R. (2011). Kinetic analysis reveals the ordered coupling of translation termination and ribosome recycling in yeast. Proc. Natl. Acad. Sci. *108*, 1392-1398

Smith, P.C., Karpowich, N., Millen, L., Moody, J.E., Rosen, J., Thomas, P.J., and Hunt, J.F. (2002). ATP binding to the motor domain from an ABC transporter drives formation of a nucleotide sandwich dimer. Mol. Cell *10*, 139-149.

Soding, J., Biegert, A., and Lupas, A.N. (2005). The HHpred interactive server for protein homology detection and structure prediction. Nucleic Acids Res. *33*, W244-248.

Song, H., Mugnier, P., Das, A.K., Webb, H.M., Evans, D.R., Tuite, M.F., Hemmings, B.A., and Barford, D. (2000). The crystal structure of human eukaryotic release factor eRF1 - mechanism of stop codon recognition and peptidyl-tRNA hydrolysis. Cell *100*, 311-321.

Spahn, C.M., Gomez-Lorenzo, M.G., Grassucci, R.A., Jorgensen, R., Andersen, G.R., Beckmann, R., Penczek, P.A., Ballesta, J.P., and Frank, J. (2004). Domain movements of elongation factor eEF2 and the eukaryotic 80S ribosome facilitate tRNA translocation. EMBO J. *23*, 1008-1019.

Spahn, C.M., and Penczek, P.A. (2009). Exploring conformational modes of macromolecular assemblies by multiparticle cryo-EM. Curr. Opin. Struct. Biol. *19*, 623-631.

Taylor, D.J., Nilsson, J., Merrill, A.R., Andersen, G.R., Nissen, P., and Frank, J. (2007). Structures of modified eEF2 80S ribosome complexes reveal the role of GTP hydrolysis in translocation. EMBO J. *26*, 2421-2431.

Trabuco, L.G., Villa, E., Mitra, K., Frank, J., and Schulten, K. (2008). Flexible fitting of atomic structures into electron microscopy maps using molecular dynamics. Structure *16*, 673-683.

Ushida, C., Himeno, H., Watanabe, T., and Muto, A. (1994). tRNA-like structures in 10Sa RNAs of *Mycoplasma capricolum* and *Bacillus subtilis*. Nucleic Acids Res. *22*, 3392-3396.
van de Vossenberg, J.L., Driessen, A.J., and Konings, W.N. (1998). The essence of being extremophilic: the role of the unique archaeal membrane lipids. Extremophiles *2*, 163-170.

van den Berg, B., Clemons, W.M., Jr., Collinson, I., Modis, Y., Hartmann, E., Harrison, S.C., and Rapoport, T.A. (2004). X-ray structure of a protein-conducting channel. Nature *427*, 36-44.

van den Elzen, A.M.G., Henri, J., Lazar, N., Gas, M.E., Durand, D., Lacroute, F., Nicaise, M., van Tilbeurgh, H., Seraphin, B., and Graille, M. (2010). Dissection of Dom34-Hbs1 reveals independent functions in two RNA quality control pathways. Nat. Struct. Mol. Biol. *17*, 1446-1474.

van Hoof, A. (2005). Conserved functions of yeast genes support the duplication, degeneration and complementation model for gene duplication. Genetics *171*, 1455 - 1461.

van Hoof, A., Frischmeyer, P.A., Dietz, H.C., and Parker, R. (2002). Exosome-mediated recognition and degradation of mRNAs lacking a termination codon. Science *295*, 2262-2264.

Villa, E., Sengupta, J., Trabuco, L.G., LeBarron, J., Baxter, W.T., Shaikh, T.R., Grassucci, R.A., Nissen, P., Ehrenberg, M., Schulten, K., and Frank, J. (2009). Ribosome-induced changes in elongation factor Tu conformation control GTP hydrolysis. Proc. Natl. Acad. Sci. *106*, 1063-1068.

Wild, K., Bange, G., Bozkurt, G., Segnitz, B., Hendricks, A., and Sinning, I. (2010). Structural insights into the assembly of the human and archaeal signal recognition particles. Acta Crystallogr. D. Biol. Crystallogr. *66*, 295-303.

Wilson, M.A., Meaux, S., and van Hoof, A. (2007). A genomic screen in yeast reveals novel aspects of nonstop mRNA metabolism. Genetics *177*, 773-784.

Winzeler, E.A., Shoemaker, D.D., Astromoff, A., Liang, H., Anderson, K., Andre, B., Bangham, R., Benito, R., Boeke, J.D., Bussey, H., Chu, A.M., Connelly, C., Davis, K., Dietrich, F., Dow, S. W., El Bakkoury, M., Foury, F., Friend, S. H., Gentalen, E., Giaever, G., Hegemann, J. H., Jones, T., Laub, M., Liao, H., Liebundguth, N., Lockhart, D.J., Lucau-Danila, A., Lussier, M., M'Rabet, N., Menard, P., Mittmann, M., Pai, C., Rebischung, C., Revuelta, J.L., Riles, L., Roberts, C.J., Ross-MacDonald, P., Scherens, B., Snyder,

M., Sookhai-Mahadeo, S., Storms, R.K., Veronneau, S., Voet, M., Volckaert, G., Ward, T.R., Wysocki, R., Yen, G.S., Yu, K., Zimmermann, K., Philippsen, P., Johnston, M., and Davis, R.W. (1999). Functional characterization of the *S. cerevisiae* genome by gene deletion and parallel analysis. Science *285*, 901-906.

Woese, C.R., and Fox, G.E. (1977). Phylogenetic structure of the prokaryotic domain: the primary kingdoms. Proc. Natl. Acad. Sci. *74*, 5088-5090.

Woese, C.R., Kandler, O., and Wheelis, M.L. (1990). Towards a natural system of organisms: proposal for the domains Archaea, Bacteria, and Eucarya. Proc. Natl. Acad. Sci. *87*, 4576-4579.

Wollerton, M.C., Gooding, C., Wagner, E.J., Garcia-Blanco, M.A., and Smith, C.W. (2004). Autoregulation of polypyrimidine tract binding protein by alternative splicing leading to nonsense-mediated decay. Mol. Cell *13*, 91-100.

Yarunin, A., Panse, V.G., Petfalski, E., Dez, C., Tollervey, D., and Hurt, E.C. (2005). Functional link between ribosome formation and biogenesis of iron-sulfur proteins. EMBO J. *24*, 580-588.

Youngman, E.M., and Green, R. (2005). Affinity purification of *in vivo*-assembled ribosomes for *in vitro* biochemical analysis. Methods *36*, 305-312.

Yu, X.K., Ge, P., Jiang, J.S., Atanasov, I., and Zhou, Z.H. (2011). Atomic model of CPV reveals the mechanism used by this single-shelled virus to economically carry out functions conserved in multishelled reoviruses. Structure *19*, 652-661.

Zimmerman, C., Klein, K.C., Kiser, P.K., Singh, A.R., Firestein, B.L., Riba, S.C., and Lingappa, J.R. (2002). Identification of a host protein essential for assembly of immature HIV-1 capsids. Nature *415*, 88-92.

8. Appendix

Supplementary Table: Contacts of aPelota and aABCE1 with the ribosome and with each other. Known mutations of or in direct neighborhood to contacting residues in aPelota and aABCE1 and their effects are given.

Ribosome		aPelota		Mutation	
Protein	**Residue**	**Domain**	**Residue**	**Residue ****	**Effect *****
LSU L10e	100-106	ce	174-176	174KKK176 to 174AAA176[1,2] (174-176)	+
L11	18-24	CTD	283-285	Y300A[3,2] (283)	+
SSU S5	79	NTD	48-49	49SKLDf53 to AAAAA[1] (47-51)	+

Ribosome		aPelota		Mutation	
RNA	**Nucleotide***	**Domain**	**Residue**	**Residue ****	**Effect *****
LSU H43	1205-1207	CTD	325-326		
H44	1234	CTD	353,354		
H69	2038-2040	ce	239-240, 243		
H72	2070-2071	ce	207-208, 231-233	G217Y[3] (208), 216PGF218 to 216AAA218[1] (207-209)	+, +
	2087	ce	235-236		
H89	2595	ce	223		
H95	2776	CTD	272-273, 276		
SSU h18	470-472, 483-484	NTD	42, 63-64, 68, 94-96	(D90-P100)A[3] (90-104)	+
h28	1357	NTD	46	F47A[3] (45), 49SKLDf53 to 49AAAAA53[1] (47-51)	++, +
h31	916	NTD	9		
h34	1004-1006, 1156	NTD	46, 94-96	F47A[3] (45), 49SKLDf53 to 49AAAAA53[1], (47-51), (D90-P100)A[3] (90-104)	++, +
h44	1449	NTD	60		

tRNA		aPelota		Mutation	
Position	**Residue**	**Domain**	**Residue**	**Residue ****	**Effect *****
P site	1	ce	172-174	174KKK176 to 174AAA176[1,2] (174-176)	+
	68	ce	163-164		
	73	ce	172		

ABCE1		aPelota		Mutation	
Domain	**Residue**	**Domain**	**Residue**	**Residue ****	**Effect *****
FeS	30-31, 33-34, 58	CTD	283, 285, 344-345	$Y300A^{3,2}$ (283)	+

	Ribosome		aABCE1		Mutation	
	Protein	**Residue**	**Domain**	**Residue**	**Residue ****	**Effect *****
LSU	L14	132	H1	324-327		
	L9	96	NBD2	434-435		

	Ribosome		aABCE1		Mutation	
	RNA	**Nucleotide***	**Domain**	**Residue**	**Residue ****	**Effect *****
SSU	h5	51	NBD1	149	$L152A^4$ (150)	-
	h8	144-145	H2	576-579, 582	$S588E^4$ (576)	++
	h14	339-341	H1	302, 304	$R311E^4$ (304)	++
			H2	563, 572, 575	$R573E^4$ (563)	++
	h15	363-364	NBD1	146-149	$R148A^4$, $L152A^4$ (146, 149)	-,-

aPelota		aABCE1		Mutation	
Domain	**Residue**	**Domain**	**Residue**	**Residue ****	**Effect *****
CTD	283, 285, 344-345	FeS	30-31, 33-34, 58	$C29S/A^{4,5}$, $C54S^6$, ΔFeS^6, (29, 58, 1-78)	-,-,++

Legend:

*   *P. furiosus* numbering

**   Numbers in brackets indicate the corresponding residues for aPelota (*T. kodakarensis*) and aABCE1 (*P. furiosus*)

***   Effect reads as: - no effect   + mild effect   ++ strong effect

1,   Passos et al., 2009

2,   van den Elzen et al., 2010

3,   Kobayashi et al., 2010

4,   Karcher et al., 2005

5,   Barthelme et al., 2007

6,   Barthelme et al., 2011

9. Acknowledgements

10. Curriculum Vitae

Personal data:

Name   Sibylle Franckenberg

Date of birth   09.02.1982

Place of birth Bamberg, Germany

Citizenship   German

Education:

2007-2012   PhD thesis at the Gene Center (Ludwig-Maximilians-Universität Munich), Prof. Dr. Roland Beckmann

2006-2007   Diploma thesis at the Max-Planck-Institute for Terrestrial Microbiology in Marburg, Prof. Dr. Andreas Brune

2002-2007   Studies of human biology, Philpps-Universität Marburg

2001   Abitur at Franz-Ludwig-Gymnasium, Bamberg

Publications:

Armache, J.P., Jarasch, A., Anger, A.M., Villa, E., Becker, T., Bhushan, S., Jossinet, F., Habeck, M., Dindar, G., **Franckenberg, S.,** Marqez, V., Mielke, T., Thomm, M., Berninghausen, O., Beatrix, B., Soding, J., Westhof, E., Wilson, D.N., and Beckmann, R. (2010a). Cryo-EM structure and rRNA model of a translating eukaryotic 80S ribosome at 5.5-Å resolution. Proc. Natl. Acad. Sci. *107*, 19748-19753.

Armache, J.P., Jarasch, A., Anger, A.M., Villa, E., Becker, T., Bhushan, S., Jossinet, F., Habeck, M., Dindar, G., **Franckenberg, S.***,* Marqez, V., Mielke, T., Thomm, M., Berninghausen, O., Beatrix, B., Soding, J., Westhof, E., Wilson, D.N., and Beckmann, R. (2010b). Localization of eukaryote-specific ribosomal proteins in a 5.5-Å cryo-EM map of the 80S eukaryotic ribosome. Proc. Natl. Acad. Sci. *107*, 19754-19759.

Becker, T., **Franckenberg, S.,** Wickles, S., Shoemaker, C.J., Anger, A.M., Armache, J.P., Sieber, H., Ungewickell, C., Berninghausen, O., Daberkow, I., Karcher, A., Thomm, M., Hopfner, K.P., Green, R., and Beckmann, R (2012). Structural basis of highly conserved ribosome recycling in eukaryotes and archaea. Nature, *482*, 501-506.